

A Booklet for External Review

Department of Astronomy, School of Science, The University of Tokyo
and
Institute of Astronomy, School of Science, The University of Tokyo

January 14, 2020

Contents

Chapter 1	Introduction	7
Chapter 2	Organization	9
Chapter 3	Education	11
3.1	Admission of Students	11
3.2	Financial Support	12
3.3	Paths after Graduation	12
3.4	Lectures for undergraduate students	12
3.5	Lectures for graduate students	15
3.6	Recent master and doctor theses	20
Chapter 4	Research Activities	29
4.1	Statistics	29
4.2	Competitive research funds	29
Chapter 5	Research Highlights	37
5.1	Tomonori Totani	37
5.1.1	The Subaru FMOS Galaxy Redshift Survey (FastSound) to Probe the Cosmic Acceleration	37
5.1.2	On the Origin of Mysterious Fast Radio Bursts	38
5.2	Motohide Tamura	39
5.2.1	Exoplanet Instrumentations	39
5.2.2	K2/TESS and Other Transiting Planet Detection and Characterization	41
5.2.3	Circular and Linear Polarization Survey of Star Forming Regions	41
5.3	Yuri Aikawa	43
5.3.1	Isotope fractionation in the star-forming regions and protoplanetary disks	43
5.3.2	Complex organic molecules in protoplanetary disks	44
5.4	Nobunari Kashikawa	45
5.4.1	High-z protocluster survey by Subaru/HSC	45
5.4.2	Subaru High-z Exploration of Low-luminosity Quasars (SHELLQs)	45
5.5	Kazuhiro Shimasaku	47
5.5.1	Galaxy evolution	47
5.5.2	Subaru Hyper Suprime-Cam Strategic Survey	47
5.6	Hideyuki Umeda	49
5.6.1	The Final Fates of Accreting Supermassive Stars	49
5.6.2	A progenitor model of SN 1987A based on the slow-merger scenario	49
5.7	Michiko Fujii	50
5.7.1	Dynamical evolution of star clusters and galaxies	50
5.8	Masao Takata	53
5.8.1	Rosette Modes of Oscillation in Rotating Stars	53
5.8.2	Asymptotic Analysis of Oscillations in Red-Giant Stars	53
5.8.3	Asteroseismic Study of Internal Rotation of Stars	54
5.9	Itsuki Sakon	55
5.9.1	The study of Mid-infrared Spectrometer and Camera (MISC) for Origins Space Telescope for US 2020 Decadal Survey	55
5.9.2	Laboratory Astrophysics and Space Exposure Experiment using International Space Station(ISS)/ExHAM	56
5.9.3	Infrared Observation of Dusty Novae	57

5.10	Noriyuki Matsunaga	58
5.10.1	The structure of the Milky Way and stellar populations therein	58
5.10.2	Near-infrared high-resolution spectroscopy	59
5.11	Mamoru Doi	61
5.11.1	Properties of Type-Ia Supernovae	61
5.11.2	Local environment of the Core-Collapse Supernova	61
5.11.3	Isophote Shapes of Early-type Galaxies	62
5.12	Kotaro Kohno (and IoA radio astronomy group)	63
5.12.1	Deep galaxy surveys using ALMA	63
5.12.2	Interstellar medium in galaxies and quasars in the EoR	63
5.12.3	Physical and chemical properties of giant molecular clouds in the Milky Way and galaxies	64
5.12.4	Development of new observing instruments and techniques	65
5.13	Takashi Miyata, Takafumi Kamizuka, Kentaro Asano	67
5.13.1	Development of Field Stacker for precise monitoring in MIR	67
5.13.2	Structure of protoplanetary disks	67
5.13.3	Studies on solar system objects	67
5.13.4	Dust formation and alteration processes around young and evolved stars	67
5.14	Masuo Tanaka	69
5.14.1	Near-infrared Narrow-band Imaging Observations in the 1.87 and 2.07 μm of Massive Star Clusters with miniTAO at Atacama: Classification of Stellar Components	69
5.15	Naoto Kobayashi	70
5.15.1	NIR High-resolution Spectroscopy of Optical Quality with WINERED	70
5.15.2	Near-infrared DIBs	70
5.15.3	Development of Immersion Grating	71
5.16	Kentaro Motohara	73
5.16.1	Star Formation Activities in Nearby LIRGs Probed by Paschen α Imaging	73
5.16.2	Development of Integral Field Unit for SWIMS	73
5.17	Takeo Minezaki	75
5.17.1	Reverberation Mapping of Active Galactic Nuclei	75
5.17.2	Development of Optical Adaptive Optics for Small Telescopes	76
5.18	Toshihiko Tanabé	77
5.18.1	Search for the MOLsphere	77
5.19	Shigeyuki Sako	78
5.19.1	Development of Tomo-e Gozen: Kiso Wide-field Video Observation System	78
5.19.2	Observations of the solar system small bodies with Tomo-e Gozen	78
5.19.3	Observations of faint meteors with Tomo-e Gozen	79
5.19.4	Development of data-driven approaches toward astronomical big data	80
5.20	Tomoki Morokuma	82
5.20.1	Electromagnetic Counterpart Identification of Gravitational Wave Sources	82
5.20.2	Electromagnetic Counterpart Identification of High-Energy Neutrino Sources	82
5.20.3	Effective Selection of Low-Mass Black Holes via Optical Rapid Variability	83
5.21	Bunyo Hatsukade	84
5.21.1	A Census of the Population of Faint Submillimeter Sources	84
5.21.2	Host Galaxies of Gamma-ray Bursts (GRBs) and Superluminous Supernovae (SLSNe)	85
5.21.3	Commissioning of a New 2-mm Receiver and Spectrometer System on LMT	85
5.22	Fumi Egusa	86
5.22.1	Lifetime of Spiral Arms in Nearby Galaxies	86
5.22.2	Molecular Gas and Star Formation in the Nearby Barred Spiral Galaxy NGC 1365	87
5.22.3	Molecular Gas Properties in the Nearby Barred Spiral Galaxy M 83 from PDF Analysis	87
5.23	Masahiro Konishi	89
5.23.1	The evaluation of atmospheric transmittance in the NIR at the TAO site	89
5.23.2	TAO enclosure design and wind analysis	89
5.24	Hidenori Takahashi	91
5.24.1	Investigation of Property of Massive Star Cluster by Near-Infrared Imaging Observation	91
5.24.2	Multi-wavelength Study of Starburst Galaxy NGC253	91
5.24.3	Development of Tunable Filter for Spectroscopic Imaging Observation	92

Chapter 6 Kiso Observatory	95
6.1 Introduction	95
6.2 Observing Facilities	95
6.2.1 105cm Schmidt Telescope	96
6.2.2 Past Instruments	97
6.2.3 New Instrument – Tomo-e Gozen –	97
6.3 Remote/Automatic Observing	99
6.3.1 Observing Efficiency	99
6.4 Science Operation	100
6.4.1 From Open-Use to Inter-university Collaboration	100
6.4.2 Open-Use	100
6.4.3 Publications	100
6.5 Observatory Long-term Science Programs	102
6.5.1 Overview	102
6.5.2 KIso Supernova Survey (KISS)	102
6.5.3 KWFC Intensive Survey of the Galactic Plane (KISOGP)	103
6.6 Education	104
6.7 Public Outreach	105
6.7.1 Galaxy School (“Ginga Gakko”)	105
6.7.2 Science Partnership Program (SPP)/Super Science High-school (SSH): “Hoshi no Kyoshitsu”	106
6.7.3 Extracurricular Lessons and Star Watching Parties	107
6.7.4 Open House	107
6.8 Accommodation Facility	108
6.9 Future Plan	109
Chapter 7 TAO project	111
7.1 Project Overview	111
7.2 Telescope Optics	112
7.3 Telescope Mount	113
7.4 Summit Facilities	114
7.5 Aluminizing Chamber	115
7.6 Site Construction Works	117
7.7 Schedule	117
7.8 First-generation Instruments	118
7.8.1 SWIMS	118
7.8.2 MIMIZUKU	119
7.8.3 NICE	121
7.9 Key Science Objectives	122
7.9.1 Probe History of Baryon Accumulation by Observations of Quasars	123
7.9.2 Origin of Earth-Type Exoplanets	124
7.9.3 Time-Domain Observations	125
7.10 Operation Plan	126

Chapter 1

Introduction

This is a booklet for the 2019 external review jointly for the two organizations: the Department of Astronomy and the Institute of Astronomy of the School of Science, the University of Tokyo, seven years after the previous review in 2012.

The University of Tokyo has the largest astronomy group among the universities in Japan and thus has significant responsibility not only in educating students in the University of Tokyo, but also in fostering future astronomers, who can lead astronomy in Japan as well as internationally, by front-line research in astronomy. We believe that this external review would be crucially useful for our future development.

In chapter 2, we introduce the organization structure. Chapter 3 describes our educational activities with statistical data. Chapter 4 summarizes statistics about our research activities, followed by research highlights in chapter 5. Finally, we describe the two observatories (the Kiso observatory and the Univ. of Tokyo Atacama Observatory) in chapters 6 and 7, respectively.

In addition to this booklet, we provide the Annual Reports of the two organizations, as a reference to the complete lists of activities (e.g., paper lists). We apologize to the international review committee members that this is written in Japanese. However, lists of refereed papers and presentations in international conferences can be read by non-Japanese members. The pdf files of the annual reports (one pdf file includes both DoA and IoA) can be downloaded from <http://www.astron.s.u-tokyo.ac.jp/en/about/annual-reports/>.

We warmly appreciate significant effort made by the external review committee. If there are any questions or you need additional information, please contact us at any time.

Chapter 2

Organization

The Astronomy Group of the School of Science, the University of Tokyo consists of the two organizations: Department of Astronomy (DoA) at the Hongo campus and Institute of Astronomy (IoA) at the Mitaka campus. There are about 30 full-time faculty members now in these two organizations. In the academic year of 2019 (2019 Apr. – 2020 Mar.), T. Totani is serving as the chair of DoA, and M. Doi is serving as the director of IoA. In addition, one full-time faculty is joining the Astronomy Group from the Research Center for the Early Universe of the School of Science. These full-time faculties are responsible for undergraduate and graduate courses of astronomy. Furthermore, 18 cooperative faculties are participating to the graduate course from organizations outside the School of Science but within the University of Tokyo, and also from those outside the Univ. of Tokyo, i.e., National Astronomical Observatory of Japan (NAOJ) and Institute of Space and Astronautical Science (ISAS) of the Japan Aerospace Exploration Agency (JAXA). The name “Department of Astronomy” is often used to include all these faculty members in a wider meaning.

The current faculty member list is shown in Table 2.1.

Table 2.1: Full-time and cooperative teaching staff

Institute	Position	Name	Speciality	
Full-time				
Department of Astronomy	Professor	T. Totani	Astrophysics	
		M. Tamura	Exoplanet Astronomy	
		Y. Aikawa	Astrophysics	
	Assoc. Prof.	N. Kashikawa	Galactic Astronomy	
		K. Shimasaku	Galactic Astronomy	
		H. Umeda	Theoretical Astrophysics	
		M. Fujii	Theoretical & Computational Astrophysics	
	Assis. Prof.	M. Takata	Astrophysics	
		I. Sakon	Infrared Astronomy	
		N. Matsunaga	Optical & Infrared Astronomy	
Institute of Astronomy	S.A. Assis. Prof.*	J. Kwon	Optical & Interstellar Physics	
		M. Doi	Galactic Astronomy	
	Professor	K. Kohno	Radio Astronomy	
		T. Miyata	Infrared Astronomy	
		M. Tanaka	Infrared Astronomy	
		N. Kobayashi	Infrared Astronomy	
	Assoc. Prof.	K. Motohara	Infrared Astronomy	
			T. Minezaki	Infrared Astronomy
		Assis. Prof.	T. Tanabé	Astrophysics
			S. Sako	Infrared & Time Domain Astronomy
T. Morokuma			Optical & Infrared Astronomy	
S.A. Assis. Prof.*		B. Hatsukade	Radio Astronomy	
		F. Egusa	Radio Astronomy	
		M. Konishi	Infrared Astronomy	
		H. Takahashi	Infrared Astronomy & Instrumentation	
		R. Ohsawa	Optical & Infrared Astronomy	
	T. Takekoshi	Radio Astronomy		
	Y. Niino	Optical Astronomy & Astrophysics		
	T. Kamizuka	Infrared Astronomy		
H. Sameshima	Optical & Infrared Astronomy			
Research Center for the Early Universe	Assoc. Prof.	T. Shigeyama	Theoretical Astrophysics	
Cooperative within the University of Tokyo				
Graduate School of Arts and Sciences Institute for Cosmic Ray Research Kavli IPMU	Professor	T. Suzuki	Theoretical Astrophysics	
		M. Ouchi	Galactic Astronomy	
		J. Silverman	Observational Cosmology	
Cooperative outside of the University of Tokyo				
Institute of Space and Astronautical Science, JAXA	Professor	K. Ebisawa	X-ray Astronomy	
	Assoc. Prof.	M. Tsuboi	Radio Astronomy	
National Astronomical Observatory Japan	Assoc. Prof.	H. Kataza	Infrared Astronomy	
		N. Gouda	Astrophysics	
	Professor	N. Ohashi	Radio Astronomy	
		E. Kokubo	Theoretical Astrophysics	
		S. Sakamoto	Radio Astronomy	
		R. Flaminio	Gravitational Wave Astronomy	
		M. Honma	Radio Astronomy	
		M. Fukagawa	Radio Astronomy	
		Assoc. Prof.	H. Hara	Solar Physics
		N. Takato	Optical & Infrared Astronomy	
Y. Katsukawa	Solar Physics			
T. Okuda	Radio Astronomy			
F. Nakamura	Theoretical Astronomy			

*Specially appointed assistant professors (non-tenured). Normal assistant professors are tenured in the Japanese system.

Chapter 3

Education

3.1 Admission of Students

Table 3.1 shows the numbers of the students who graduated the undergraduate, master, and doctor course of astronomy for 2013 – 2019.

Every year, 9–10 students enter the undergraduate course of DoA as new third-year students. Education for undergraduate students is done in Japanese. Unlike many universities, the subject of the major study is not determined at the time when undergraduate students enter the University of Tokyo. Students experience various fields in the College of Arts and Sciences for one and a half years. Admission into a specialty department is decided in the autumn of the second year. Decisions of allowing students to enter an oversubscribed department are based on their achievements (score/grades) in the College of Arts and Sciences. Among various subjects, the DoA places its emphasis on physics. Astronomy is a highly popular field, and normally it is highly oversubscribed and hence students coming to DoA have top-level grades in the College of Arts and Sciences.

About 25 Japanese students enter as the 1st year master course graduate students every year, by passing the entrance examination open to anyone who can take the examination in Japanese. As a result, more than half of master course students are from Japanese universities other than UTokyo. There is no preferential treatment for undergraduate UTokyo students at the entrance examination. About half of those who graduated the master course go up to the doctor course, and hence 10–15 doctor course students get PhD every year. These numbers stay roughly constant over the last 10 years.

On average, female students constitute 14% of all Japanese undergraduate students, and 12% of all Japanese graduate students entering the master course. There is no affirmative action in the process of selecting undergraduate or graduate students to DoA. As a reference, the fraction of female students is 18.6% of all undergraduate students of UTokyo, and it is 12.2% for the School of Science. There is a financial support (30,000 JPY per month) for female undergraduate students who need housing in the city of Tokyo.

Apart from the undergraduate entrance examination for Japanese students, we also have entrance examination for foreign students, evaluating by GRE (Physics), undergraduate scores, and TOEFL. Every year, a few foreign students enter our course by this system.

Table 3.1: The numbers of students who graduated

Academic Year	2013	2014	2015	2016	2017	2018
Undergraduate	9 (2)	9 (1)	9 (0)	10 (0)	9 (2)	9 (3)
Graduate (Master)						
<i>Japanese</i>	24 (0)	18 (2)	18 (5)	16 (2)	17 (1)	18 (3)
<i>Foreign</i>	1 (0)	2 (1)	3 (0)	0 (0)	3 (0)	5 (0)
<i>Total</i>	25	20	21	16	20	23
Graduate (PhD)						
<i>Japanese</i>	12 (2)	9 (0)	8 (4)	14 (0)	8 (0)	7 (2)
<i>Foreign</i>	1 (0)	0 (0)	1 (0)	1 (0)	2 (1)	3 (0)
<i>Total</i>	13	9	9	15	10	10

Note: the numbers in parentheses are those of female students.

Table 3.2: The number of PhD students with JSPS fellowship

Academic Year	2013	2014	2015	2016	2017	2018
Total number of PhD students	42	48	49	44	35	35
Number of PhD students with JSPS fellowship	17	19	18	19	14	12

Table 3.3: Career paths after graduation

Academic Year	2013	2014	2015	2016	2017	2018
Undergraduate students						
<i>Graduate schools</i>	8	9	9	10	9	9
<i>Companies</i>	0	0	0	0	0	0
Graduate students (Master)						
<i>PhD courses</i>	18	13	14	10	10	15
<i>Companies</i>	7	7	6	5	10	7
<i>Academic institutes</i>	0	0	0	0	0	0
Graduate students (PhD)						
<i>Companies</i>	2	3	9	8	2	3
<i>Academic institutes</i>	10	7	5	9	7	5

3.2 Financial Support

Table 3.2 shows the number of the JSPS (Japan Society for Promotion of Science) research fellows in the doctor course in 2013–2018 together with the number of the doctor course students. PhD course students in Japan can apply for the JSPS fellow, and selection is based on evaluation of their research achievement and research plan. If a student fails to get this fellowship, she/he can apply again next year during the PhD course. If they get the fellowship, they receive stipend (about 200,000 JPY per month) as well as the research grant (about 900,000 JPY per year), which support their research efficiently. On average nearly half of PhD students become JSPS research fellows. This number can be compared with the nation-wide average; 19% of applicants get the fellowship every year.

A fraction of master and PhD students enroll the International Graduate Program for Excellence (IGPE) in Earth-Space Science and that for Photon Science in the University of Tokyo. Especially promising foreign students may get a pass to the Global Science Graduate Course (GSGC) of the School of Science, or they may get the MEXT (Ministry of Education, Culture, Sports, and Science and Technology of Japan) scholarships. Students who get enrolled at these programs receive stipend of a similar amount to JSPS fellows.

Those who could not get the JSPS or IGPE fellowships are financially supported by the University of Tokyo as research and teaching assistants, which amounts to about a half of their tuition fees.

Interest-free scholarships can be loaned to most students who wish from the Japan Student Services Organization (JASSO). Return of the loan is exempted for a small fraction of students with an excellent research achievement.

3.3 Paths after Graduation

Table 3.3 shows the statistics of the paths after graduation in 2013–2018. Practically all undergraduate students go to a graduate course of an university. About 90% of them go to the Department of of Astronomy in the University of Tokyo. About half of master degree students go to the doctor course, whereas the other half quit astronomy and go to companies. More than 50% of students who graduated the doctor course continue astronomy as post-docs either in Japan or abroad.

3.4 Lectures for undergraduate students

Here is the list of the lectures given to the undergraduate students of DoA (3rd and 4th year students). This lists include only the lecturers given by DoA. In addition to these lectures, DoA students need to take lectures on basic physics (e.g., quantum physics) given by Department of Physics.

Subject ID	Subject name	Units	Term	Grade	Lecturer
0520013	Extragalactic Astronomy	2	summer	3,4	Kazuhiro Shimasaku and Nobunari Kashikawa
Lecture on fundamental properties of galaxies and large-scale structure, the standard theory of galaxy formation, and observations of distant galaxies.					
0520015	Astronomical Observation Technique	2	summer	3,4	Mamoru Doi and Takashi Miyata
Lecture on telescopes, instruments, optical and infrared detectors, data processing, and related techniques for astronomical observations.					
0520021	Stellar Evolution	2	summer	4	Hideyuki Umeda
Lecture on stellar evolution, supernova explosion, gamma-ray bursts, stellar nucleosynthesis, as well as recent topics on these research fields.					
0520022	Cosmology	2	summer	4	Tomonori Totani
Lecture on the basic principles, applications, and the current status of cosmology and structure formation.					
0520028	Topical Study in Astronomy and Astrophysics I	3	~ 20 days	4	All academic staff
Students will study a specific topic in various fields of astronomy.					
0520029	Topical Study in Astronomy and Astrophysics II	3	~ 20 days	4	All academic staff
Students will study a specific topic in various fields of astronomy.					
0520031	Computational Astronomy I	2	summer	3,4	Michiko Fujii
Introductory lectures and exercises on numerical analyses with computers using problems related to astronomy.					
0520033	Radiative Processes in Astrophysics I	2	autumn	3,4	Masuo Tanaka
Lecture on basic radiative processes in astrophysics for appropriate handling of astronomical data.					
0520034	Exercise in Astrophysics II	2	summer	3,4	Fumi Egusa
The purpose of this class is, by solving problems, to understand and master the basics in quantum mechanics, statistical physics, classical mechanics, and electromagnetism which are closely related to astronomy.					
0520036	Radiative Processes in Astrophysics II	2	autumn	4	Toshikazu Shigeyama
Lecture on radiation mechanisms and radiation from supernovae, supernova remnants, pulsars, galaxies and clusters of galaxies.					
0520038	Textbook Reading	2	autumn	3,4	Itsuki Sakon and Bunyo Hatsukade
Students will learn basic ways of thinking, presentation, and communication in astronomy by reading English textbooks and papers in turn.					
0520040	Practice in Astronomical Experiments	2	summer	3,4	All academic staff
Through experiments of analog circuits and optics, students will understand basic technologies used in observational astronomy.					
0520041	Practice in Astronomical Observations	4	~ 15 days	3,4	All academic staff
By using observational devices and/or facilities, students will learn basic methods of astronomical observations and data analysis.					
0520042	Positional Astronomy and Celestial Mechanics	2	summer	3,4	Makoto Yoshikawa
Lecture on the basics of positional astronomy and celestial mechanics.					
0520043	Interstellar Physics I	2	summer	4	Yuri Aikawa and Masuo Tanaka
Lecture on the properties of interstellar matter in various phases in our Galaxy primarily based on optical and infrared observations.					

Subject ID	Subject name	Units	Term	Grade	Lecturer
0520044	Interstellar Physics II	2	summer	4	Kotaro Kohno and Kentaro Motohara
Lecture on the basics and methodology of interstellar physics using optical to submillimeter data of galaxies at various cosmic times.					
0520045	Exoplanets	2	summer	4	Masahiro Ikoma and Yuri Aikawa
Lecture on the basis of theories and observation of exoplanet studies.					
0520046	Solar and Stellar Physics	2	autumn	3,4	Takaaki Yokoyama, Takashi Sekii, and Hirohisa Hara
Lecture on the basics and methodology of solar physics and physical processes occurring inside and on the surface of the Sun and stars.					
0520801	Research Ethics	0.5	summer	3,4	Nobunari Kashikawa
Lecture on best research practices, research funding, refereeing, compliance with laws and regulations, authorship, dual publication, conflict of interest, and research misconduct.					

3.5 Lectures for graduate students

In addition to the basic credits given to the research activities of students for master and doctor theses under supervision of their advisors, we provide lecture series to educate basic knowledge on various topics in astronomy. Subjects and lecturers change every year. A fraction of lectures are given by guest lecturers outside the Department of Astronomy. Here is the list of lecture series in the latest three years.

Lecture Subjects of Year 2019—Department of Astronomy, Graduate School of Science

Subject	Lecturer	Contents
Celestial Mechanics, Advanced Course V	Eiichiro Kokubo	Lecture overviews the basic dynamics that are important to understand the structure, formation, and evolution of planetary systems. The subjects include, two-body problem, three-body problem, Hill problem, many-body problem, orbital resonances, orbital stability, tidal evolution, planetary accretion, planetary rings etc.
Optical Infrared Astronomy, Advanced Course I	Kouichi Kataza	Lecture overviews of the basic concepts observations in the infrared astronomy. Various effects which limit the real observations is discussed to help planning new observation projects. Technologies for optics and detectors is reviewed to understand more deeply about the limits of observation.
Theoretical Astrophysics, Advanced Course I	Hideyuki Umeda	Lecture describes how the formations of Supermassive Blackholes and Blackhole binaries can be understood in the theories of primordial Pop III star formation and evolution.
Solar Physics, Advanced Course V	Yukio Katsukawa	Lectures on diagnostics of solar and stellar magnetic fields using polarization measurements. Basic principles of polarized radiation from magnetized atmosphere as well as techniques to measure the polarized light are introduced. Recent progresses of solar magnetic fields are also covered.
Radio Astronomy, Advanced Course II	Takeshi Okuda	Lecture on basic knowledge of radio astronomical observations by understanding not only radio telescopes and radio astronomical instruments but also observing systems and observational methods of radio sign-dish telescopes and radio interferometers.
Extragalactic Astronomy, Advanced Course V	Kazuhiro Shimasaku	Lecture on the basics of optical observations, galaxies, and galaxy evolution.
Stellar Physics, Advanced Course IV	Masuo Tanaka	Lecture on basic radiative processes in astrophysics for appropriate handling of astronomical data.
Interstellar Physics, Advanced Course I	Fumitaka Nakamura	Lecture on the physical properties of interstellar medium and their role in process of star formation.
High Energy Astronomy, Advanced Course I	Hiroya Yamaguchi	Lecture overviews various high-energy phenomena in the Universe by referring to real observational data as needed. The lecture also covers the physics of X-ray/gamma-ray detectors and the theory of radiative processes.
Exoplanets, Advanced Course I	Masahiro Ikoma and Yuri Aikawa	Lecture on the basics of theories of exoplanet studies.
Exoplanets, Advanced Course II	Motohide Tamura and Yasushi Suto	Lecture on the basics of observations of exoplanet studies.
Gravitational-wave Physics	Kipp Cannon and Raffaele Flaminio	Lecture on the method of operation of gravitational-wave detectors, astrophysical sources of gravitational waves, and the techniques used to identify and study the signals.
English for Scientific Reser- chers I	Peter Maksym	Lecture on how to communicate scientific results effectively, how scientists communicate and how to distinguish good and bad style.

Subject	Lecturer	Contents
Observational Astronomy, Advanced Course I	Sigeru Yoshida	Lecture on the mechanisms of cosmic neutrino productions in energy range from TeV to EeV, and their implications to the yet-unknown origin of cosmic rays.
Theoretical Astronomy, Ad- vanced Course VII	Masaomi Tanaka	Lecture on theory and observations of explosive transients in the Universe.
Theoretical Astronomy, Ad- vanced Course VIII	Wakako Ishibashi	Lecture on black hole, active galactic nuclei, and accretion disks.

Lecture Subjects of Year 2018—Department of Astronomy, Graduate School of Science

Subject	Lecturer	Contents
Optical Infrared Astronomy, Advanced Course III	Naruhisa Takato	Lecture on Adaptive Optics. Overview various atmospheric effects on optical-IR astronomical observations, focusing on a basic theoretical model of wave propagation through turbulent medium and imaging through the atmosphere.
Theoretical Astrophysics, Advanced Course III	Tomonori Totani	Lecture on Cosmic Background Radiation and Global Distribution of Energy in the Cosmos.
Solar Physics, Advanced Course II	Takashi Sekii	Lecture on helioseismology as an observational tool to investigate the interiors of the Sun, to study its internal structure and dynamical processes.
Radio Astronomy, Advanced Course V	Nagayoshi Ohashi	Lecture on how star-planet system like our solar system is formed, based on results of observational research including those conducted recently.
Extragalactic Astronomy, Advanced Course IV	Masami Ouchi	Lecture on the framework of galaxy formation, dark-matter halo and star formation, in the Big Bang Universe, and then review pictures of galaxy formation history based on the latest deep observations.
Stellar Physics, Advanced Course II	Toshikazu Shigeyama	Lecture on special-relativistic fluid mechanics, shock, and gamma-ray burst.
Stellar Physics, Advanced Course IV	Masuo Tanaka	Lecture on basic radiative processes in astrophysics for appropriate handling of astronomical data.
Interstellar Physics, Advanced Course IV	Masato Tsuboi	Lecture on interstellar physics of the galaxy by radio observations.
High Energy Astronomy, Advanced Course V	Takehiro Mihara	Lecture on x-ray astronomy : all-sky x-ray monitoring from international space station.
Exoplanets, Advanced Course I	Yuri Aikawa, Masahiro Ikoma and Yasushi Suto	Lecture on the basics of theories of exoplanet studies.
Exoplanets, Advanced Course II	Yuri Aikawa, Masahiro Ikoma and Yasushi Suto	Lecture on the basics of observations of exoplanet studies.
Gravitational-wave Physics	Kipp Cannon and Raffaele Flaminio	Lecture on the method of operation of gravitational-wave detectors, astrophysical sources of gravitational waves, and the techniques used to identify and study the signals.
English for Scientific Researchers I	Peter Maksym	Lecture on how to communicate scientific results effectively, how scientists communicate and how to distinguish good and bad style.
Theoretical Astronomy, Advanced Course VI	Michael Famiano	Lecture provides an introduction to the application of fundamental principles of the production of atomic nuclei along the cosmic evolution. An emphasis will be placed on, first, the formation processes of the elements and, second, the molecules of life, i.e. the amino acids, in various astrophysical conditions in space from a perspective of fundamental interactions of elementary particles and nuclei.

Lecture Subjects of Year 2017—Department of Astronomy, Graduate School of Science

Subject	Lecturer	Contents
Celestial Mechanics, Advanced Course III	Toshio Fukushima	Lecture on the basic part of astrometry and celestial mechanics within the general relativistic framework, focusing on the equation of motion of photon and masspoints and their approximate solutions.
Optical Infrared Astronomy, Advanced Course V	Kentaro Motohara	Lecture on instrumentation, element technologies, and their background concepts used in for the observations in the optical-infrared wavelength.
Theoretical Astrophysics, Advanced Course IV	Takeru Suzuki	Lecture on mass and energy transfer processes in astrophysics based on hydro- and magnetohydrodynamics.
Solar Physics, Advanced Course IV	Taro Sakao	Lecture on observations of flares, production of radiation and particles in flares, mechanisms of flare formation, plasma phenomena, and influences on the interplanetary space.
Radio Astronomy, Advanced Course I	Hideyuki Kobayashi	Lecture on the radio telescope and observation equipment system, including the future plan.
Extragalactic Astronomy, Advanced Course III	Mamoru Doi	Lecture on the basics of optical-infrared astronomy, observational cosmology, galaxies and supernovae, especially as the standard candles.
Stellar Physics, Advanced Course IV	Masuo Tanaka	Lecture on basic radiative processes in astrophysics for appropriate handling of astronomical data.
Interstellar Physics, Advanced Course II	Takashi Onaka	Lecture on the basic properties of solid particles in the Universe based on observations and theories.
Exoplanets, Advanced Course I	Motohide Tamura, Masahiro Ikoma and Yasushi Suto	Lecture on the basics of theories of exoplanet studies.
Exoplanets, Advanced Course II	Motohide Tamura, Masahiro Ikoma and Yasushi Suto	Lecture on the basics of observations of exoplanet studies.
Gravitational-wave Physics	Kipp Cannon and Raffaele Flaminio	Lecture on the method of operation of gravitational-wave detectors, astrophysical sources of gravitational waves, and the techniques used to identify and study the signals.
English for Scientific Reser- chers I	Hiroaki Aihara	Lecture on how to communicate scientific results in English and to effectively communicate with non-Japanese speaking researchers.
Observational Astronomy, Advanced Course VII	Aurora Simionescu	Lecture on the evolution of the universe, from the near-uniform matter distribution implied by the cosmic microwave background to present-day galaxies, clusters of galaxies, and the cosmic web. The lecture also cover the dynamics of the homogeneous, expanding universe, then discuss simple models of spherical collapse leading up to the formation of the first stars, galaxies, and hierarchical growth of structure.
Observational Astronomy, Advanced Course VIII	Matthew W Johns	Lecture on the conceptualization and development of modern ground-based optical telescopes. The emphasis will be on technical development but some program management details will be included. Subjects to be covered include project planning and structure, systems engineering, project phases, and key issues in telescope and facility design and construction.

Subject	Lecturer	Contents
Theoretical Astronomy, Advanced Course III	Kentaro Nagamine	Lecture the basics of modern cosmology that is based on the general relativity theory. The lecture includes how the current concordance cosmological model was established by the physical theories and astronomical observations, through discussions on the following topics: Friedmann models, Big Bang universe, thermal history of the Universe, cosmological perturbation theory, nonlinear structure formation, galaxy clustering, cosmological simulations, high-redshift universe, dark matter, etc.
Theoretical Astronomy, Advanced Course IV	Yamac Deliduman	Lecture aims to give an introduction to the neutrinos as important astrophysical messengers and as key participants in various astrophysical processes.

3.6 Recent master and doctor theses

Here we list the master and PhD theses in the recent three years.

Master thesis defended in 2019

氏名 (Name)	指導教員 (Adviser)	論文題目 (Title)
金岡 慧 KANAOKA Satoru	梅田 秀之 UMEDA Hideyuki	バリオンの超音速流による初代星の星団形成 Formation of the first stellar clusters by baryon supersonic flow
有馬 宣明 ARIMA Noriaki	土居 守 DOI Mamoru	スペクトル分類に基づいた Ia 型超新星の多様性を探る研究 Research on diversity of type Ia supernova based on spectral classification
石塚 典義 ISHIDUKA Noriyoshi	原 弘久 HARA Hirohisa	太陽フレア中のプラズモイドの成長過程に関する観測的研究 Observational study on the growth process of plasmoids in solar flares
柏田 祐樹 KASHIWADA Yuki	郷田 直輝 GODA Naoteru	太陽運動の解析における星の速度分散の効果の定量評価 Quantitative evaluation of the effect of stellar velocity dispersion in solar motion analysis
菊地原 正太郎 KIKUCHIHARA Shotaro	大内 正己 OUCHI Masami	重力レンズ効果と可視・近赤外深撮像観測で探る形成初期の低質量銀河の性質 Properties of low-mass galaxies in the early stages of formation explored by near-infrared deep imaging and gravitational lens
桑原 滉 KUWABARA Ko	鈴木 建 SUZUKI Kakeru	原始惑星系円盤中における磁気駆動円盤風のダスト成長への影響 Effects of magnetically driven disk wind on dust growth in protoplanetary disks
河野 志洋 KOHNO Yukihiro	本原 顕太郎 MOTOHARA Kentaro	近赤外線面分光装置 SWIMS-IFU の開発 Development of near infrared integral field spectrometer SWIMS-IFU
小島 悠人 KOJIMA Yuto	小林 尚人 KOBAYASHI Naoto	木曾超広視野高速 CMOS カメラの性能評価及び高速移動する地球接近天体の広視野探査 Performance evaluation of Kiso ultra-wide-field high-speed CMOS camera and wide-field exploration of fast-moving objects approaching the Earth
財前 真理 ZAIZEN Masamichi	梅田 秀之 UMEDA Hideyuki	Failed supernovae の高密度環境下でのニュートリノ集団振動とその観測への影響 Neutrino collective oscillations in the high-density environments in Failed supernovae and their effects on observations
佐藤 一樹 SATO Kazuki	阪本 成一 SAKAMOTO Seiichu	野辺山 45m 電波望遠鏡を用いた銀河系内域のホットコア無バイアスサーベイ An unbiased survey of hot cores in the inner Galaxy with the Nobeyama 45m radio telescope
下向 怜歩 SHIMOMUKAI Reiho	海老沢 研 EBISAWA Ken	成層圏気球 VLBI 観測の実現に向けた地上実験 Ground-based experiment for realization of stratospheric balloon VLBI observation
武井 勇樹 TAKEI Yuki	茂山 俊和 SHIGEYAMA Toshikazu	星周物質との衝突による相互作用によって光る超新星における光度曲線の研究 A study of light curves of supernovae that shine by collisions with circumstellar matter
谷本 悠太	柏川 伸成	若いランジット惑星候補を伴う PTFO 8-8695 の可視赤外同時観測による減光イベントの起源の探究

TANIMOTO Yuta	KASHIKAWA Nobunari	Identifying the source of fading events of PTFO 8-8695 with a young transiting planet candidate by simultaneous optical and infrared observations
陳 家偉 CHIN Kaul	川邊 良平 KAWABE Ryohei	超広帯域ミリ波サブミリ波多色カメラに向けたオンチップフィルター開発 Development of on-chip filter for ultra-wideband millimeter-wave submillimeter-wave multicolor camera
寺田 由佳 TERADA Yuka	田村 元秀 TAMURA Motohide	ヘイズの存在が期待されるウォームジュピター WASP-80b の大気観測 Atmospheric observation of WASP-80b, a warm jupiter that is expected to have haze
長谷川 大空 HASEGAWA Taku	藤井 通子 FUJII Michiko	星団形成期の周囲の星による星周円盤の破壊 Destruction of circumstellar disks by surrounding stars during star cluster formation
山下 祐依 YAMASHITA Yui	河野 孝太郎 KOHNO Kotaro	Swift 衛星で選択された近傍超臨界降着活動銀河核の低温分子ガスに関する観測的研究 Observational study on cold molecular gas in nearby supercritical active galactic nuclei selected by Swift satellite
吉田 泰 YOSHIDA Yutaka	宮田 隆志 MIYATA Takashi	Mon R2 IRS3 の近赤外線変光観測と TAO/MIMIZUKU 用天体導入プログラムの開発 Near-infrared observation of Mon R2 IRS3 and development of guiding program for TAO/MIMIZUKU
李 建鋒 LI Kenho	河野 孝太郎 KOHNO Kotaro	HSC で選択された赤方偏移 4-6 のクェーサーにおける強電波比率とその赤方偏移および光度への依存性 The radio-loud fraction of z 4-6 HSC-selected quasars and its dependences on redshift and luminosity
郭 康柔 GUO Kangrou	小久保英一郎 KOKUBO Eiichiro	連星系における微惑星の軌道進化 Planetesimal Dynamics in the Presence of a Massive Companion
李 秀珍 EIE Sujin	本間希樹 HONMA Mareki	マグネターアウトバーストの電波域での観測的研究 : XTE J1810-197 の再活性化 Observational Study of Magnetar Outburst in the Radio Bands: Re-activation of XTE J1810-197

Master thesis defended in 2018

氏名 (Name)	指導教員 (Adviser)	論文題目 (Title)
安藤 亮 ANDO Ryo	河野孝太郎 KOHNO Kotaro	輝線と吸収線で探る紫外線に照らされた星間ガスの多様な分子化学組成 Diverse chemical compositions of UV-irradiated interstellar molecular gas investigated with emission and absorption line observations
黒瀬 一平 KUROSE Ipppei	相川祐理 AIKAWA Yuri	ALMA による原始星 L1448-mm の星周構造の観測 Observation of the circumstellar structure of the protostar L1448-mm by ALMA
辰馬 未沙子 TATSUUMA Misako	小久保英一郎 KOKUBO Eiichiro	原始惑星系円盤中の多孔質ケイ酸塩ダスト集合体で構成されるダスト層の重力不安定性 Gravitational Instability of a Dust Layer Composed of Porous Silicate Dust Aggregates in a Protoplanetary Disk
石田 剛	河野孝太郎	重力レンズ効果の高解像像復元と高赤方偏移爆発的星形成銀河の観測的研究

ISHIDA Tsuyoshi	KOHNO Kotaro	High resolution reconstruction of the gravitational lensing effect and observational study of high-redshift starburst galaxies
一木 真 ICHIKI Makoto	土居 守 DOI Mamoru	可視高速周期変動天体探査のための Crab パルサーの試験観測 Test observation of Crab pulsar for exploration of visible high-frequency periodic celestial bodies
猪岡 皓太 INOOKA Kota	山下卓也 YAMASHITA Takuya	木曾広視野 CMOS カメラによるふたご座領域の高速撮像サーベイ High-speed imaging survey of Gemini region with Kiso wide-field CMOS camera
入倉 和志 IRIKURA Kazushi	嶋作一大 SHIMASAKU Kazuhiro	原始銀河団探査における新手法の開発 Development of a new method to search for proto-clusters
大澤 健太郎 OSAWA Kentaro	田中培生 TANAKA Masuo	miniTAO/ANIR の観測に基づく Wolf-Rayet 星の星風モデルの研究 Study on the stellar wind model of Wolf-Rayet stars based on miniTAO / ANIR observations
大橋 宗史 OHASHI Fumihiro	本原顕太郎 MOTOHARA Kentaro	LIRG の空間分解した星形成活動 Spatially resolved observation of star-formation activities in LIRG
木下 聖也 KINOSHITA Seiya	海老沢研 EBISAWA Ken	すざく衛星の観測中に偶然発見された X 線変動天体の研究 Study of X-ray variable objects serendipitously discovered by Suzaku satellite
木村 智幸 KIMURA Tomoyuki	尾中 敬 ONAKA Takashi	赤外線分光に基づく大質量星形成領域におけるダストの観測的研究 Observational study of the dust species in a massive star-forming region based on infrared spectroscopy
崔 仁士 SAI Jinshi	大橋永芳 OHASHI Nagayoshi	ALMA による Class I 原始星 L1489 IRS の観測的研究 Observational studies of Class I protostar L1489 IRS using ALMA
須藤 貴弘 SUDO Takahiro	戸谷友則 TOTANI Tomonori	宇宙論の未解明問題と銀河形成—宇宙定数と高エネルギーニュートリノ Galaxy Formation and Unsolved Problems in Cosmology: the Cosmological Constant and Very High Energy Neutrinos
田中 祐輔 TANAKA Yusuke	田村元秀 TAMURA Motohide	すばる望遠鏡 Hyper Suprime Cam を用いた超低質量星探査 Exploration of ultra-low-mass stars with the Subaru Telescope Hyper Suprime Cam
森 寛治 MORI Kanji	梶野敏貴 KAJINO Toshitaka	炭素融合反応に対する量子力学的制限と Ia 型超新星へのインパクト Quantum Mechanical Constraint on Carbon Fusion Reaction and Its Impact on Type Ia Supernovae
山口 淳平 YAMAGUCHI Junpei	宮田隆志 MIYATA Takashi	中間赤外線観測装置 MIMIZUKU における検出器システムの性能評価 Performance evaluation of detector system of mid-infrared observational instrument MIMIZUKU
山口 正行 YAMAGUCHI Masayuki	川邊良平 KAWABE Ryohei	スパースモデリングによる原始惑星系円盤 HD 142527 の超解像イメージング Super-resolution imaging of the protoplanetary disk HD 142527 by sparse modeling
DE LEON Jerome Pitogo	田村元秀	低密度ホットジュピターに対する多色同時トランジット観測

	TAMURA Motohide	Multi-color Simultaneous Transit Observations of Low Density Hot Jupiters
HILMI Miftahul	大内正己 OUCHI Masami	赤方偏移 $z = 3.8 - 5.0$ における星形成銀河の電離光子生成効率：宇宙再電離への示唆 Ionizing Photon Production Efficiency of Star-Forming Galaxies at $z = 3.8 - 5.0$: Implications for Cosmic Reionization
JIAN Mingjie	田村元秀 TAMURA Motohide	近赤外線高分散スペクトル中の吸収線強度比に基づく恒星物理量指標 Line-depth ratios as indicators of stellar parameters in near-infrared high-resolution spectra
LIN Haoxiang	戸谷友則 TOTANI Tomonori	連星中性子星合体 GW170817 からの非熱的放射の物理 Physics of Non-thermal Emission from the Binary Neutron Star Merger GW170817
LUO Yudong	中村文隆 NAKAMURA Fumitaka	宇宙磁場揺らぎに起因する粒子の非マクスウェル分布とビッグバン元素合成への影響 Fluctuating Cosmic Magnetic Field, Non-Maxwellian distribution, and Impact on Big-Bang Nucleosynthesis

Master thesis defended in 2017

氏名 (Name)	指導教員 (Adviser)	論文題目 (Title)
池内綾人 IKEUCHI Ayato	尾中敬 ONAKA Takashi	あかり、スピッツァー、ハーシェル宇宙望遠鏡の観測に基づくヒクソン・コンパクト銀河群のダストの性質 Dust Properties of Hickson Compact Groups Revealed by AKARI, Spitzer and Herschel Observations
石川聡一 ISHIKAWA Soichi	坪井昌人 TSUBOI Masato	銀河系中心領域の ALMA による観測：SgrA* とミニスパイラルのサブミリ波スペクトル ALMA observation of the Galactic Center: Submillimeter spectrum of SgrA* and mini spiral
石塚将斗 ISHIDUKA Masato	田村元秀 TAMURA Motohide	すばる望遠鏡用ドップラー法赤外線分光器 IRD のためのファイバーモードスクランブラー試験 Fiber mode scrambler experiments for the Subaru Infrared Doppler Instrument (IRD)
岡村拓 OKAMURA Taku	嶋作一大 SHIMASAKU Kazuhiro	高赤方偏移における銀河ディスクの角運動量進化 Angular momentum evolution of stellar discs at high redshifts
楠絵莉子 KUSUNOKI Eriko	海老沢研 EBISAWA Ken	セイファート銀河が示す広帯域 X 線スペクトル変動の統一的な解釈 Unified interpretation of broadband X-ray spectrum of Seyfert galaxies
酒井伊織 SAKAI Iori	小林行泰 KOBAYASHI Yukiyasu	α 線を用いた Nano-JASMINE 搭載用 CCD の放射線耐性実験 Experiments on radiation resistance of CCD for Nano-JASMINE using α -ray
佐々木宏和 SASAKI Hirokazu	梶野敏貴 KAJINO Toshitaka	ニュートリノ集団振動と超新星における元素合成への応用 Collective neutrino flavor oscillations and application to supernova nucleosynthesis
谷口由貴 TANIGUCHI Yuki	土居守 DOI Mamoru	活動銀河核における低質量ブラックホールの可視光度変動タイムスケール Optical Variability Timescale of Low-mass Black Holes in Active Galactic Nuclei
寺尾恭範	本原顕太郎	近赤外線 2 色同時多天体分光撮像装置 SWIMS の検出器システム開発

TERAO Yasunori	MOTOHARA Kentaro	Development of detector system for the near infrared two-color simultaneous multi-object spectral imaging device SWIMS
野田和弘 NODA Kazuhro	茂山俊和 SHIGEYAMA Toshikazu	Ia 型超新星を生き延びた伴星の理論モデル Theoretical model of companion star surviving type Ia supernova
藤井善範 FUJII Yoshinori	FLAINIO Raffaele	KAGRA における低周波防振装置の開発、及び重力波検出器による階層的な検出ネットワークを用いた連星合体の方向特定に関する研究 Development of a low frequency vibration isolation system for KAGRA, and study of the localization of coalescing binaries with a hierarchical network of gravitational wave detectors
藤田彩豊 FUJITA Ayato	郷田直輝 GODA Naoteru	銀河系回転や太陽運動の解析に及ぼす軌道共鳴の影響 Effect of orbital resonance on analysis of galaxy rotation and solar motion
藤本空 FUJIMOTO Sora	梅田秀之 UMEDA Hideyuki	電子陽電子対生成型超新星のニュートリノスペクトル Neutrino spectrum of electron-positron pair-generating supernovae
向江志朗 MUKAE Shiro	大内正己 OUCHI Masami	可視・近赤外線探査に基づく赤方偏移 2-3 の銀河-銀河間物質関係の研究 Connection between Galaxy and Inter-Galactic Medium at $z \sim 2 - 3$ Studied by Optical and Near-Infrared Observations
毛利清 MOURI Kiyoshi	宮田隆志 MIYATA Takashi	次世代中間赤外線装置における低温チョッピング実現に向けた超伝導リニアモーターの開発 Development of a superconducting linear motor for realizing low-temperature chopping in next-generation mid-infrared devices
山崎 翔太郎 YAMASAKI Shotaro	戸谷友則 TOTANI Tomonori	フェルミガンマ線サーベイと連星中性子星合体シミュレーションで探る高速電波バーストの起源 Probing the Origin of Fast Radio Bursts by Fermi Gamma-ray Survey and Simulations of Binary Neutron Star Mergers
FENG Chien-Chang	梅田秀之 UMEDA Hideyuki	ブラックホール形成時の重力エネルギー損失による弱い超新星爆発 Weak Supernovae Induced by the Gravitational Energy Loss in the Black Hole Formation
ZHANG Jin	尾中敬 ONAKA Takashi	あかり衛星による大マゼラン雲の近赤外線分光サーベイの研究 A Study of the Near-infrared Spectroscopic Survey of the Large Magellanic Cloud Based on Observations with AKARI

PhD thesis defended in 2019

氏名 (Name)	指導教員 (Adviser)	論文題目 (Title)
上原 顕太 UEHARA Kenta	坪井昌人 TSUBOI Masato	銀河系中心星形成分子雲における多重構造の性質に関する統計的研究 Statistical Study on the Properties of Multi-Structures in Star-Forming Molecular Clouds of the Galactic Center
MARCHIO Manuel	FLAMINIO Raffaele	KAGRA サファイア鏡及び新たな高反射性結晶コーティングの評価のための光吸収測定システムの開発 Development of an optical absorption measurement system to characterize KAGRA sapphire mirrors and new high-reflectivity crystalline coatings

LIVINGSTON John Henry	田村元秀 TAMURA Motohide	地上及び宇宙観測による K2 惑星の発見とキャラクター化 Discovery and characterization of K2 planets from the ground and space
内山 允史 UCHIYAMA Masahito	宮田隆志 MIYATA Takashi	中間赤外線高精度モニタ観測に向けた二視野合成機構 フィールドスタッカーの開発 Development of a two-field combining device "Field Stacker" for accurate monitoring observations at mid-infrared wavelengths
鷗山 太智 UYAMA Taichi	田村元秀 TAMURA Motohide	若い惑星の直接撮像と特徴付け Direct Imaging and Characterizations of Young Exoplanets
姜 継安 JIANG Jian	土居守 DOI Mamoru	(Ia 型超新星の早期測光観測とその解釈 The Early-phase Photometric Behavior of Type Ia Supernovae and Its Implications
日下部 晴香 KUSAKABE Haruka	嶋作一大 SHIMASAKU Kazuhiro	Ly α 輝線銀河の性質: 星形成率、星質量、ダークマターハロー質量 The nature of Ly α emitters: SFR, stellar mass, and dark matter halo mass
藤本 征史 FUJIMOTO Seiji	大内正己 OUCHI Masami	ALMA で探る冷たい宇宙: 星間及び銀河周辺物質から宇宙の構造までの統計研究 Demographics of the Cold Universe with ALMA: From Inter-Stellar and Circum-Galactic Media to Cosmic Structures
増山 美優 MASUYAMA Miyu	茂山俊和 SHIGEYAMA Toshikazu	マグネターが付随する超新星残骸の起源の理論的研究 Theoretical study on the origin of supernova remnants associated with magnetars
山口 裕貴 YAMAGUCHI Yuki	河野孝太郎 KOHNO Kotaro	ALMA 連続波天体の多波長解析と無バイアスマリ波輝線銀河探索に基づく宇宙星形成活動史の研究 Study of the cosmic star formation history based on a multi-wavelength analysis of ALMA continuum sources and an unbiased search of millimeter line emitters

PhD thesis defended in 2018

氏名 (Name)	指導教員 (Adviser)	論文題目 (Title)
李 民主 LEE Minju	川邊良平 KAWABE Ryohei	銀河団形成期における星形成銀河の性質および環境依存性に関する研究 The nature of star forming galaxies and environmental influence during cluster formation
漆畑 貴樹 URUSHIBATA Takaki	梅田秀之 UMEDA Hideyuki	恒星合体シナリオを基にした SN1987A の親星の数値モデル Numerical Models of the Progenitor Star of SN 1987A Based on the Stellar Merger Scenario
加藤 裕太 KATO Yuta	阪本成一 SAKAMOTO Seiichi	ハーシェル宇宙望遠鏡とアルマ望遠鏡で探る赤方偏移 2-3 原始銀河団における爆発的星形成銀河の研究 A Study of Dusty Star-Forming Galaxies in the z=2-3 Protoclusters with Herschel and ALMA
川俣 良太 KAWAMATA Ryota	嶋作一大 SHIMASAKU Kazuhiro	再電離期の銀河のサイズと光度および銀河形成へのそれらの示唆 The Size and Luminosity Distributions of Galaxies in the Reionization Era and Their Implications for Galaxy Formation
酒井 大裕	小林秀行	VERA による銀河系中心方向の VLBI アストロメトリに関する研究

SAKAI Daisuke	KOBAYASHI Hideyuki	Study of VLBI astrometry toward the Galactic center with VERA
谷口 暁星 TANIGUCHI Akio	河野孝太郎 KOHNO Kotaro	相関雑音除去に基づくミリ波サブミリ波分光のための周波数変調観測手法の開発 Development of a Frequency Modulation Observing Method for Millimeter and Submillimeter Wave Spectroscopy Based on Correlated Noise Removal
平居 悠 HIRAI Yutaka	梶野敏貴 KAJINO Takatoshi	矮小銀河の化学力学進化モデルによる重元素の化学進化の理解 Understanding the enrichment of heavy elements by the chemodynamical evolution models of dwarf galaxies
BELL Aaron Christopher	尾中敬 ONAKA Takashi	全天サーベイによる赤外線マイクロ波帯での星間ダスト放射の研究 Investigation of Interstellar Dust Emission in the Infrared-Microwave Range with All-sky Surveys
水本 岬希 MIZUMOTO Misaki	海老沢研 EBISAWA Ken	活動銀河核の鉄 K バンドにおける X 線スペクトルの変動性について On the X-ray spectral variability in the Fe-K band of active galactic nuclei
満田 和真 MITSUDA Kazuma	土居守 DOI Mamoru	表面測光で探る早期型銀河の運動学的性質の進化 Evolution of Kinematic Properties of Early-Type Galaxies Investigated by Surface Photometry

PhD thesis defended in 2017

氏名 (Name)	指導教員 (Adviser)	論文題目 (Title)
麻生 有佑 ASO Yusuke	大橋永芳 OHASHI Nagayoshi	ALMA を用いた星形成初期段階における円盤形成の研究 ALMA Observations Revealing Disk Formation in Early Phases of Star Formation
大橋 聡史 OHASHI Satoshi	阪本成一 SAKAMOTO Seiichi	巨大分子雲における分子雲コアの化学的物理的性質 The chemical and dynamical nature of dense cores in giant molecular clouds
北川 祐太朗 KITAGAWA Yutaro	本原顕太郎 MOTOHARA Kentaro	空間分解したスターバースト銀河研究のための近赤外線面分光ユニットの開発 The Development of a Near-Infrared Integral Field Unit for Spatially Resolved Studies of Starburst Galaxies
小久保 充 KOKUBO Mitsuru	土居守 DOI Mamoru	クエーサー降着円盤紫外可視域連続光放射の光度変動および偏光現象の研究 Variability and Polarization of the Ultraviolet-optical Continuum Emission of Quasar Accretion Disks
今野 彰 KONNO Akira	大内正己 OUCHI Masami	すばる望遠鏡ライマンアルファ輝線天体探査による銀河進化と宇宙再電離史の研究 Galaxy Evolution and Cosmic Reionization History Studied by Subaru Lyman α Emitter Surveys
斉藤 俊貴 SAITO Toshiki	川辺良平 KAWABE Ryohei	近傍高光度赤外線相互作用銀河の分子ガスの物理状態 Physical Conditions of Molecular Gas in Nearby Merging Luminous Infrared Galaxies
佐藤 裕史 SATO Yushi	蜂須泉 HACHISU Izumi	二重白色矮星連星合体の SPH シミュレーション: Ia 型超新星の親星としての検証 SPH simulations of mergers of double white dwarf binaries: Possible progenitors of Type Ia supernovae
佐野 圭	海老沢研	OBE/DIRBE により観測された近赤外線拡散放射の起源

SANO Kei	EBISAWA Ken	Origin of the Diffuse Near-Infrared Radiation Observed with COBE/DIRBE
柴垣 翔太 SHIBAGAKI Shota	梶野敏貴 KAJINO Toshitaka	磁気回転駆動型超新星爆発と極限天体環境における元素合成 Magneto-rotational core-collapse supernovae and nucleosynthesis in extreme astrophysical environments
関口 繁之 SEKIGUCHI Shigeyuki	関本裕太郎 SEKIMOTO Yutaro	マイクロ波力学的インダクタンス検出器用広視野・広帯域冷却光学系の開発 Development of Wide Field and Broadband Cryogenic Optics with Microwave Kinetic Inductance Detectors
高橋 亘 TAKAHASHI Ko	梅田秀之 UMEDA Hideyuki	大質量初代星の進化と元素合成 Evolution and nucleosynthesis of massive first stars
田川 寛通 TAGAWA Hiromichi	郷田直輝 GODA Naoteru	多重恒星質量ブラックホールの合体過程 The merger processes of multiple stellar-mass black holes

Chapter 4

Research Activities

4.1 Statistics

Table 4.1 shows statistics about research activities about publications and presentations in international conferences by the full-time faculty members in Department of Astronomy and Institute of Astronomy. For the complete lists of papers and presentations in conferences, please see the annual reports that can be downloaded from <http://www.astron.s.u-tokyo.ac.jp/en/about/annual-reports/>. In the annual report of 2018, paper lists are found in §1.6.1 英文報告 (DoA) and §2.6.1 英文報告 (IoA), and presentations in international meetings are found in §1.7.5 国際研究会 (DoA) and §2.7.4 国際研究会 (IoA). The format of the annual reports in other years is almost the same. In addition, as an indicator of international collaboration and exchange activities, the number of foreign visitors is also shown.

4.2 Competitive research funds

As an indicator of research activities, the lists of competitive research funds (mostly Grant-in-Aids from MEXT, Japan, i.e., KAKENHI) obtained by the full-time faculty members in Department of Astronomy and Institute of Astronomy are given in Table 4.2 and 4.3.

Table 4.1: Statistics about research activities by full-time faculties in DoA and IoA.

year	refereed papers	international conferences ^a	foreign guests ^b
2013	155	90	31
2014	162	76	31
2015	167	70	40
2016	206	68	37
2017	218	67	48
2018	247	75	47

^a All talks and posters presented in interenational meetings

^b Sum of guests from foreign countries or non-Japanese guests

Table 4.2: List of competitive funds obtained by the members of DoA. The types of *KAKENHI* (Grants-in-Aid from Japan Society for the Promotion of Science) are abbreviated or shortened as: *Kiban (S, A, B, C)* for Grant-in-Aid for Scientific Research, *Exploratory Research* for Grant-in-Aid for challenging Exploratory Research, *Innovative Areas* for Grant-in-Aid for Scientific Research Innovative Areas, *Joint International (A, B)* for Grant-in-Aid for Fostering Joint International Research (A, B), *Promoted Research* for Grant-in-Aid for Specially Promoted Research, and *Young (A, B)* for Grant-in-Aid for Young Scientists (A, B). The table also includes grants from other institutes such as National Astronomical Observatory of Japan (*NAOJ*) and Japan Aerospace Exploration Agency (*JAXA*). The total amount of each fund is given if the member is the PI, but the amount is not given otherwise.

Name	Year(s)	Type	Amount (JPY, given only if PI)
Totani	2018–2021	<i>KAKENHI–Kiban (C)</i> Evolution of the universe probed by fast radio bursts and gamma-ray bursts	2,800,000
Totani	2015–2017	<i>KAKENHI–Kiban (C)</i> Early universe probed by transient objects	2,300,000
Totani	2012–2016	<i>KAKENHI–Promoted Research</i> Extreme universe revealed by high energy gamma-rays	— <i>CoI</i> —
Totani	2011–2014	<i>KAKENHI–Young (A)</i> Study on dark energy by Subaru FMOS galaxy redshift survey	14,400,000
Tamura	2018–2022	<i>KAKENHI–Innovative Areas</i> Innovation of Infrared Observations of Young Planets and Habitable Planets	264,000,000
Tamura	2015–2019	<i>KAKENHI–Kiban (A)</i> Earth-like Planet Search on the Subaru Telescope	32,000,000
Tamura	2010–2014	<i>KAKENHI–Promoted Research</i> Development of Exoplanet Researches with New IR Technologies	396,900,000
Aikawa	2018–2022	<i>KAKENHI–Kiban (S)</i> Molecular composition and its evolution in the protoplanetary disk forming region	— <i>CoI</i> —
Aikawa	2019–2021	<i>NAOJ Grant (ALMA)</i> The Chemistry of Protoplanetary Disks	3,000,000
Aikawa	2016–2018	<i>KAKENHI–Exploratory Research</i> Theoretical challenge to astrobiology by computational science	2,600,000
Aikawa	2016–2017	<i>KAKENHI–Innovative Areas</i> Gas-grain chemistry in star and planetary system formation: molecular evolution and observational tracers of circumstellar structures	3,300,000
Kashikawa	2017–2020	<i>KAKENHI–Kiban (A)</i> Cosmic HydrOgen Reionization Unveiled with Subaru (CHORUS)	— <i>CoI</i> —
Kashikawa	2015–2018	<i>KAKENHI–Kiban (B)</i> Exploring the first black hole formation and cosmic reionization using high-z quasars	12,600,000

Table 4.2: —continued.

Name	Year(s)	Type	Amount (JPY, given only if PI)
Shimasaku	2019–2021	<i>KAKENHI–Kiban (C)</i> Evolution of cluster galaxies based on a systematic survey	2,100,000
Shimasaku	2017–2020	<i>KAKENHI–Kiban (A)</i> Cosmic HydrOgen Reionization Unveiled with Subaru (CHORUS)	— <i>CoI</i> —
Shimasaku	2016–2018	<i>KAKENHI–Kiban (C)</i> A comprehensive study of forming galaxies	2,800,000
Shimasaku	2011–2014	<i>KAKENHI–Kiban (A)</i>	11,800,000
Umeda	2017–2020	<i>KAKENHI–Kiban (C)</i> Exploring the evolution of rotating super-massive stars in the early universe	3,500,000
Umeda	2017–2020	<i>KAKENHI–Kiban (A)</i> Revealing a Universal mechanism for the formation of compact objects by the study of multi-dimensional evolution and explosion of massive stars	— <i>CoI</i> —
Umeda	2014–2018	<i>KAKENHI–Innovative Areas</i> Constructing comprehensive observation system of neutrinos from nearby celestial objects and research about celestial activities	— <i>CoI</i> —
Umeda	2014–2017	<i>KAKENHI–Kiban (C)</i> Developing data base of massive star evolution for the observational and theoretical studies of supernovae	— <i>CoI</i> —
Umeda	2014–2016	<i>KAKENHI–Kiban (C)</i> Revealing the evolution and fate of super massive stars as seeds of super massive blackholes	3,700,000
Umeda	2010–2013	<i>KAKENHI–Kiban (C)</i> Construction of progenitors of electron capture supernovae	2,800,000
Fujii	2019–2021	<i>KAKENHI–Kiban (B)</i> Study on the formation of binary black holes in star clusters using galaxy simulations	13,200,000
Fujii	2017–2021	<i>KAKENHI–Innovative Areas</i> Theoretical study on the formation scenario of binary black holes	— <i>CoI</i> —
Fujii	2015–2017	<i>KAKENHI–Kiban (B)</i> Planet formation simulation with 100 million particles using GPU clusters	— <i>CoI</i> —
Fujii	2014–2017	<i>KAKENHI–Young (B)</i> Star cluster formation in the Galactic disk and the origin of the variation of star clusters	2,900,000
Takata	2018–2020	<i>KAKENHI–Kiban (C)</i> Mystery of depressed dipolar modes of oscillation in red giants study based on the asymptotic theory	3,500,000
Takata	2014–2017	<i>KAKENHI–Kiban (C)</i> Study on the interaction between oscillation and rotation in stars based on rosette modes	3,600,000
Sakon	2019–2021	<i>KAKENHI–Kiban (C)</i> Understanding the process of dust formation by evolved stars based on infrared observation and experiment	3,400,000
Sakon	2018–2020	<i>KAKENHI–Kiban(C)</i> Study of evolution and processing of interstellar dust based on infrared satellite data	— <i>CoI</i> —
Sakon	2019	<i>JAXA Grant (International Joint Mission)</i> Completion of the Final Study Report on the Origins Space Telescope (Origins) / Mid-Infrared Spectrometer and Camera (MISC) for the US 2020 Decadal Survey	300,000
Sakon	2018	<i>JAXA Grant (International Joint Mission)</i> The Concept 2 Study of the Origins Space Telescope (OST) / Mid-Infrared Imager, Spectrometer, Coronagraph (MISC) for the US 2020 Decadal Survey	1,500,000

Table 4.2: —continued.

Name	Year(s)	Type	Amount (JPY, given only if PI)
		Properties of low-mass galaxies at cosmic noon	
Sakon	2016–2018	<i>KAKENHI—Young (A)</i> Challenges towards the understanding of the properties of interstellar dust based on experiments and observations	18,500,000
Sakon	2017–2018	<i>JSPS Bilateral Program (with DST, India)</i> Investigation of Interstellar Polycyclic Aromatic Hydrocarbons(PAHs), pure and substituted: a combined approach	1,920,000
Sakon	2017	<i>JAXA Grant (International Joint Mission)</i> The Study of the Origins Space Telescope (OST) / Mid-Infrared Imager, Spectrometer, Coronagraph (MISC) for the US 2020 Decadal Survey	1,500,000
Sakon	2016	<i>KAKENHI—Innovative Areas</i> New Frontiers of Extrasolar Planets: Exploring Terrestrial Planets	— CoI —
Sakon	2014–2015	<i>KAKENHI—Innovative Areas</i> Identification of the carriers of the unidentified infrared bands and the investigation of the effect of their deuteration on the infrared spectra	3,800,000
Sakon	2014–2015	<i>JSPS Bilateral Program (with DST, India)</i> Observational investigation of PAH and dust features in galactic and extra-galactic environments	2,000,000
Sakon	2011–2015	<i>KAKENHI—Innovative Areas</i> New Frontiers of Extrasolar Planets: Exploring Terrestrial Planets	— CoI —
Sakon	2011–2015	<i>KAKENHI—Innovative Areas</i> Direct imaging and spectroscopy of gas giants and detection of terrestrial planets	— CoI —
Matsunaga	2019–2022	<i>KAKENHI—Joint International (B)</i> Near-infrared spectroscopy to investigate the synthesis of neutron-capture elements in unexplored regions of the Galactic disk	12,900,000
Matsunaga	2018–2020	<i>KAKENHI—Kiban (B)</i> Study on evolutionary processes of the Galactic disk based on multi-dimensional data of Cepheid variable stars	12,200,000
Matsunaga	2016–2020	<i>KAKENHI—Promoted Research</i> Search for cold exoplanets and free-floating planets by near infrared gravitational microlensing observation	— CoI —
Matsunaga	2019	<i>NAOJ Grant (Supporting Universities)</i> Calibration and application of absorption lines by r-process elements in NIR YJ-bands	3,600,000
Matsunaga	2015–2016	<i>JSPS Bilateral Program (with NRF, South Africa)</i> Studies of the Milky Way galaxy	3,960,000
Matsunaga	2014–2017	<i>KAKENHI—Kiban (B)</i> Stellar abundance analysis based on near-infrared high-resolution spectra and applications to studies on the Milky Way	13,700,000
Matsunaga	2013	<i>NAOJ Grant (Supporting Universities)</i> Acceleration of stellar astronomy by combining large-scale variability search and spectroscopic follow-up observations	900,000
Matsunaga	2011–2014	<i>KAKENHI—Young (A)</i> Surveys and spectroscopic observations of Cepheid variable stars to reveal the Galactic structure and evolution	6,500,000

Table 4.3: The same as Table 4.2, but for IoA.

Name	Year(s)	Type	Amount (JPY, given only if PI)
Doi	2018–2022	<i>KAKENHI—Kiban (S)</i> Identifying the origin of the type-Ia supernova by observations just after the explosion	147,400,000
Doi	2016–2020	<i>KAKENHI—Kiban (S)</i> A Study of binary neutron star merger by high cadence optical observations	— <i>CoI</i> —
Doi	2018–2019	<i>KAKENHI—Innovative Area</i> Studying the progenitor of the type-Ia supernova by early phase observations with HSC	2,900,000
Doi	2016–2017	<i>KAKENHI—Innovative Area</i> Studying the progenitor of the type-Ia supernova with multi-band early phase photometry	1,700,000
Doi	2015–2016	<i>KAKENHI—Innovative Area</i> Identifying Gravitational Wave Sources and their Environments with Optical Simultaneous Imaging	4,600,000
Doi	2014–2016	<i>KAKENHI—Kiban (B)</i> Studying the environment of supernova explosion sites with narrow-band multi-color imaging	12,900,000
Doi	2014–2015	<i>KAKENHI—Innovative Area</i> A Study of Exo-planet Atmospheres by Optical High-precision Multi-band and Spectro Photometry	4,400,000
Doi	2011–2013	<i>KAKENHI—Kiban (B)</i> Mass Constraints for the Progenitor of the Core Collapse Supernova	14,000,000
Kohno	2017–2022	<i>NAOJ Grant (ALMA)</i> Study of dust-obscured activities in galaxies and their evolution	10,000,000
Kohno	2017–2021	<i>KAKENHI—Kiban (S)</i> Study of cosmic star formation history based on an unbiased survey of mm/submm-wave emission line galaxies	163,700,000
Kohno	2019	<i>NAOJ Grant (Co-development)</i> Development of optical filters for submillimeter-waves using flexible printed circuit technology	1,940,000
Kohno	2017	<i>KAKENHI—Kiban (A)</i> Study of growth process of dust-enshrouded super-massive blackholes	33,800,000
Kohno	2017	<i>NAOJ Grant (Co-development)</i> Development of a multi-chroic transition-edge sensor array	2,400,000
Kohno	2013–2016	<i>KAKENHI—Kiban (A)</i> Demonstration of on-chip low-dispersion ultra-wideband spectrograph for submm wavelengths using super-conducting resonators	32,300,000
Miyata	2013–2016	<i>KAKENHI—Kiban (A)</i> Pioneering study of mid infrared time domain astronomy by newly developed simultaneous observing system	29,200,000
Kobayashi	2019–2023	<i>KAKENHI—Joint International (B)</i> Exploring the synthesis of neutron-capture elements in the frontiers of the Galactic disk based on near-infrared spectroscopy	— <i>CoI</i> —
Kobayashi	2019–2020	<i>NAOJ Grant (Supporting Universities)</i> Calibration and application of absorption lines by r-process elements in NIR YJ-bands	— <i>CoI</i> —
Kobayashi	2018–2020	<i>NAOJ Grant (TMT)</i> Development of CdZnTe immersion grating for TMT MIR 10–20 μm	8,600,000
Kobayashi	2018–2020	<i>KAKENHI—Kiban (B)</i> Study on evolutionary processes of the Galactic disk based on multi-dimensional data of Cepheid variable stars	— <i>CoI</i> —

Table 4.3: —continued.

Name	Year(s)	Type	Amount (JPY, given only if PI)
Kobayashi	2018–2019	<i>NAOJ Grant (Supporting Universities)</i> Exploiting high-resolution spectroscopy at 1- μm band for deep space with NIR high-resolution spectrograph WINERED and the Magellan 6.5 m telescope	— <i>CoI</i> —
Kobayashi	2018–2019	<i>NAOJ Grant (Co-development)</i> Development of VINROUGE: highly-efficient NIR high-resolution spectrograph using reflective optical systems made of ultra-low expansion ceramics	— <i>CoI</i> —
Kobayashi	2014–2018	<i>MEXT Grant (Private Universities)</i> Establishment of Laboratory of Infrared High-resolution Spectroscopy for Astronomy	— <i>CoI</i> —
Kobayashi	2017–2018	<i>NAOJ Grant (TMT)</i> Athermality performance evaluation of reflective optical system made of ultra-low thermal expansion ceramics	— <i>CoI</i> —
Kobayashi	2017–2018	<i>JAXA-ISAS Grant (Space-borne Instruments)</i> Demonstrating high-resolution spectroscopy with 2–10 μm highly-efficient Ge-immersion grating at cryogenic temperatures	— <i>CoI</i> —
Kobayashi	2016–2017	<i>JSPS Bilateral Program (with DST, India)</i> Identifying Essential Mechanisms of Star Cluster Formation with Wide-field Optical Observations	1,513,600
Kobayashi	2016–2017	<i>NAOJ Grant (TMT)</i> Development of athermal optical system using off-axis non-spherical mirrors made of ceramics	— <i>CoI</i> —
Kobayashi	2015–2017	<i>JAXA-ISAS Grant (Space-borne Instruments)</i> Evaluation of optical performances of high-efficiency Ge-immersion grating for 2–10 μm	8,850,000
Kobayashi	2014–2017	<i>KAKENHI—Kiban (B)</i> Stellar abundance analysis based on near-infrared high-resolution spectra and applications to studies on the Milky Way	— <i>CoI</i> —
Kobayashi	2014–2017	<i>KAKENHI—Kiban (A)</i> High-resolution Spectroscopic Study of the Structure around Active Galactic Nuclei	— <i>CoI</i> —
Kobayashi	2015–2016	<i>NAOJ Grant (TMT)</i> Performance evaluation of high-efficiency Ge-immersion grating	4,600,000
Kobayashi	2013–2014	<i>JSPS Bilateral Program (with DST, India)</i> Identifying Essential Mechanism in Star Formation Using Young Clusters in the Galaxy	1,844,000
Motohara	2015–2019	<i>KAKENHI—Kiban (A)</i> Development of a Wide-Wavelength-Coverage Integral Field Spectrograph Unit to Probe Galaxy Evolution	32,600,000
Motohara	2012–2016	<i>KAKENHI—Innovative Areas</i> New Development in Astrophysics through Multimessenger Observations of Gravitational Wave Sources	— <i>CoI</i> —
Motohara	2015	<i>NAOJ Grant (Co-development)</i> Development of cryogenic IFU mirror arrays made from a special aluminum by ultra-high precision machining	1,000,000
Motohara	2014–2015	<i>JSPS Bilateral Program (with Chile)</i> Basic development of a near-infrared echelle spectrograph to observe dust-enshrouded ionized gas clouds	47,468,000
Motohara	2014	<i>NAOJ Grant (Co-development)</i> Development of an element technology for image-slicer type IFUs in TMT era	3,200,000
Motohara	2011–2013	<i>KAKENHI—Kiban (C)</i> Development of an Integral Field Unit for a Near Infrared Spectrograph SWIMS	3,900,000

Table 4.3: —continued.

Name	Year(s)	Type	Amount (JPY, given only if PI)
Minezaki	2018–2019	<i>KAKENHI—Innovative Areas</i> Preparation of new facility for the optical follow-up observation	4,000,000
Minezaki	2016–2019	<i>KAKENHI—(A)</i> Development of a new-generation near-infrared spectrometer for a new AGN distance ladder	— <i>CoI</i> —
Minezaki	2013–2015	<i>KAKENHI—Kiban (B)</i> Development of a low-cost adaptive optics system in optical for small telescopes	14,500,000
Minezaki	2013–2015	<i>KAKENHI—Kiban (B)</i> Uncovering the origin of primordial dark-matter minihalo by gravitationally lensed quasars	— <i>CoI</i> —
Tanabe	2011–2013	<i>KAKENHI—(C)</i> Systematic search for MOLsphere	3,800,000
Sako	2017–2021	<i>KAKENHI—Innovative Areas</i> Gravitational wave physics and astronomy: Genesis	— <i>CoI</i> —
Sako	2018–2020	<i>KAKENHI—Kiban (B)</i> Study of Size Distribution of Small Bodies by Detection of High-speed Moving Objects	— <i>CoI</i> —
Sako	2018–2020	<i>KAKENHI—Kiban (B)</i> High-speed Wide-field Survey of Trans-Neptunian Small Bodies	— <i>CoI</i> —
Sako	2019	<i>NAOJ Grant (Co-development)</i> Development of CMOS Camera Module for High-speed Time Domain Astronomy	1,700,000
Sako	2016–2019	<i>KAKENHI—Kiban (A)</i> Deaths of Massive Stars and Supernova Explosions Revealed by High-Cadence Wide-Field Observations	— <i>CoI</i> —
Sako	2015–2018	<i>JST Grant (PREST)</i> Development of Fast Real-time Processing Methods for Astronomical Time-domain Data	37,720,000
Sako	2014–2017	<i>KAKENHI—Kiban (A)</i> Survey of Trans-Neptunian Objects with Wide-field High-speed camera	— <i>CoI</i> —
Sako	2013–2017	<i>NAOJ Grant (TMT)</i> Development of Component Technology of MICHI(Mid-Infrared Camera, High-disperser, and IFU)	— <i>CoI</i> —
Sako	2015–2016	<i>NAOJ Grant (Co-development)</i> Development of Readout System of High-sensitivity CMOS Sensor for Astronomical Observations	5,800,000
Sako	2013–2016	<i>KAKENHI—Young (A)</i> Search for Traces of Giant Impacts of Rocky Planets with Silica Feature	14,400,000
Sako	2013–2014	<i>KAKENHI—Innovative Areas</i> Development of High-sensitivity CMOS Sensor for Astronomical Observations	3,600,000
Morokuma	2018–2019	<i>KAKENHI—Innovative Areas</i> A Wide-Field Search for Optical Counterparts of Gravitational Wave Sources with Tomo-e Gozen	3,800,000
Morokuma	2016–2019	<i>KAKENHI—Kiban (A)</i> Deaths of Massive Stars and Supernova Explosions Revealed by High-Cadence Wide-Field Observations	35,100,000
Morokuma	2016–2017	<i>KAKENHI—Innovative Areas</i> A Search for Low-Mass Black Holes By Optical Variability	1,600,000
Morokuma	2015–2018	<i>KAKENHI—Kiban (A)</i> Exploring the Frontier of Time Domain Astronomy with Large Transient Surveys	— <i>CoI</i> —
Morokuma	2013–2015	<i>KAKENHI—Young (B)</i> Optical Survey for Supernova Shock Breakouts	3,200,000

Table 4.3: —continued.

Name	Year(s)	Type	Amount (JPY, given only if PI)
Hatsukade	2017–2020	<i>MEXT Leading Initiative for Excellent Young Researchers</i> Revealing the environments of gamma-ray bursts through high spatial resolution observations of molecular gas and dust	24,000,000
Hatsukade	2019	<i>NAOJ Grant (Supporting Universities)</i> Do long-duration gamma-ray bursts occur in special environments?: Constraining the environment of long-duration gamma-ray bursts through molecular gas observations of host galaxies	900,000
Hatsukade	2019–2021	<i>KAKENHI—Kiban (C)</i> A detailed study of obscured star formation and molecular gas in the host galaxies of superluminous supernovae	3,200,000
Hatsukade	2015–2018	<i>KAKENHI—Young (B)</i> Revealing the environments of long-duration gamma-ray bursts with molecular gas and dust observations	2,600,000
Egusa	2017–2020	<i>KAKENHI—Young (B)</i> Lifetime of spiral structures in nearby galaxies	3,100,000
Konishi	2015–2016	<i>KAKENHI—Young (B)</i> A CFD study for the development of wind control system on a telescope enclosure	3,100,000
Takahashi	2018–2021	<i>KAKENHI—Kiban (B)</i> Development of Near-Infrared Tunable Filter for Research of Star-formation Activity by 3D Spectroscopy	13,300,000
Takahashi	2013–2016	<i>KAKENHI—Kiban (C)</i> Development of Near-Infrared Fabry-Perot Spectrometer and Spectroscopic Observation of Massive Stars	3,800,000

Chapter 5

Research Highlights

Here we presents selected researches by the full-time faculty members in Department of Astronomy and Institute of Astronomy.

5.1 Tomonori Totani

5.1.1 The Subaru FMOS Galaxy Redshift Survey (FastSound) to Probe the Cosmic Acceleration

The FastSound project is a galaxy redshift survey for cosmology, which has been approved as a Strategic Program of the Subaru Telescope (Tonegawa et al. 2015). T. Totani served as the PI of the project. The project used a unique instrument FMOS (fiber multi object spectrograph), which is a near-infrared spectrograph having 400 fibers in 30 arcmin diameter field-of-view. The scientific goal is to test the theory of gravity on the cosmological scale for the first time at distant universe ($z > 1$), by measuring the growth speed of large scale structure from the reshift space distortion effect. Such a test sheds light on the problem of dark energy (or accelerating universe), which is the most serious, important, and fundamental problem in modern physical cosmology.

The survey successfully completed in 2015, by surveying 30 square degrees in total, in the four fields of the Canada-France-Hawaii Telescope Legacy Survey Wide (CFHTLS-W), producing 3,000 redshifts ($z = 1.2$ – 1.5) of $H\alpha$ emitting galaxies detected in a wavelength coverage of 1.45–1.65 μm . The galaxy catalog is open to public, and the final result is reported as a measurement of structure growth rate, $f\sigma_8 = 0.482 \pm 0.116$ at $z = 1.4$ (Okumura et al. 2016). This is consistent with the standard prediction of the ΛCDM with the Einstein’s gravity, giving a further support for the cosmological constant Λ as the cause of accelerated expansion of the universe. Measurements of this quantity at various redshifts are now recognized as a very important cosmological test, and the FastSound measurement marks the first robust detection beyond $z = 1$. The paper of Okumura et al. (2016) has been cited 76 times.

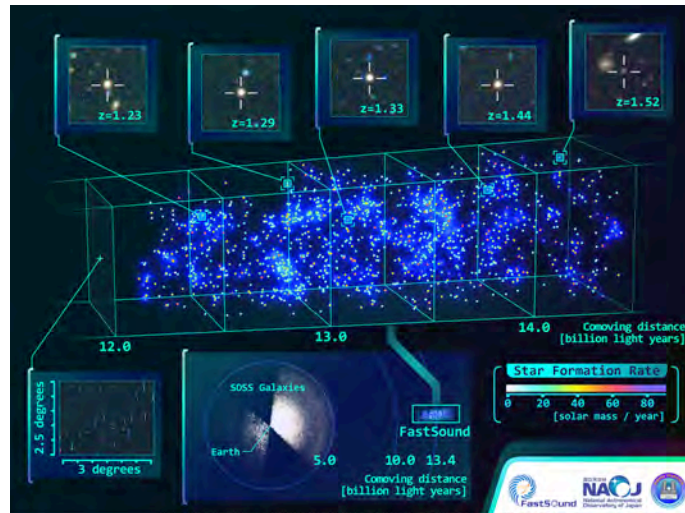


Figure 5.1: The three-dimensional large scale structure at $z \sim 1.4$ revealed by the FastSound survey.

References

- Okumura, T. et al. 2016, PASJ, 68, 38
Tonegawa, M. et al. 2015, PASJ, 67, 81

5.1.2 On the Origin of Mysterious Fast Radio Bursts

Fast radio bursts (FRBs) are a mysterious transient phenomenon first reported in 2007. Intensive research started after the report of four new FRBs in 2013. They are a burst detected in radio, lasting only a few msec. Their dispersion measure (DM) is too large to explain by electrons in the Galaxy, and if their large DM comes from electrons in intergalactic medium, their redshifts should be 0.5–1, i.e., cosmological distances. Up till now, about 100 FRBs have been detected. Only a small fraction ($\sim 10\%$) of them show a repeating activity, and apparently non-repeating FRBs may be a different population from the repeaters. The first unambiguous identification of the host galaxy was achieved for the first-detected repeater, FRB 121102, and the host galaxy is a dwarf and actively star-forming galaxy, similar to those for long gamma-ray bursts, favoring a young stellar population for the origin of FRBs. However, recently the host galaxies were identified for a few non-repeating FRBs, and they are weakly star-forming, massive galaxies. This implies that FRBs also occur in old stellar population.

T. Totani (2013) proposed that a merger of binary neutron stars is the origin of non-repeating FRBs, showing that both the event rate and radio flux can be reasonably explained. This is recognized as one of the major theoretical candidates about the origin of FRBs, which has been cited 173 times. Furthermore, Totani's student S. Yamasaki et al. (2018) investigated this scenario using a simulation data of a binary neutron star merger, and showed that matter ejection occurs a few msec after the rotation speed of the merged neutron star gets maximum, and hence there is a time window in which radio signal from the rotating merged neutron star can propagate to an observer. Yamasaki et al. (2018) also proposed that repeater FRBs may be a massive neutron star remnant after a binary merger. A fraction of binary neutron star mergers would leave such a massive and stable neutron star, depending on total stellar mass and equation of state. Such a remnant neutron star can be a repeater FRB, after the ejected mass expands and the surrounding medium gets transparent to radio signals.

T. Totani also led a FRB follow-up program using the Subaru Telescope. Especially, Subaru played a crucial role to identify a possible host galaxy and taking its spectrum to determine the redshift for FRB 150418 (Keane et al. 2016, cited 180 times). Though a possibility that this galaxy is not related to FRB 150418 but a radio flaring AGN cannot be excluded, this is one of the earliest multi-wavelength campaign for FRBs.

References

- Keane, E. et al. 2016, Nature, 530, 453
Totani, T. 2013, PASJ, 65, L12
Yamasaki, S. et al. 2018, PASJ, 70, 39

5.2 Motohide Tamura

5.2.1 Exoplanet Instrumentations

Prof. Motohide Tamura and his collaborators inside and outside of the Department have been conducting various instrument developments for exoplanet detection and characterization. Each of these is briefly summarized below. Reference papers are only from 2016 to present.

IRD (InfraRed Doppler) instrument IRD is a near-infrared high-precision radial velocity spectrometer for the 8.2-m Subaru telescope equipped with a laser-frequency comb. IRD aims at detection of Earth-like habitable planets around late M stars. It is completed in 2018 and started a Subaru Strategic Program in 2019. It is one of the most high-precision spectrometers working at infrared wavelengths. Tamura is the PI and Dr. Takayuki Kotani is the Co-PI of IRD. The original fund is from JSPS Grant-in-Aid for Scientific Research and IRD is currently operated by the Astrobiology Center (ABC). ABC is contributing to unifiedly operate Subaru exoplanet instruments including IRD, SCEXAO, and CHARIS. A copy of IRD is under development for the 1.7-m IR telescope PRIME (PRime-focus Infrared Microlensing Experiment) with a new MEXT fund (2018-2022). The Osaka University and SAAO (South African Astronomical Observatory) are the main institutes of PRIME.

SCEXAO (Subaru Coronagraphic Extreme Adaptive Optics) instrument SCEXAO is a modular high-contrast instrument installed on the Subaru telescope. SCEXAO benefits from a first stage of wavefront correction with AO188 and a second stage with the 2000-actuator deformable mirror. It splits the 600-2400 nm spectrum towards a variety of modules, in visible and near infrared, optimized for a large range of science cases. The integral field spectrograph CHARIS makes SCEXAO a prime instrument for exoplanet/disk detection and characterization. The newest addition is the 20k-pixel Microwave Kinetic Inductance Detector (MKIDS) Exoplanet Camera (MEC). These continuous developments using Subaru/SCEXAO as a testbed brings SCEXAO closer to the future TMT exoplanet instrument, PSI. Dr. Olivier Guyon is the PI of the SCEXAO project. UTokyo is contributing various aspects including polarimetry, coronagraph, and funding.

MuSCAT (Multi-color Simultaneous Camera for studying Atmospheres of Transiting exoplanets) instrument series MuSCAT and MuSCAT2 are multi-band optical cameras for a follow-up and characterization of transiting planets. MuSCAT is a 3-band camera used on the 1.88-m telescope at Okayama Astro-Complex (OAC), Japan, while MuSCAT2 is a 4-band camera installed on the 1.52-m Carlos Sanchez Telescope at Teide Observatory in the Canary Islands, Spain. MuSCAT2 supports TESS validations with 162 dedicated observing nights per year. Dr. Norio Narita is the PI of both instruments. MuSCAT3 is also under development to achieve a 24-hour continuous observation from the northern hemisphere.

WFIRST coronagraph (CGI) CGI is an optical coronagraph with space adaptive optics for the 2.4-m WFIRST (Wide Field Infrared Survey Telescope) mission under development by NASA. It is currently a technology demonstration instrument but it aims at achieving a contrast of 10^9 at 0.2-1 arcsec, enabling detection of reflected light from large-to-mid size planets. Motohide Tamura and his collaborators inside and outside of the Department have been developing the polarization module and mask substrate for CGI. The optical design using a dual beam polarimetry is newly proposed and is completed in 2019. The EM manufacturing will start soon. An involvement in the WFIRST/CGI and space coronagraph technology will be crucial to a possible Japanese contribution to the future flagship missions such as HabEx and LUVOIR.

References

- Beichman, C. et al. 2019, RNAAS, 3, 89
 Narita, N. et al. 2019, JATIS, 5a5001
 Ishiduka, M. et al. 2018, PASP, 130f5003I
 Kuzuhara, M. et al. 2018, SPIE, 10702E
 Kotani, T. 2018, SPIE, 10702E11K
 Gaudi, B. S. et al. 2018, SPIE, 10698E.0P
 Lozi, J. 2018, SPIE, 10703E59
 Watanabe, M. 2018, SPIE, 10702E3V
 Takizawa, K. et al. 2017, NatSR, 7, 7561
 Ishizuka, M. et al. 2016, SPIE, 9912E1
 Kokubo, T. et al. 2016, SPIE, 9912E1RK
 Guyon, O. and Tamura, M., 2016, JATIS, 2a0901G
 Yoneta, K. et al. 2016, SPIE, 9912E6I

Murakami, N. et al. 2016, SPIE., 9912E6G
Jovanovic, N. et al. 2016, SPIE, 9909E0W
Mennesson, B. et al. 2016, SPIE, 9904E0L

Direct Imaging and Spectroscopy of Exoplanets and Disks (SEEDS/Post-SEEDS projects and others)

After the success of the Subaru SEEDS survey project of exoplanets and disks (2009-2015), Motohide Tamura and his collaborators inside and outside of the Department have been promoting the Post-SEEDS project. This program organizes the direct imaging and spectroscopy of exoplanets and disks using Subaru's extreme AO (SCEXAO) and IFU instrument CHARIS and tries to produce more sciences beyond the technical demonstration of these cutting edge-instruments. The papers using the SEEDS survey data are also being published even after the main survey and its activities are extended to ALMA and theoretical studies.

References

Mayama et al. 2019, in press
Uyama et al. 2019a,b, in press
Gerard, B. L. et al. 2019, AJ, 158, 36
Currie, T. et al. 2019, ApJ, 877, L3
Rich, E. A. et al. 2019, ApJ, 875, 38
Asensio-Torres, R. et al. 2019
Currie, T. et al. 2018, AJ., 156, 291
Goebel, S. et al. 2018, AJ, 156, 279
Johnson, M. C. et al. 2018, MNRAS.481, 596
Mizuki, T. et al. 2018, ApJ, 865, 152
Bonnefoy, M. 2018, A&A, 618, 63
Takami, M. 2018, ApJ, 864, 20
Livingston, J. H. 2018, AJ., 156, 78
Uyama, T. et al. 2018, AJ, 156, 63
Yang Y. et a. 2018, ApJ, 861, 133
Dong, R. et al. 2018, ApJ, 860, 124
Long, Z. C. et al. 2018, ApJ, 858, 112
Kuhn, J. et al. 2018, PASP, 130c5001K
Rich, E. A. et al. 2017, MNRAS, 472, 1736
Brandt, T. D. et al. 2017, JATIS, 3d8002
Uyama, T. et al. 2017, AJ, 154, 90
Uyama, T. et al. 2017, AJ, 153, 106
Currie, T. et al. 2017, ApJ, 836, L15
Dong, R. et al. 2017, ApJ, 836, 201
Garcia, E. V. et al. 2017, ApJ, 834, 162
Yang, Y. et al. 2017, AJ, 153, 7
Kooistra, R. et al. 2017, A&A, 597, 132
Konishi, M. et al. 2016, PASJ, 68, 92
Akiyama, E. et al. 2016, AJ, 152, 222
Helminiak, K. G. et al. 2016, ApJ, 832, 33
Oh, D. et al. 2016, ApJ, 831, L7
Mizuki, T. et al. 2016, A&A, 595, 79
Lomax, J. R. et al. 2016, ApJ, 828, 2
Schneider, G. et al. 2016, AJ, 152, 64
Asensio-Torres, R. et al. 2016, A&A, 593, 73
Ohta, Y. et al. 2016, PASJ, 68, 53
Ryu, T. et al. 2016, ApJ, 825, 127
Oh, D. et al. 2016, PASJ, 68, L3
Honda, M. 2016, ApJ, 821, 2
Liu, H. B. et al. 2016, SciA, 2E0875
Tamura, M. 2016, PJAB, 92, 45
Konishi, M. et al. 2016, ApJ, 818, L23

5.2.2 K2/TESS and Other Transiting Planet Detection and Characterization

Dr. John Livingston and Dr. Norio Narita and their collaborators inside and outside of the Department have been conducting validation of exoplanet candidates detected by the NASA K2 mission. Our team is concentrating on high-resolution imaging and published many papers so far including 3 refereed papers as the first author of Dr. Livingston. Among these the paper entitled “44 Validated Planets from K2 Campaign 10” was press-released by the UTokyo both in Japanese and English and caught a broad attention including the Japan Times. Including a subsequent discovery of 60 planets from K2 C5-8, the total number of his validated planets is well more than 100. Therefore he is currently a record holder of exoplanet discovery in Japan. Due to the relatively bright and moderately inactive host star, many planets he validated are compelling targets for future characterization via radial velocity mass measurements and transmission spectroscopy. As the first known star with multiple transiting planets in the Hyades cluster, the system should be helpful for testing theories of planet formation and migration. This approach has been extended to the TESS planet candidate follow-up with MuSCAT and MuSCAT2 multi-band optical camera build by Dr. Narita and his collaborators.

References

- Barragan, O. et al. 2019, MNRAS, 490, 698
 Parviainen, H. et al. 2019, in press
 Fukui, A. et al. 2019, AJ, 158, 206
 Quinn, S. N. et al. 2019, AJ, 158, 177
 Parviainen, H. et al. 2019, A&A, 630, 89
 Crossfield, I. J. M. et al. 2019, ApJ, 883, L16
 Persson, C. M. et al. A&A, 628, 64
 Luque, R. et al. 2019, A&A, 628, 39
 Alsubai, K. et al. 2019, AJ, 157, 224
 Livingston, J. H. et al. 2019, MNRAS.484, 8
 Livingston, J. H. et al. 2019, AJ, 157, 102
 Alsubai, K. et al. 2019, AJ, 157, 74
 Deibert, E. K. 2019, AJ, 157, 58
 Hirano, T. et al. 2018, AJ, 155, 127
 Livingston, J. H. et al. 2018, AJ, 155, 115
 Narita, N. et al. 2017, PASJ, 69, 29
 Henderson, C. B. et al. 2016, PASP, 12814401
 Hirano, T. et al. 2016, ApJ, 825, 53
 Hirano, T. 2016, ApJ, 820, 41.

5.2.3 Circular and Linear Polarization Survey of Star Forming Regions

Dr. Jungmi Kwon and her collaborators inside and outside of the Department have been conducting unique and extensive polarization surveys of various star forming regions (SFRs) and other objects at near-infrared wavelengths (J, H, Ks simultaneously). This is not only linear polarimetry but also circular polarization survey using the IRSF 1.4-m telescope in South Africa. This is the only infrared circular polarization survey in the world and only Dr. Kwon’s team is publishing the circular data. The data are crucial not only for proving magnetic and dust-scattering field structures in SFRs but also for implicating the origin of homochirality of life on Earth by demonstrating the ubiquity of extended high circularly polarized regions around massive YSOs. The team is also contributing to the submillimeter polarimetry projects such as JCMT/BISTRO. In fact her paper for the Oph cloud core is the first BISTRO-J paper.

References

- Kwon, Y. G. et al. 2019, A&A, 629, 121
 Sugitani, K. et al. 2019, PASJ.tmp, 89
 Coude, S. et al. ApJ, 877, 88
 Liu, J. et al. 2019, ApJ, 877, 43
 Wang, J.-W. et al. 2019, ApJ, 876, 42
 Kusune, T. et al. 2019, PASJ, tmp, 57
 Tamaoki, S. et al. 2019, ApJ, 875, L16
 Kandori, R. et al. 2018, ApJ, 868, 94
 Kandori, R. 2018ApJ, 865, 121
 Soam, A. 2018, ApJ, 861, 65
 Kwon, J. et al. 2018, AJ, 156, 1

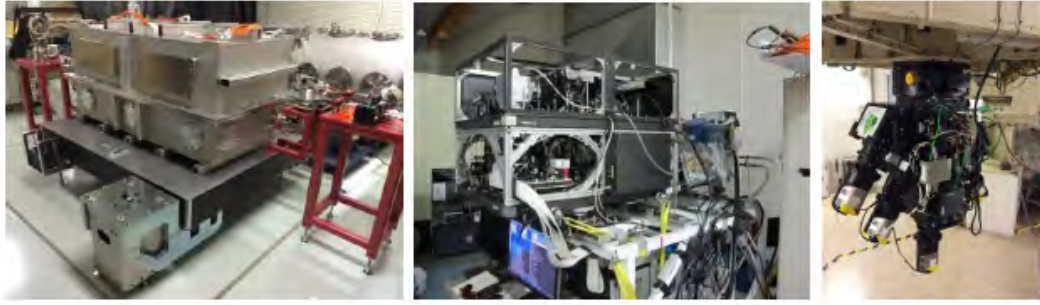


Figure 5.2: IRD (left), SCEXAO (middle), and MuSCAT2 (right).

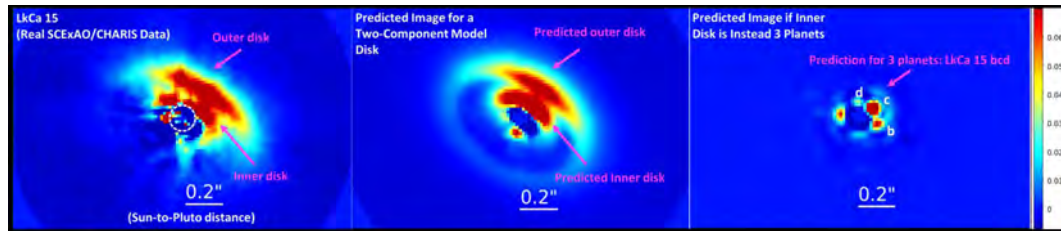


Figure 5.3: SCEXAO image of LkCa 15 (left). Model image in the case of disk scenario (middle). Model image in the case of planet scenario (right). SCEXAO data are consistent with the disk model and LkCa 15b is most likely a part of the disk.

- Kwon, J. et al. 2018, ApJ, 859, 4
 Kandori, R. et al. 2018, ApJ, 857, 100
 Kwon, J. 2018, ApJS, 234, 42
 Eswaraiah, C. et al. 2017, ApJ, 850, 195
 Kandori, R. et al. 2017, ApJ, 848, 110
 Kandori, R. 2017, ApJ, 845, 32
 Ward-Thompson, D. et al. 2017, ApJ, 842, 66
 Chen, Z. et al. 2017, ApJ, 838, 80
 Kim, J. et al. 2017, AJ, 153, 126
 Kusune, T. et al. 2016, ApJ, 830, L23
 Kwon, J. et al. 2016, AJ, 152, 67
 Kwon, J. et al. 2016, ApJ, 824, 95
 Chen, Z. 2016, ApJ, 822, 114
 Kim, J. et al. 2016, ApJS, 222, 2



Figure 5.4: Cartoon of the K2-187 planetary system. The planet sizes are 1.3, 1.8, 3.2, and 2.4 times of the Earth size. The inner most is a ultra short period planet.

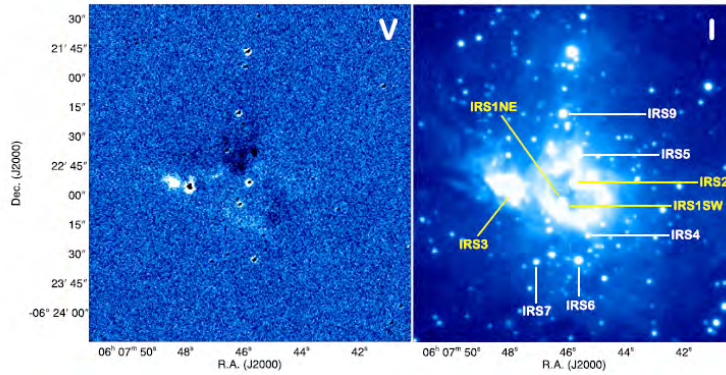


Figure 5.5: Stokes V (left) and I (right) of Mon R2 in the Ks band. The white and black colors indicate positive and negative Stokes V, respectively, and the blue background indicates zero levels.

5.3 Yuri Aikawa

5.3.1 Isotope fractionation in the star-forming regions and protoplanetary disks

The primordial Solar system material such as comets and meteorites show isotope anomalies; the molecular isotope ratios are significantly different from the elemental abundance ratio. Since the isotope fractionation is caused in specific physical conditions, such as low temperature and intense UV irradiation, the isotope ratios have been investigated as indicators of the origin and thermal history of the Solar system material.

While various isotope fractionations are observed and investigated in molecular clouds, the fractionation proceeds in protoplanetary disks, as well. In recent years, the spatially resolved observations of deuterated molecules become possible using ALMA (Huang et al. 2017). Spatial distributions of DCO^+ and DCN are found to be different, which indicates that these molecules are deuterated via different reactions. Motivated by these observations, Aikawa et al. (2018) revisited the deuterium fractionation in protoplanetary disks to reveal the spatial variation of the most effective deuteration path for each molecule. The OPR of H_2 , which affects the efficiency of the deuteration, is also investigated and found to be almost thermal except in the cold midplane. Analytical formulae of D/H ratio of simple species are also derived. Y. Aikawa is currently participating as a co-PI in the ALMA Large Program MAPS (PI: K. Öberg), in which various molecular emission lines, including those of deuterated species, are observed with a high spatial resolution.

The isotope ratio of $^{15}\text{N}/^{14}\text{N}$ is known to be higher in comets, while its ratio in N_2H^+ in a prototypical prestellar core L1544 is lower than the elemental abundance ratio. Although the $^{15}\text{N}/^{14}\text{N}$ enhancement in comets had been considered to originate in exothermic exchange reactions in molecular clouds, the recent quantum chemical study by Roueff et al. (2015) found significant activation barriers in representative exchange reactions of nitrogen isotopes. Furuya & Aikawa (2018) then proposed that the N-isotope fractionation in comets and prestellar cores would originate in the converging flow of molecular cloud formation; ^{15}N is preferentially incorporated to ice, and is depleted from the gas phase, by the

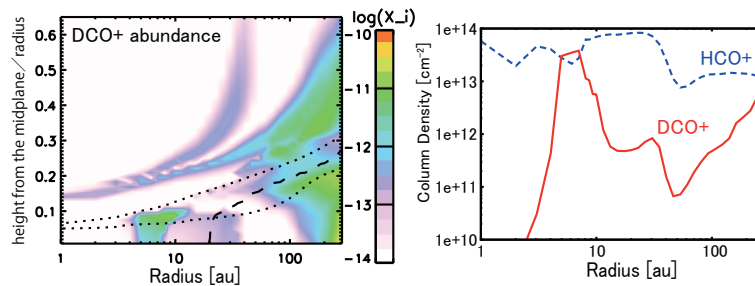


Figure 5.6: Distribution of DCO^+ in a protoplanetary disk.

combination of photo-dissociation of gaseous $^{15}\text{N}^{14}\text{N}$ and freeze-out of ^{15}N to form icy molecules on grain surfaces. The work is press-released in April, 2018.

References

- Furuya, K., Aikawa, Y., 2018, *ApJ*, 857, 105
 Aikawa, Y., Furuya, K., Hincelin, U., Herbst, E., 2018, *ApJ*, 855, 119
 Huang, J., Öberg, K. I., Qi, C., Aikawa, Y., Andrews, S. M., Furuya, K., Guzmán, V. V., Loomis, R. A., van Dishoeck, E. F., Wilner, D. J., 2017, *ApJ*, 835, 231

5.3.2 Complex organic molecules in protoplanetary disks

Observations and analysis of comets and meteorites show that the Solar nebula, i.e. the protoplanetary disk of our Solar system, was rich in organic molecules. While these organic molecules are formed in a star-forming core via the interactions of gas-phase and grain surface chemistry (Lu et al. 2018), the formation proceeds in protoplanetary disks, as well (Furuya & Aikawa 2014; Yoneda et al. 2016). The large organic molecules are expected to be abundant as ice in protoplanetary disks, but the detections of icy molecules need absorption band observations in infrared, which is difficult in disks. We thus depend on radio observations of gaseous emission lines to detect these organic molecules in disks, although their gas-phase abundances are expected to be much lower than those in ice mantles. In recent years, detections of complex organic molecules, such as CH_3OH and CH_3CN become possible with ALMA (Öberg et al. 2015; Walsh et al. 2016), which is currently further pursued in the ALMA Large Program MAPS.

While the gas-phase abundance of large organic molecules are low in usual quiescent disks due to their relatively high sublimation temperatures (~ 100 K), they can be freshly and abundantly sublimated in disks in a large outburst, e.g. FU Ors. Y. Aikawa has been serving as a coordinator of JCMT monitoring survey of luminosity outbursts in YSOs (e.g. Johnstone et al. 2018)(PI: Greg Herczeg). In the course of this collaboration, Aikawa proposed an observation of COMs in a FU Ori star using ALMA, which is performed towards V883 Ori; Lee et al. (2019) detected various organic molecules such as CH_3OH and CH_3CHO around the extended snow line in the disk. This result is press-released in February 2019.

References

- Furuya, K. Aikawa, Y., 2014, *ApJ*, 790, 97
 Öberg, K. I., Guzmán, V. V., Furuya, K., Qi, C., Aikawa, Y., Andrews, S. M., Loomis, R., Wilner, D. J., 2015, *Nature* 520, 198
 Yoneda, H., Tsukamoto, Y., Furuya, K., Aikawa, Y., 2016, *ApJ*, 833, 105
 Walsh, C., Loomis, R. A., Öberg, K. I., Kama, M., van 't Hoff, M. L. R., Millar, T.J., Aikawa, Y., Herbst, E., Widicus Weaver, S. L., Nomura, H., 2016, *ApJL*, 823, L10
 Lu, Y., Chang, Q., Aikawa, Y. 2018, *ApJ*, 869, 165
 Johnstone, D. et al. 2018, *ApJ*, 854, 31
 Lee, J.-E. Lee, S., Baek, G., Aikawa, Y., Cieza, L., Yoon, S.-Y. Herczeg, G., Johnstone, D., Cassasus, S., 2019, *Nature Astronomy*, 3, 314-319

5.4 Nobunari Kashikawa

5.4.1 High- z protocluster survey by Subaru/HSC

The evolution of galaxies is well known to be closely linked to their surrounding environments. The environmental dependence of the stellar population of galaxies appears at $z \sim 2 - 3$; however, we are still not sure about when the distinct characteristics of cluster galaxies emerge, and what process is responsible. Due to the extremely small number density of protoclusters, which is defined as a structure that will collapse into a galaxy cluster (i.e. a virialized object of $> 10^{14}M_{\odot}$ at $z = 0$), we know only ~ 20 confirmed protoclusters at $z > 3$. To overcome this paucity of protoclusters, we have constructed the largest and the most systematic sample of candidate protoclusters at $z \sim 4$ to date (Toshikawa et al. 2018) by using the data from Hyper Suprime-Cam Subaru Strategic Program (HSC-SSP). Due to its large coverage field (121deg^2) and depth (e.g. ~ 25.8 mag in i -band at 5σ), Toshikawa et al. (2018) identified 179 unique protocluster candidates based on the overdensity of g -dropout galaxies.

The unprecedented size of our protocluster candidate catalog allowed us to perform, for the first time, an angular clustering analysis of the systematic sample of protocluster candidates. We find a correlation length of $35.0h^{-1}\text{Mpc}$, corresponding to the halo mass of $2 \times 10^{13}M_{\odot}$. The relation between correlation length and number density of $z \sim 4$ protocluster candidates is consistent with the prediction of the ΛCDM model, and the correlation length is similar to that of rich clusters in the local universe.

We find that only two out of 151 luminous quasars at $z \sim 4$ reside in the protocluster regions (Uchiyama et al. 2018). The distributions of the distances between quasars and the nearest protoclusters and the significance of the overdensity at the positions of quasars are all statistically identical to those found for g -dropout galaxies, suggesting that quasars tend to reside in almost the same environment as star-forming galaxies at this redshift. These findings are consistent with a scenario in which luminous quasars at $z \sim 4$ reside in structures that are less massive than those expected for the progenitors of today's rich clusters of galaxies. We also found two pairs of quasars residing in protoclusters (Onoue et al. 2018). Quasars are rare and pairs of them are even rarer. The fact that both pairs were associated with protoclusters suggests that quasar activity is perhaps synchronous in protocluster environments.

On the other hand, stacking the images of the 179 candidate protoclusters, the combined infrared (IR) emission of the protocluster galaxies in the observed $12 - 850\mu\text{m}$ wavelength range is successfully detected (Kubo et al. 2019). This is the first time that the average IR spectral energy distribution (SED) of a protocluster has been constrained at $z \sim 4$. The observed IR SEDs of the protoclusters exhibit significant excess emission in the mid-IR with $> 5\sigma$ significance with Planck compared to that expected from typical star-forming galaxies (SFGs). They are reproduced well using SED models of intense starburst galaxies with warm/hot dust heated by young stars, or by a population of active galactic nuclei (AGN)/SFG composites.

We also found that the proto-BCG (Brightest Cluster Galaxy) candidates and their surrounding galaxies are found to have different rest-UV color ($i - z$) distributions to field galaxies and other galaxies in protoclusters that do not host proto-BCGs (Ito et al. 2019). The result suggests that specific environmental effects or assembly biases have already emerged in some protoclusters as early as $z \sim 4$. These results are web released to public on the Subaru telescope HP.

References

- Toshikawa et al. 2018, PASJ, 70, S12
 Uchiyama et al. 2018, PASJ, 70, S32
 Onoue et al. 2018, PASJ, 70, S31
 Ito, K. et al. 2019, ApJ, 878, 68
 Kubo, M. et al. 2019, ApJ, accepted
<https://subarutelescope.org/Pressrelease/2018/03/04/index.html>

5.4.2 Subaru High- z Exploration of Low-luminosity Quasars (SHELLQs)

Quasars at high redshift ($z > 6$) are an important and unique probe of the distant Universe, for understanding the origin and progress of cosmic reionization, the early growth of supermassive black holes (SMBHs). However, despite two decades of intensive efforts by past surveys, our knowledge about high- z quasars is limited to the most luminous ($M_{1450} < -24\text{mag}$) quasars at $z < 6.5$, with only a few examples known at lower luminosity. Those poorly-explored regions are likely one of the most important and exciting sites of cosmic evolution; numerous low-luminosity quasars may be (at least partly) reionizing the Universe and SMBHs are rapidly growing along with their host galaxies at this epoch. We are on-going the project called Subaru High- z Exploration of Low-Luminosity Quasars (SHELLQs). We selected distant quasar candidates from the sensitive HSC-SSP survey data, then carried out an intensive observational campaign to obtain spectra of those candidates, using the Subaru Telescope, the Gran Telescopio Canarias, and the Gemini telescope. The survey has revealed 83 previously unknown at $z \sim 6$ (e.g. Matsuoka et al. 2019a), including one quasar at $z = 7.07$ (Matsuoka et al. 2019b).

This finding increases the number of black holes known at that epoch considerably, and reveals, for the first time, how common SMBHs are early in the universe’s history.

The luminosity function (LF) was calculated (Matsuoka et al. 2018) with a complete sample of 110 quasars at $5.7 < z < 6.5$, which includes 48 SHELLQs quasars discovered over 650 deg^2 and 63 brighter quasars. This is the largest sample of $z \sim 6$ quasars with a well-defined selection function constructed to date, which has allowed us to detect significant flattening of the LF at its faint end. A double power-law function fit to the sample yields a faint-end slope $\alpha = -1.23_{-0.34}^{+0.44}$, a bright-end slope $\beta = -2.73_{-0.31}^{+0.23}$, a break magnitude $M_{1450}^* = -24.90_{-0.90}^{+0.75}$. Integrating the best-fit model over the range $-18 < M_{1450} < -30 \text{ mag}$, quasars emit ionizing photons at the rate of $\dot{N}_{\text{ion}} = 10^{48.8 \pm 0.1} \text{ s}^{-1} \text{ Mpc}^{-3}$ at $z = 6.0$. This is less than 10% of the critical rate necessary to keep the intergalactic medium ionized, which indicates that quasars are not a major contributor to cosmic reionization.

We also executed deep near-infrared spectroscopy of six quasars at $6.1 < z < 6.7$. From single-epoch mass measurements based on Mg II $\lambda 2798$, we find a wide range in BH masses, from $M_{\text{BH}} = 10^{7.6}$ to $10^{9.3} M_{\odot}$ (Onoue et al. 2019). The Eddington ratios $L_{\text{bol}}/L_{\text{Edd}}$ range from 0.16 to 1.1, but the majority of the HSC quasars are powered by $M_{\text{BH}} \sim 10^9 M_{\odot}$ SMBHs accreting at sub-Eddington rates. The Eddington ratio distribution of the HSC quasars is inclined to low accretion rates, suggests that the global Eddington ratio distribution is wider than has previously been thought. The presence of $M_{\text{BH}} \sim 10^9 M_{\odot}$ SMBHs at $z \sim 6$ cannot be explained with constant sub-Eddington accretion from stellar remnant seed BHs. Therefore, we may be witnessing the first buildup of the most massive BHs in the first billion years of the universe, the accretion activity of which is transforming from active growth to a quiescent phase.

We performed ALMA [CII] line and far-infrared (FIR) continuum observations of seven $z > 6$ HSC quasars (Izumi et al. 2019). Most of the HSC quasars studied thus far show [CII]/FIR luminosity ratios similar to local star-forming galaxies. Using the [CII]-based dynamical mass (M_{dym}) as a surrogate for bulge stellar mass (M_{bulge}), we find that a significant fraction of low-luminosity quasars are located on or even below the local $M_{\text{BH}}?M_{\text{bulge}}$ relation, particularly at the massive end of the galaxy mass distribution. In contrast, previous studies of optically luminous quasars have found that black holes are overmassive relative to the local relation. Given the low luminosities of our targets, we are exploring the nature of the early co-evolution of supermassive black holes and their hosts in a less biased way. Almost all of the quasars presented in this work are growing their black hole mass at much higher pace at $z \sim 6$ than the parallel growth model, in which supermassive black holes and their hosts grow simultaneously to match the local $M_{\text{BH}}?M_{\text{bulge}}$ relation at all redshifts. As the low-luminosity quasars appear to realize the local co-evolutionary relation even at $z \sim 6$, they should have experienced vigorous starbursts prior to the currently observed quasar phase to catch up with the relation. These results are web released to public on the U. Tokyo HP.

References

- Matsuoka et al. 2019a, ApJ, 883, 183
 Onoue et al. 2019, ApJ, 880, 77
 Izumi et al. arXiv:1904.07345
 Matsuoka et al. 2019b, ApJ, 872, L2
 Matsuoka et al. 2018, ApJ, 869, 150
<https://www.s.u-tokyo.ac.jp/ja/info/6297/>

5.5 Kazuhiro Shimasaku

5.5.1 Galaxy evolution

Size evolution of galaxies Sizes of high-redshift galaxies provide important information on the evolution of galactic structure. We analyze extremely deep Hubble Space Telescope images toward six gravitational lensing clusters (“the Hubble Frontier Fields”) and make a large sample of $z \sim 6 - 9$ galaxies whose sizes and luminosities are corrected for gravitational lensing effects using our own precise cluster mass models. Using this sample combined with lower- z results in the literature, we find that the disk size of galaxies increases with cosmic time and that the ratio of the disk half-light radius to the virial radius of the host dark matter halo is almost constant at $\sim 3\%$ independent of cosmic time. This implies that angular momenta are conserved when disks are formed and grow (Kawamata et al. 2015, 2018). We also obtain similar constant ratios for $z \sim 2 - 4$ galaxies using other deep HST data (Okamura et al. 2018). We also present the most accurate size-luminosity relation after correction for surface-brightness dependent detection completeness for $z \sim 6 - 9$ galaxies (Kawamata et al. 2018).

References

- Kawamata, R., Shimasaku, K. et al. 2015, ApJ, 804, 103
 Okamura, T., Shimasaku, K., & Kawamata, R. 2018, ApJ, 854, 22
 Kawamata, R., Shimasaku, K. et al. 2018, ApJ, 855, 4

Comprehensive study of Lyman α emitters Lyman α emitters (LAEs) are one of the major galaxy populations at high-redshift, but their fundamental properties such as dark halo masses and star formation rates remain to be well constrained. Using the largest sample of LAEs at $z \sim 2$ obtained with the Subaru Telescope combined with careful clustering and stellar population analyses, we accurately estimate their halo masses, stellar masses, and star formation rates. We find that LAEs are normal star-forming galaxies lying on the star-formation main sequence, except that they are efficiently converting the gas of host haloes into stars (Kusakabe et al. 2015, 2018). We also find that diffuse Lyman α haloes around LAEs (whose origin is a long-lasting problem) are primarily caused by Lyman α photons escaping from the main body and then scattering in the circum-galactic medium (Kusakabe et al. 2019).

References

- Kusakabe, H., Shimasaku, K. et al. 2015, ApJ, 800, L29
 Kusakabe, H., Shimasaku, K. et al. 2018, PASJ, 70, 4
 Kusakabe, H., Shimasaku, K. et al. 2019, PASJ, 71, 55

The relation between supermassive black holes and host dark matter haloes How supermassive black holes (SMBHs) and their host galaxies co-evolve is an open question. We examine the SMBH mass - host dark halo mass relation for ~ 50 $z \sim 6$ quasars using literature data, and find that a vast majority of these SMBHs are more massive than expected from the local relation. This indicates that the growth of SMBHs in $z \sim 6$ quasars precedes that of hosting haloes. We also find that half or more of the host galaxies are consistent with $z \sim 6$ average galaxies without hosting a quasar in terms of star formation rate and perhaps stellar mass.

References

- Shimasaku, K. & Izumi, T. 2019, ApJ, 872, L29

5.5.2 Subaru Hyper Suprime-Cam Strategic Survey

The Hyper Suprime-Cam Strategic Survey is a 300 night program of the 8.2m Subaru Telescope that conducts a wide and deep multiband imaging survey with Hyper Suprime-Cam, a wide-field (1.8 square degrees) prime-focus optical imager of Subaru. The survey consists of three layers: Wide (g, r, i, z, y bands; 1400 deg^2 down to $r \simeq 25$ mag), Deep (g, r, i, z, y and 3 narrow bands; 27 deg^2 , $r \simeq 26$ mag), and Ultra Deep (g, r, i, z, y and 3 narrow bands; 3.5 deg^2 , $r \simeq 27$ mag) (Aihara et al. 2018a). This program started observations in 2014 and is still on-going as of 2019, but it has already been producing many important results in galactic and extragalactic astronomy and observational cosmology. Initial data have been publicly released (Aihara et al. 2018b). As a core member of this program, I was in charge of the high-redshift galaxies section of the proposal and acted as a co-chair of the high-redshift galaxies working group. I am also a Co-I of many science papers.

References

- Aihara, H., Shimasaku, K. et al. 2018a, PASJ, 70, S4
Aihara, H., Shimasaku, K. et al. 2018b, PASJ, 70, S8

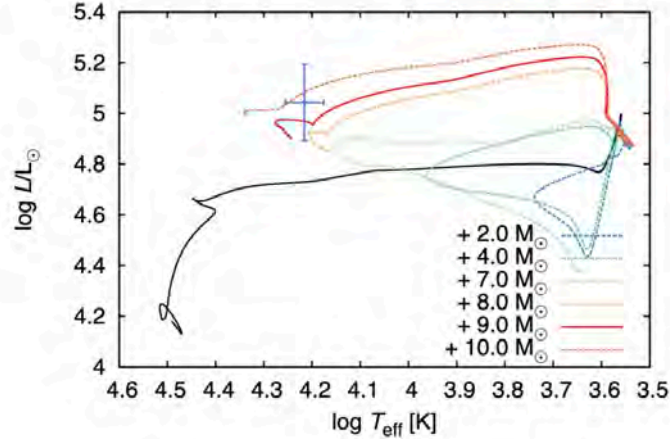


Figure 5.7: Hertzsprung-Russell diagram. The observed position of Sk-69°202 is shown by the cross. The values in the legends indicate the M_2 of models.

5.6 Hideyuki Umeda

5.6.1 The Final Fates of Accreting Supermassive Stars

The formation of supermassive stars (SMSs) via rapid mass accretion and their direct collapse into black holes (BHs) is a promising pathway for sowing seeds of supermassive BHs in the early universe. We calculate the evolution of rapidly accreting SMSs by solving the stellar structure equations including nuclear burning as well as general relativistic (GR) effects up to the onset of the collapse. We find that such SMSs have a less concentrated structure than a fully convective counterpart, which is often postulated for non-accreting ones. This effect stabilizes the stars against GR instability even above the classical upper mass limit $\gtrsim 105M_\odot$ derived for the fully convective stars. The accreting SMS begins to collapse at the higher mass with the higher accretion rate. The collapse occurs when the nuclear fuel is exhausted only for cases with $\dot{M} \lesssim 0.1M_\odot\text{yr}^{-1}$. With $\dot{M} \simeq 0.3\text{--}1M_\odot\text{yr}^{-1}$, the star becomes GR unstable during the helium-burning stage at $M \simeq 2 - 3.5 \times 10^5 M_\odot$. In an extreme case with $10M_\odot\text{yr}^{-1}$, the star does not collapse until the mass reaches $\simeq 8.0 \times 10^5 M_\odot$, where it is still in the hydrogen-burning stage. We expect that BHs with roughly the same mass will be left behind after the collapse in all the cases. (Umeda et al. 2016)

5.6.2 A progenitor model of SN 1987A based on the slow-merger scenario

Even after elaborate investigations spanning 30 years, it is still not understood how the progenitor of SN 1987A has evolved. In order to explain the unusual red-to-blue evolution, previous studies have suggested that in the red giant stage an increase either in the surface helium abundance or in the envelope mass was necessary. It is usually supposed that the helium enhancement is caused by rotational mixing, and that the mass increase is the result of a binary merger. We have thus investigated these scenarios thoroughly. We found that rotating single-star models do not satisfy all the observational constraints and that the enhancement of the envelope mass alone does not explain the observations. Here, we consider a slow-merger scenario in which both the helium abundance and the envelope mass enhancements are expected to occur. We show that most of the observational constraints, such as the red-to-blue evolution, lifetime, total mass and position in the Hertzsprung-Russell diagram at collapse, and the chemical anomalies are well reproduced by a merger model with 14 and 9 M_\odot stars. We also discuss the effects of the added envelope spin in the merger scenarios. The Evolution in the HR diagram for our progenitor model is shown in Figure 5.7. (Urushibata et al. 2018)

References

- Umeda, H., Hosokawa, T., Omukai, K. & Yoshida, N. 2016, ApJ, 830, L34
 Urushibata, T., Takahashi, K., Umeda, H. & Yoshida, T. 2018, MNRAS, 473, L101-105

5.7 Michiko Fujii

5.7.1 Dynamical evolution of star clusters and galaxies

Formation and dynamical evolution of star clusters Star clusters are one of fundamental building blocks of disk galaxies. We investigated the formation process of star clusters, especially their early dynamical evolution, using hydrodynamic and N -body simulations. We first performed hydrodynamic simulations of turbulent molecular clouds for roughly one free-fall time. For the next step, we generated the initial stellar distributions based on the results of hydrodynamic simulations by replacing some gas particles to stellar particles. We then performed N -body simulations only with stellar particles up to 10 Myr. The stellar systems finally formed several star clusters. We found that molecular clouds typical in our Galaxy form open clusters and associations, while molecular clouds typical in starburst galaxies form dense massive clusters (see Figure 5.8).

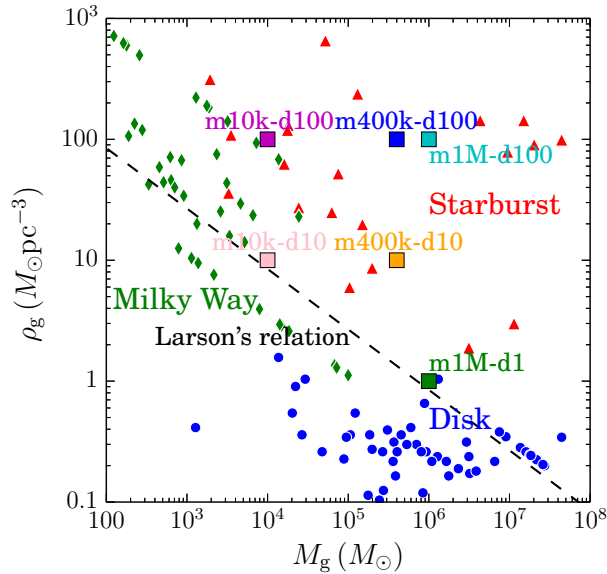


Figure 5.8: Mass-density relation of observed molecular clouds (triangles, circles, and diamonds) and our initial conditions (squares). Green diamonds indicate individual molecular clouds in the Milky Way galaxy. Blue circles and red triangles are for molecular clouds typical in individual local disk and starburst galaxies, respectively. Each point indicates one galaxy. The data are from Krumholz et al. (2012). The dashed line indicates the mass-density relation following Larson's relation. (Figure 7 in Fujii & Portegies Zwart 2016)

Formation of intermediate-mass black holes in first star clusters If first stars formed as a star cluster, runaway collisions of stars may cause the formation intermediate-mass black holes (IMBHs) in the first star clusters. We performed N -body simulations of first star clusters embedded in dark matter halo using initial conditions taken from a cosmological simulation. In these simulations, both star clusters and dark matter halos are modeled as N -body systems. We estimated that first clusters can form typically $\sim 1000M_{\odot}$ IMBHs and that the tidal disruption rate around the IMBHs is $\sim 0.3\text{Myr}^{-1}(M_{\text{IMBH}}/1000M_{\odot})$.

Survival rate of planets in open clusters In dense stellar environment such as star clusters, planets can be ejected due to the close encounters among stars. In Pleiades cluster, no planet has been found yet. We estimated the survival rate of planets in open clusters using N -body simulations of star clusters. We found that only 1.5% of close-in planets within 1 AU and 7% of planets between 1 and 10 AU are ejected even in relatively dense open clusters 5.9. This result suggest that we should find exoplanets in star clusters as well as around field stars.

Modeling the Milky-Way galaxy The dynamical evolution and current structure of the Milky-Way (MW) galaxy is of particular interest since Gaia started to provide the observed data. We modeled the MW galaxy using maximum eight billion particles, which is the largest number of particles for a MW galaxy model. We modeled the disk, bulge, and dark matter halo as N -body systems and resolved them with the same mass resolution. We performed N -body simulations up to 10 Gyr. We ran simulations ~ 50 models. From these simulations, we found that initial halo spin is necessary to

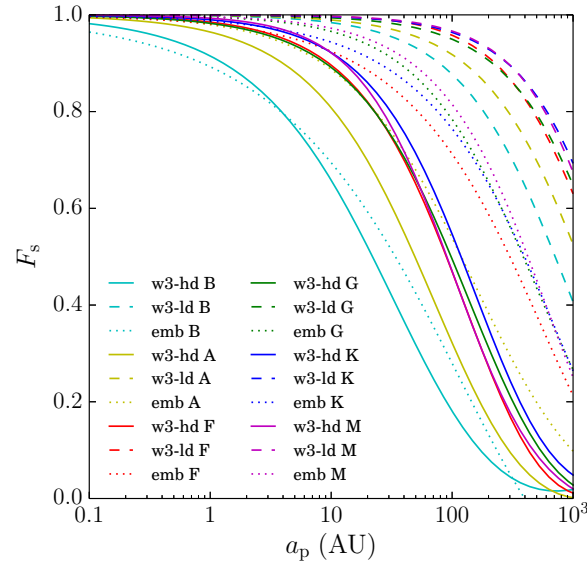


Figure 5.9: Survival fraction of planets around each spectral type of star as a function of the semi-major axis of planets (Fig. 5 in Fujii & Hori 2019).

maintain a short and fast rotating bar (see Figure 5.10). This model can also reproduce the observed dynamics of the MW galaxy such as velocity dispersion of stars in the disk and bulge regions.

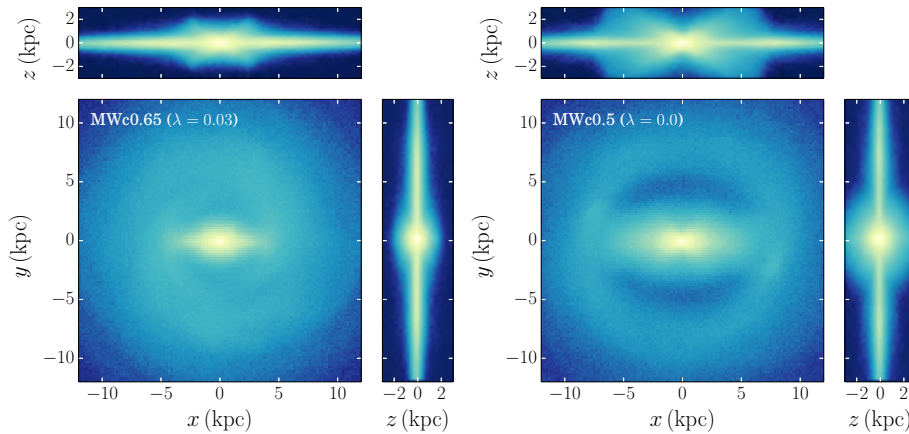


Figure 5.10: Surface density of models with high and low initial halo spin (left) and without halo spin (right). (Figure 7 in Fujii et al. 2019).

Gravitational wave emission from merging binary black holes formed in star clusters Since the first gravitational wave detection from the merging binary black holes (BBHs), several gravitational wave signals from merging BBHs have already been detected and the number is now increasing. One of possible formation channel of BBHs is dynamical interaction of BBHs in dense star clusters. Using the results of N -body simulations of star clusters including black holes (BHs), we estimated the merger and detection rate of BBHs originated from star clusters. We estimated that the detection rate of BBHs formed in star clusters is comparable to that expected from isolated binaries (see Figure 5.11). We also estimated that the the merger rate of BBHs formed in open clusters is 20–50% of that formed in typical globular clusters, considering the cluster mass function with a power of -2 .

Development of new N -body codes We have developed a new Particle-Particle Particle-Tree code, PENTACLE, in which gravitational force from neighbor particles is evaluated and integrated with individual timesteps, while force from far-away particles is calculated using tree code and integrated with a shared timestep. This code was developed

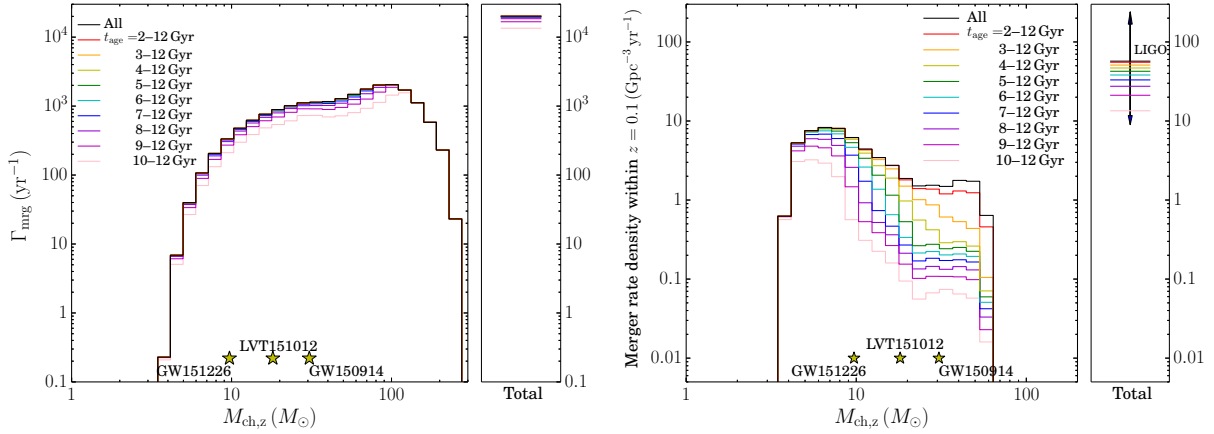


Figure 5.11: Merger rate distribution as a function of redshifted chirp mass and the total merger rates for all BBH mergers (left), and merger rate density distribution as a function of redshifted chirp mass and the total merger rate density for mergers within $z = 0.1$ (right). (Fig. 6 in Fujii et al. 2017)

particularly for planet formation N -body simulation, but applicable for other N -body problems such as star clusters. The code is already public. <https://github.com/PENTACLE-Team/PENTACLE>.

References

- Fujii M. S., Portegies Zwart S., 2016, *ApJ*, 817, 4
 Sakurai Y., Yoshida N., Fujii M. S., Hirano S., 2017, *MNRAS*, 472, 1677
 Iwasawa M., Oshino S., Fujii M. S., Hori Y., 2017, *PASJ*, 69, 81
 Fujii M. S., Tanikawa A., Makino J., 2017, *PASJ*, 69, 94
 Hirai Y., Ishimaru Y., Saitoh T. R., Fujii M. S., Hidaka J., Kajino T., 2017, *MNRAS*, 466, 2474
 Fujii M. S., Bédorf J., Baba J., Portegies Zwart S., 2018, *MNRAS*, 477, 1451
 Hirano S., Yoshida N., Sakurai Y., Fujii M. S., 2018, *ApJ*, 855, 17
 Fujii M. S., Bédorf J., Baba J., Portegies Zwart S., 2019, *MNRAS*, 482, 1983
 Fujii M. S., Hori Y., 2019, *A&A*, 624, A110
 Trani A. A., Fujii M. S., Spera M., 2019, *ApJ*, 875, 42
 Kumamoto J., Fujii M. S., Tanikawa A., 2019, *MNRAS*, 486, 3942
 Fujii M. S., 2019, *MNRAS*, 486, 3019
 Trani A. A., Spera M., Leigh N. W. C., Fujii M. S., 2019, *ApJ*, 885, 135

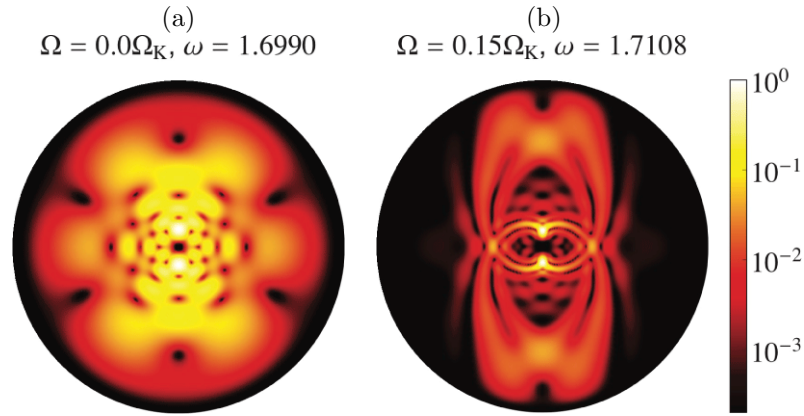


Figure 5.12: Distribution of the kinetic energy of (a) an ordinary low-frequency mode (gravity mode) and (b) a rosette mode on a meridional plane of a polytropic model with index 3.

5.8 Masao Takata

The research topics of Takata can be divided into two categories: (1) theoretical study of stellar oscillation and (2) its application to asteroseismology, which is the study of the internal structure of stars based on the properties of oscillations detected at the surface. The results described in sections 5.8.1 and 5.8.3 are those of (1) and (2), respectively, while those in section 5.8.2 are related to the both categories.

5.8.1 Rosette Modes of Oscillation in Rotating Stars

Rotation is an important unsolved problem in stellar physics. It can significantly influence the structure and evolution of stars through various types of instabilities and material mixing. It is also deeply related to the generation and maintenance of stellar magnetic field (dynamo mechanism). Still, the physical processes associated with stellar rotation have not been understood very well yet.

Study of oscillations in rotating stars is expected to shed light on this problem from a different angle. Although the subject has fairly a long history, a new phenomenon has recently been discovered in numerical simulations. It is a unique type of eigenmodes of oscillation with low frequencies, called rosette modes. Unlike other types of modes, the oscillation energy of these modes concentrates on special ‘rosette’ patterns (cf. Fig. 5.12). Takata & Saio (2013) develop a detailed theory of rosette modes to show that they originate from a group of eigenmodes with close frequencies (in the limit of no rotation), which interact with each other through the second-order effect of the Coriolis force. It is demonstrated in the subsequent papers that these modes are not necessarily axisymmetric with respect to the rotation axis (Saio & Takata 2014), and that the rosette structure can be described by a simple analytical expression, which is derived under the assumption of the much shorter wavelength of constituent waves than the scale height of the equilibrium stellar structure (Takata 2014). Due to their special structure, these modes could have a unique contribution to the angular momentum transport inside main sequence stars with intermediate mass.

References

- Takata, M. & Saio, H. 2013, PASJ, 65, 68
 Saio, H. & Takata, M. 2014, PASJ, 66, 58
 Takata, M. 2014, PASJ, 66, 80

5.8.2 Asymptotic Analysis of Oscillations in Red-Giant Stars

Thanks to recent space missions for exoplanet study, such as CoRoT and *Kepler*, very high-quality data for asteroseismology have been obtained. One of the most successful examples is the detection of solar-like oscillations in low-luminosity red giant stars. They are composed of a lot of eigenmodes with tiny amplitude excited by the turbulent convection near the surface. The most remarkable feature of the oscillations is that they include a special class of eigenmodes, called mixed modes. These modes are constructed from acoustic waves in the low-density envelope and internal gravity waves in the compact core. Therefore, their properties can be used to extract information about both of the core and envelope.

While a lot of observational studies have been conducted to analyze the mixed modes of red giants in recent years, there still remains a lot of room to improve their theory. In fact, the original theoretical analysis of the mixed modes was

conducted a few decades ago, much before their detection in red-giant stars. A major revision of the theory of mixed modes is presented by Takata (2016a, 2016b). He carefully applies the asymptotic analysis to the problem, which can be justified for the short-wavelength oscillations, to obtain in particular the formulae of two observables, (1) the coupling factor and (2) the gravity offset. Quantity (1) is a measure of the strength of interaction between the gravity-wave oscillation in the core and the acoustic oscillation in the envelope. The new formula successfully removes the known discrepancy between the old theory and the recent observations (Mosser et al. 2017). Quantity (2) indicates a small phase shift of the core oscillation that was originally introduced in the data analysis without clear physical justification. Pinçon et al. (2019) show that the new formula can explain the observed behavior of the quantity very well. The revised analysis of the mixed modes should be of fundamental use when we examine the core structure of red giants by asteroseismology.

References

- Takata, M. 2016a, PASJ, 68, 91
 Takata, M. 2016b, PASJ, 68, 109
 Mosser, B., Pinçon, C., Belkacem, K., Takata, M. et al. 2017, A&A, 600, 1
 Pinçon, C., Takata, M., Mosser, B. 2019, 626, 125

5.8.3 Asteroseismic Study of Internal Rotation of Stars

One of the hottest topics in asteroseismology is the internal rotation of stars. While helioseismology already achieved major success in this problem for the Sun a few decades ago, it is only recently that we start to obtain reliable results for other stars. Kurtz et al. (2014) discover an A-type main-sequence star, KIC 11145123, which has been observed by the *Kepler* spacecraft. The star shows the signals of oscillations in two different ranges of periods (of the order of an hour and a day). The oscillations of the short (long) periods are interpreted as composed of acoustic (internal-gravity) waves, which propagate in the envelope (core) region of the star. Using these oscillations, they succeed in inferring the average rotation periods of the both regions. This is the first robust determination of the rotation of the deep core and surface of a main-sequence star. Although the rotation periods are equal to about 100 days in the both regions, that in the envelope is shown to be shorter than the core by a few per cent with high statistical significance. The unusually long period (of 100 days) and the faster rotation of the envelope than the core pose a very interesting problem about the formation of the star. In fact, some additional studies follow to investigate this star in more detail. With the very precise oscillation frequencies measured by *Kepler*, Gizon et al. (2016) put a constraint on the oblateness of the star to claim that it is the roundest natural object in the universe. Hatta et al. (2019) extend the seismic analysis to determine the two-dimensional structure of internal rotation.

Takata has also been involved in the asteroseismic study of other stars. Saio et al. (2015) disclose the nearly uniform rotation of an F-type main-sequence star, KIC 9244992, while Benomar et al. (2015) find no significant difference in the rotation period between the surface and the envelope of a few dozens of F and G-type main-sequence stars that exhibit solar-like oscillations. Moreover, Benomar et al. (2018) succeed in measuring the latitudinal dependence of the internal rotation of solar-type stars (for the first time except for the Sun). The existing numerical simulations are challenged by their results that the fast-rotating stars (compared to the Sun) tend to show more rapid rotation in the equatorial region than the polar region.

The common results of nearly uniform rotation (in the radial direction) for KIC 11145123 (Kurtz et al. 2014), KIC 9244992 (Saio et al. 2015) and solar-type stars (Benomar et al. 2015) suggest that a significant amount of angular momentum is transported from the core to the surface during the main-sequence stage. This is actually consistent with the results for red giants by different research groups. The physical mechanism responsible for the angular momentum transport in these stars is one of the most active topics in the field.

References

- Kurtz, D. W., Saio, H., Takata, M. et al. 2014, MNRAS, 444, 102
 Saio, H., Kurtz, D. W., Takata, M. et al. 2015, MNRAS, 447, 3264
 Benomar, O., Takata, M., Shibahashi, H. et al. 2015, MNRAS, 452, 2654
 Gizon, L., Sekii, T., Takata, M. et al. 2016, Science Advances, 2, 1777
 Benomar, O., Bazot, M., Nielsen, M. B. et al. (including Takata, M. as the sixth author) 2018, Science, 361, 1231
 Hatta, Y., Sekii, T., Takata, M. et al. 2019, ApJ, 871, 135

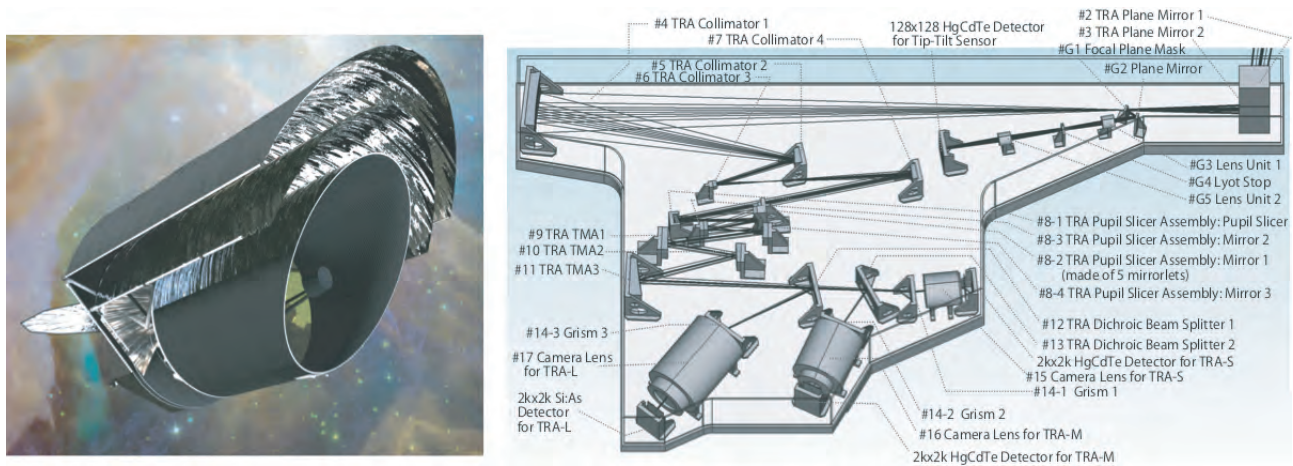


Figure 5.13: (left) The Origins Space Telescope. (right) The optics and structure design of Origins/MISC instrument.

5.9 Itsuki Sakon

5.9.1 The study of Mid-infrared Spectrometer and Camera (MISC) for Origins Space Telescope for US 2020 Decadal Survey

The Origins Space Telescope (Origins; Meixner et al. 2018; Leisawitz et al. 2019) is one of the four mission concepts studied for the 2020 US astrophysics decadal survey in the framework of Science and Technology Definition Team (STDT) activity. I have participated in this STDT activity of Origins as a JAXA liaison from the kick-off of the study team in May 2016. Origins mission is designed to have enhanced measurement capabilities relative to those of the Herschel Space Observatory, such as a three order of magnitude gain in sensitivity, angular resolution sufficient to overcome spatial confusion in deep cosmic surveys or to resolve protoplanetary disks, and new spectroscopic capability. The Origins has two mission concepts; Mission concept 1 is composed of a cryogenically cooled 9.1 m off-axis telescope and five instruments covering wavelengths from 5 to 660 μm , while Mission Concept 2 of a cryogenically cooled 5.9 m on-axis telescope with JWST-sized collecting area and four instruments covering wavelengths from 5 to 660 μm . The Mid-infrared Spectrometer and Camera (MISC; Sakon et al. 2018) is one of the instruments studied both for the Origins Space Telescope (Origins) Mission Concept 1 and 2 (cf., OSS, Bradford et al. 2018; FIP, Staguhn et al. 2018; HERO, Wiedner et al. 2018). I have led the study of the MISC as an instrument principal investigator (PI). The mid-infrared transit spectrometer (TRA) is the primary function of the MISC instrument and is base-lined in the final concept. The MISC TRA employs the densified pupil spectroscopic design (Matsuo et al. 2016) to achieve < 5 ppm of spectro-photometric stability and covers 2.8–20 μm with $R = 50\text{--}300$. The highest ever spectro-photometric stability achieved by MISC TRA enables to detect bio-signatures (e.g., ozone, water, and methane) in habitable worlds in both primary and secondary transits of exoplanets and makes the Origins a powerful tool to bring a revolutionary progress in exoplanet sciences. The mid-infrared wide-field imaging and low-resolution spectroscopic function of the MISC instrument, which provides the Origins not just with a focal plane guiding function but also with a powerful tool to diagnose the physical and chemical condition of the ISM using dust features, molecules lines and atomic and ionic lines, is also presented in the final report as an up-scoped version of the MISC instrument. I have made a primary contribution to writing the MISC instrument part both in the interim and final study reports. The Origins team has submitted the Origins' final study report to the decadal committee on 23 August 2019.

References

- Sakon, I., et al. 2018, Proc. of SPIE, 10698, 1069817 (9pp.)
 Meixner, M., et al. 2018, Proc. of SPIE, 10698, 106980N (11pp.)
 Leisawitz, D., et al. 2019, Proc. of SPIE, 11115, 111150Q (12pp.)
 Bradford, M., et al. 2018, Proc. of SPIE, 10698, 1069818 (17pp.)
 Staguhn, J., et al. 2018, Proc. of SPIE, 10698, 106981A (6pp.)
 Wiedner, M. C., et al. 2018, Proc. of SPIE, 10698, 106981B (10pp.)
 Matsuo, T., et al. 2016, ApJ, 823, 139
http://exoplanets.astron.s.u-tokyo.ac.jp/OST/MISC/index_misc.html (Origins/MISC team page)
https://asd.gsfc.nasa.gov/firs/docs/OriginsVolume1MissionConceptStudyReport_11Oct2019.pdf (final study report)

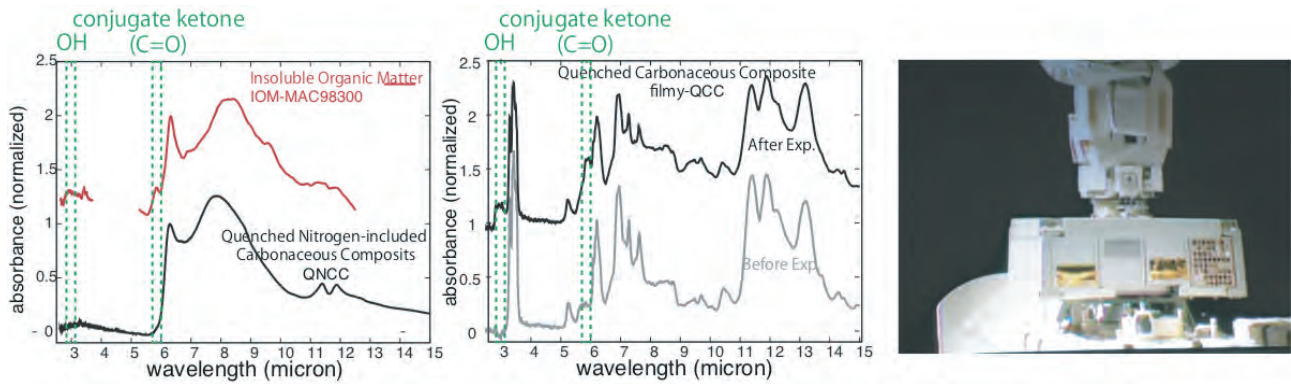


Figure 5.14: (Left) Comparison of infrared spectra between QNCC (Laboratory synthesized organics) and IOM extracted from the carbonaceous condorite. Close similarity in the general characteristics including the presence of broad features at $6.2 \mu\text{m}$, $8 \mu\text{m}$ and $11.3 \mu\text{m}$ and $12 \mu\text{m}$ are recognized. (middle) The comparison of infrared spectra of filmy-QCC between before and after the exposure experiment. In the infrared spectrum of filmy QCC collected after the exposure experiment exhibits the features of OH and conjugated ketone ($>\text{C}=\text{O}$). These features are also recognized in the spectrum of IOM. (right) The image of space exposure experiment using International Space Station (ISS)/KIBO/ExHAM.

5.9.2 Laboratory Astrophysics and Space Exposure Experiment using International Space Station(ISS)/ExHAM

Based on the synthesis experiment of organics by using 2.45 GHz microwave plasma generation apparatus, we found that the organics (Quenched Nitrogen-included Carbonaceous Composite; QNCC, hereafter) synthesized by rapidly cooling the plasma generated from hydrocarbon dust and nitrogen molecular gas exhibit quite similar infrared spectral properties to the ‘Class C’ UIR bands observed in dusty novae, which is characterized by the presence of broad $8 \mu\text{m}$ feature instead of the normal UIR $7.7 \mu\text{m}$ and $8.6 \mu\text{m}$ bands. As a result of the detailed analyses and measurements of properties of QNCC, we found that the N/C atomic ratio is 3–5%, that the amine structure is responsible for the broad $8 \mu\text{m}$ feature (Sakon et al. 2015; Endo et al. 2018). Although ‘Class C’ UIR bands are relatively minor members compared with the ‘Class A’ and/or ‘Class B’ UIR bands, the present result has a great impact in that we have succeeded in producing laboratory synthesized organics that must be the probable candidate of the carrier of the UIR bands in classical novae. We also found a similarity between the infrared and X-ray properties of the QNCC and those of insoluble organic molecules (IOM) extracted from the carbonaceous condorite (Endo et al. in prep.).

I have carried out the space exposure experiment of various kinds of carbonaceous solids using International Space Station (ISS)/KIBO/ExHAM as a principal investigator (PI). The major goal of this project is to understand how the carbonaceous dust particles synthesized in the stellar ejecta from evolved stars are chemically and physically altered in nature in the circumstellar environment until it becomes a member of the interstellar medium. In particular, we aim to investigate the properties of ‘astronomical’ polycyclic aromatic hydrocarbons (PAHs), the carrier of the unidentified infrared (UIR) bands, which have been observed ubiquitously in various astrophysical environments. So far, we have brought three experiment samples to the ISS. Each experiment sample has a $10 \text{ cm} \times 10 \text{ cm}$ exposure surface and has 64 slots for exposure experiment materials. In total, more than 40 kinds of materials including quenched carbonaceous composites (QCCs), deuterated quenched carbonaceous composites (deut-QCCs), nitrogen-included carbonaceous composites (NCCs), anthracite, graphite, and silicates are installed in the experiment samples. Among the three samples, two of them (EE64-I and EE64-II) were attached on ExHAM-1 and were exposed in the space exposure environment for 384 days from 26 May 2015 to 13 June 2016. The final sample (EE64-III) was attached on ExHAM-1 and was exposed for 386 days from 29 June 2016 to 19 July 2017. The preliminary results of the comparison of the IR and X-ray spectral characteristics of the filmy QCC between the unexposed and exposed samples, we recognized the emergence of O-H feature at $2.95 \mu\text{m}$ and conjugated Ketone ($>\text{C}=\text{O}$) feature at $5.95 \mu\text{m}$. These characteristics are commonly seen in the infrared absorption spectrum of IOM extracted from the carbonaceous condorite (Sakon et al. in prep.).

References

- Sakon, I., et al. 2015, Asian Journal of Physics, 24, 8, 1143-1150
 Endo, I., et al. 2018, JAXA Special Publication, JAXA-SP-17-009E, 305-308

5.9.3 Infrared Observation of Dusty Novae

Our knowledge of the dust formation process itself is essentially lacking. A classical nova is an important phenomenon, which provides us valuable opportunity to trace temporal development of dust condensation events and chemical/physical evolution processes of circumstellar dust on a practical timescale for human beings. I have collected multi-epoch N- and Q-band imaging and N-band low-resolution spectroscopic datasets of dusty nova V1280 Sco in 2007–2011; Day 150 with Subaru/COMICS and Days 1272, 1616, and 1947 with Gemini-South/TReCS. Long-term monitoring observations in the optical to near-infrared wavelengths have also been made continuously from the very initial phase of the outburst to date with several Japanese ground-based facilities in the framework of inter-university collaboration. Mid-Infrared spectral energy distributions (SEDs) of V1280 Sco collected at 1272, 1616 and 1947 have shown the presence of both carbonaceous and silicate dust in emission. As a result of detailed analyses of the temporal evolution of the SEDs of V1280 Sco, the dust formation history in V1280 Sco has been demonstrated such that the amorphous carbon dust is formed in the nova ejecta followed by the formation of silicate dust behind the optically thick carbon dust shell (Sakon et al. 2016).

References

Sakon, I., et al. 2016, ApJ, 817, 145 (23 pp.)

5.10 Noriyuki Matsunaga

5.10.1 The structure of the Milky Way and stellar populations therein

Variable stars with period–luminosity relations (PLRs), such as Cepheids and Miras, are good tracers of the Milky Way. The PLRs enable us to determine the accurate distances of the variables, and their ages are also available based on the theory of stellar evolution and pulsation. Classical Cepheids which represent young stellar populations (10–300 Myr) are particularly useful for studying the Galactic disk as we reviewed in Matsunaga et al. (2018). Following up our discovery of the first Cepheids within 200 pc of the Galactic center (Matsunaga et al. 2011), we have investigated the Galactic structure and stellar populations traced with variables.

Cepheid variables in the flared outer disk of our galaxy Flaring and warping of the Galactic disk had been inferred from observations of atomic hydrogen, but stars associated with flaring had not been reported. Among dozens of Cepheids found by the Optical Gravitational Lensing Experiment towards the Galactic center, we investigated five Cepheids in detail; we measured their distances based on near-infrared photometry from Infrared Survey Facility (IRSF) and the radial velocities using the Robert Stobie spectrograph on the Southern African Large Telescope (SALT). Based on these observations, we found that the five Cepheids are located within the Galactic disk beyond the Galactic center. Moreover, they are at one to two kiloparsecs above or below the Galactic plane. The presence of young stars like Cepheids are consistent with the flaring observed with atomic hydrogen, thereby giving the first evidence of stars in the flared part of the disk. This result was reported in Feast et al. (2014), and our conclusion has been supported by recent and much more complete surveys of Cepheids.

A lack of Cepheids in the inner disk and discovery of Cepheids in the surrounding region We used Infrared Survey Facility (IRSF, 1.4-m telescope at South Africa) to make surveys of variable stars in the inner part of the Galaxy. In particular, Matsunaga et al. (2016) discovered nearly 30 Cepheids towards the bulge region, $-10^\circ < l < +10^\circ$. Selecting an appropriate extinction law (the wavelength dependency of the interstellar extinction), we found that all of them are located further than the Galactic center except the four Cepheids we had reported in the earlier papers (Matsunaga et al. 2011, 2015). Moreover, except the four which are located within the Nuclear Stellar Disk (the 200-pc disk around the center), we found no Cepheids within 2.5 kpc of the Galactic center. This suggests that star formation is inactive in the central kiloparsecs of the Galaxy where the barred bulge is dominant. In addition, in other surveys conducted with IRSF targeting the inner Galaxy, we found a few Cepheids located at 4–6 kpc from the Galactic center (Tanioka et al. 2017; Inno et al. 2019). Most of these Cepheids are affected by severe interstellar extinction and could only be found in the infrared wavelengths.

While we have been studying the kinematics of Cepheids in the solar neighborhood using the Gaia early data releases (Baba et al. 2018, Kawata et al. 2019), a significant fraction of the Cepheids discovered in our infrared surveys are too much obscured behind the interstellar extinction. Their kinematics may be investigated with infrared astrometric measurements in the future such as the JASMINE project (NAOJ) and infrared spectroscopic follow-up. For example, we measured radial velocities of four Cepheids near the Galactic center using the IRCS at Subaru telescope (Matsunaga et al. 2015). Recent large-scale surveys in the infrared, such as Vista Variables in the Via Láctea Survey (VVV), are discovering thousands of new Cepheids spread across the Galactic disk. Those new Cepheids will play a crucial role in studying the structure and evolution of the Galaxy. One of our future targets is to make spectroscopic follow-up of the new Cepheids and use them as tracers of the Galactic chemical evolution, but some basic studies for establishing analysis methods of near-infrared spectroscopy is required (see the next sub-section).

Discovery of carbon-rich Miras in the Galactic bulge Miras are pulsating stars in the last stage of the Asymptotic Giant Branch evolved from low- and intermediate-mass stars. There are two distinct groups characterized by different surface chemistry, oxygen-rich and carbon-rich, of which carbon-rich Miras are considered to represent intermediate-age stars (a few Gyr) if evolved from single stars. Interestingly, only one carbon-rich Mira had been suggested as a member of the Galactic bulge and it is in a symbiotic system, i.e., evolved from a binary system. By taking low-resolution spectra of candidates selected with the infrared colors, $(J - K_s)$ and $([9] - [18])$, we confirmed eight carbon-rich Miras towards the Galactic bulge. Our near-infrared photometry infers that two of these, including the known symbiotic, are closer than the main body of the bulge while a third is a known foreground object. The remaining five, in contrast, seem to be carbon-rich Miras actually located in the bulge. The age of these carbon stars and the evolutionary process which produced them remain uncertain. They could be old and the products of either binary mass transfer or mergers, but we cannot rule out the possibility that they belong to a small in situ population of metal-poor intermediate age (< 5 Gyr) stars in the bulge or that they have been accreted from a dwarf galaxy. Reported in Matsunaga et al. (2017).

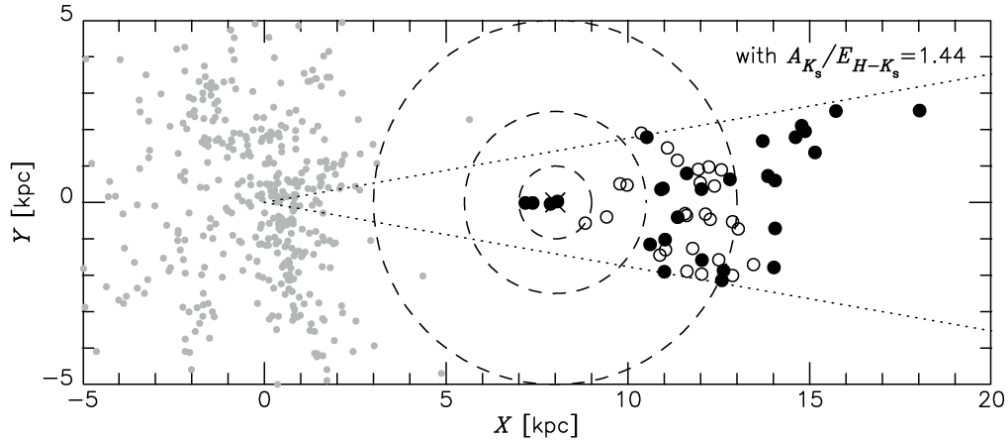


Figure 5.15: Distribution of Cepheids, ours (Matsunaga et al. 2016) and those in Dékány et al. (2015, ApJ, 812, L29) indicated by filled and open circles, respectively, on the face-on view of the Galactic disk. The Sun is located at the origin, and the Galactic center is indicated by the cross at the assumed distance of 8 kpc. Dashed circles mark 1, 2.5, and 5 kpc from the Galactic center, and the longitude range of our survey, $|l| < 10^\circ$, is illustrated by dotted lines. Reproduced from Matsunaga et al. (2016).

References

- Matsunaga et al. 2011, Nature, 477, 188
 Feast et al. 2014, Nature, 509, 342 (Matsunaga, 4th)
 Matsunaga et al., 2015, ApJ, 799, id. 46
 Matsunaga et al., 2016, MNRAS, 462, 414
 Matsunaga et al., 2017, MNRAS, 469, 4949
 Tanioka et al. 2017, ApJ, 842, 104 (Matsunaga, 2nd)
 Matsunaga et al., 2018, Space Science Reviews, 214, id. #74
 Baba et al. 2018, ApJ, 853, L23 (Matsunaga, 3rd)
 Inno et al., 2019, MNRAS, 482, 83 (Matsunaga, 3rd)
 Kawata et al., 2019, MNRAS, 482, 40 (Matsunaga, 3rd)

5.10.2 Near-infrared high-resolution spectroscopy

We are working on near-infrared high-resolution spectroscopy mainly making use of the WINERED spectrograph which covers the zYJ bands (the URL of the WINERED web site is given below). Recently developed spectrographs for the near-infrared wavelengths are becoming more and more powerful for producing a large number of high-quality spectra, and they have advantages in studying stellar populations in the Milky Way. However, there are some issues to be solved before they could be fully utilized. For example, infrared spectra are contaminated with strong telluric lines. We have developed a method of removing the telluric lines to the precision of $\sim 1\%$ (Sameshima et al. 2018). Furthermore, identification and characterization of absorption lines in the infrared range remain to be fulfilled, and we are trying to establish the list of lines of various elements including Fe (Kondo et al. 2019), α elements, and neutron-capture elements (see below). We are preparing for observations with the WINERED attached to Magellan 6.5-m telescope at Las Campanas Observatory, Chile. The high sensitivity of the WINERED would allow us to make the world leading spectroscopy in the zYJ band with the limiting magnitude of ~ 14 mag (S/N=100 with 1 hr integration) when attached to the Magellan.

Identification of near-infrared absorption lines of neutron-capture elements Stellar absorption lines of heavy elements can give us various insights into the chemical evolution of Galaxy and nearby galaxies. We searched for lines of the elements heavier than Ni in the Y (9760–11100 Å) and J (11600–13200 Å) bands. We identified 23 lines of 8 elements (Zn I, Sr II, Y II, Zr I, Ba II, Sm II, Eu II, and Dy II) in WINERED spectra of 13 supergiants and giants within FGK spectral types (spanning 4000–7200 K in the effective temperature). They are potentially useful diagnostic lines of the Galactic chemical evolution, especially in the regions for which interstellar extinction hampers detailed chemical analyses with spectra in shorter wavelengths. We also reported the detection of lines whose presence was not predicted by the synthetic spectra. To be soon published in ApJS (Matsunaga et al. in press).

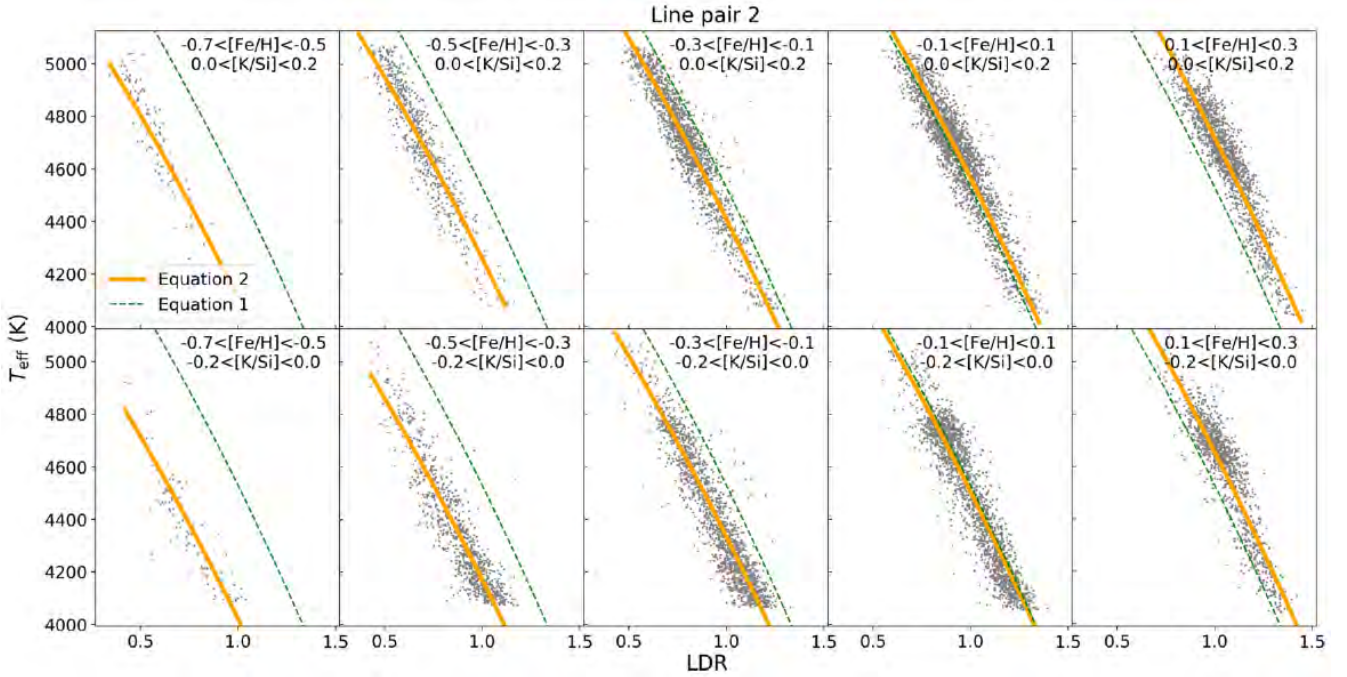


Figure 5.16: An example of the LDRs depending on the metallicity. The grey dots indicate objects within the labeled abundance range; the temperatures given by the APOGEE DR14 are plotted against the LDR of K I 15168.38/Si I 15376.83 we measured with the APOGEE spectra. The orange curve shows the LDR– T_{eff} relation at the given abundance in each panel, while the green curve indicates the relation for the solar-metal objects. Taken from Jian et al. (2019).

Line-depth ratios as the temperature indicator A line-depth ratio (LDR) of two spectral lines with different excitation potentials is expected to be tightly correlated with the effective temperature (T_{eff}), and it serves as a good T_{eff} indicator. Combining dozens or hundreds of LDR– T_{eff} relations allows us to estimate T_{eff} to the level of ~ 10 K, and the LDR method has been used mostly with optical spectra. We have been establishing this method for near-IR spectra. Not only discovering good LDR– T_{eff} relations in the YJ band (Fukue et al. 2015) and H band (Taniguchi et al. 2018), we found that many of the relations are affected by the metallicity and the surface gravity to some extent (Jian et al. 2019, see Fig. 5.16 in this report; Jian et al. in prep). Such dependency, if ignored, would limit the accuracy of T_{eff} based the LDR method, but we can instead use the LDR relations to estimate T_{eff} together with the metallicity and the surface gravity simultaneously.

References

- Fukue et al., 2015, ApJ, 812, 64 (Matsunaga, 2nd)
- Sameshima et al., 2018, PASP, 130, 074502 (Matsunaga, 2nd)
- Taniguchi et al., 2018, MNRAS, 473, 4993 (Matsunaga, 2nd)
- Jian et al., 2019, MNRAS, 485, 1310 (Matsunaga, 2nd)
- Kondo et al., 2019, ApJS, 875, 129 (Matsunaga, 3rd)
- Matsunaga et al., ApJS, in press (arXiv:1911.11277)
- WINERED web site, <http://merlot.kyoto-su.ac.jp/LIH/WINERED/>

5.11 Mamoru Doi

5.11.1 Properties of Type-Ia Supernovae

Type-Ia Supernova (SNIa) has been used as a standard candle to measure Cosmological expansion rate. We worked for calibrating photometry of SNeIa observed by SDSS-II Supernova Survey, and obtained cosmological parameters (Betoule, M. et al. 2014) based on the SDSS bands (Doi, M. et al. 2010). We show that the $\sim 2\sigma$ disagreement previously observed for SNLS survey is largely eliminated, and confirmed the concordance Cosmological mode.

To improve the accuracy of cosmological measurements with SNeIa, we have studied properties of SNeIa. We carried out a Subaru Hyper-Suprime Cam (HSC) SN survey for early phase SNeIa in 2016 lead by Ji-an Jiang, a former graduate student, and found a unique SNIa about half day after its explosion (Jiang et al. 2017, Maeda et al. 2018, Figure 5.17). The early light curve excess (Figure 5.18) and two component characteristics of its spectra were interpreted that a thin helium shell was first detonated, and then the deflagration of the white dwarf was ignited. This is the first case to show one specific mechanism of SNIa explosion observationally.

Then we studied early light curve excess of archived SNIa observations, and found that early excess was almost always observed for luminous SNeIa, while the excess was very rare for normal luminosity SNeIa. Although sample is very small, early excess was observed for sub-luminous SNeIa. These give very interesting clue for the progenitor and explosion mechanism of SNeIa (Jiang et al. 2018).

We also studied SDSS SNIa photometry without assuming any dust extinction models. Although we could not discriminate the intrinsic relation of color and luminosity of SNeIa from the dust extinction, we show that at least there exist two subgroups of SNeIa possible depending on host environment (Takanashi et al. 2017, Figure 5.19).

References

- Doi, M. et al. 2010, AJ, 139, 1628
 Betoule, M. et al. 2014, A&A, 568, id.A22
 Jiang, J. et al. 2017, Nature, 550, 80
 Jiang, J. et al. 2018, AJ, 865, id.149
 Maeda, K. et al. 2018, ApJ, 861, id.78
 Takanashi, N. et al. 2017, MNRAS, 465, 1274

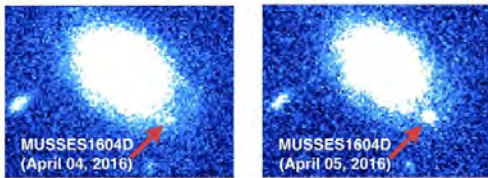


Figure 5.17: A very early phase SNIa found with Subaru/HSC. Arrows show the location of the supernova, and dates are shown in the panels. The left and right images were taken with HSC, estimated ~ 0.5 day and ~ 1.5 day after its explosion (Jiang et al. 2017).

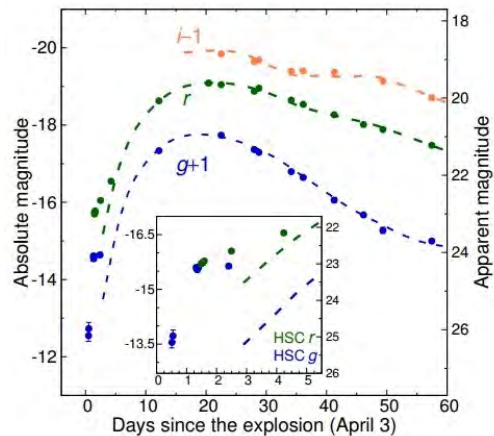


Figure 5.18: The observed light curves of the helium detonated SNIa (Jiang et al. 2017).

5.11.2 Local environment of the Core-Collapse Supernova

We have studied local environment of the explosion site of the Core-Collapse Supernova using optical-NIR IFU spectrographs. No significant metallicity differences are observed among distinct supernova types. Statistically significant

differences in progenitor initial mass are observed only when comparing supernovae II_n with other subclasses. Stripped-envelope SN progenitors with initial mass estimates lower than $25 M_{\odot}$ are found; they are thought to be the result of binary progenitors. Confirming previous studies, these results support the notion that core-collapse supernova progenitors cannot arise from single-star channels only, and both single and binary channels are at play in the production of core-collapse supernovae. These studies have been lead by a former graduate student, Hanindyo Kuncarayakti.

References

- Kuncarayakti, H. et al. 2013, AJ, 146, id.30
 Kuncarayakti, H. et al. 2013, AJ, 146, id.31
 Kuncarayakti, H. et al. 2014, PKAS, 30, 139
 Kuncarayakti, H. et al. 2016, MNRAS, 458, 2063
 Kuncarayakti, H. et al. 2018, A&A, 613, id.35

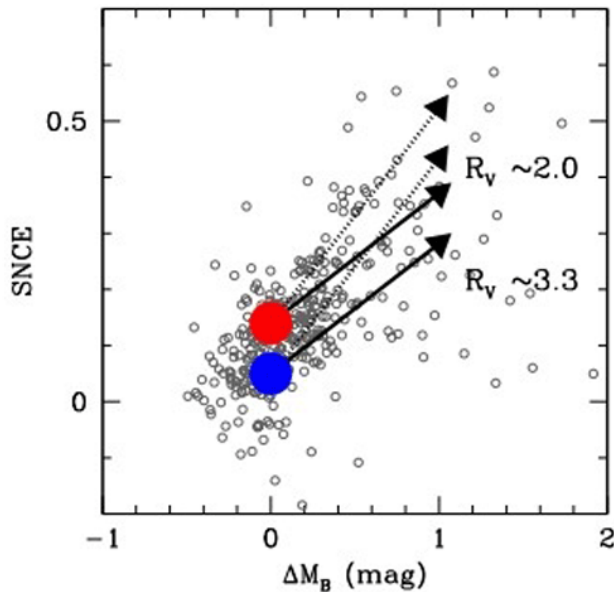


Figure 5.19: A plot for ΔM versus SNCE for SNeIa found by the SDSS-II SN survey. ΔM indicates how faint each SNIa is from typical values of bluest-brightest SNeIa, and SNCE indicates how much bluer each SNIa is from typical values of bluest-brightest SNeIa. There may be at least two SNIa subgroups with different intrinsic colors. Arrows show possible interpretation of dust extinction (Takanashi et al. 2017).

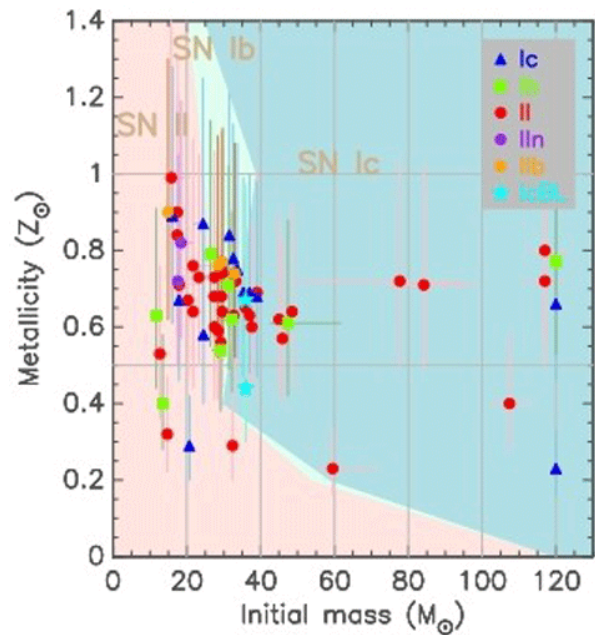


Figure 5.20: Diagram showing the plane of progenitor star initial mass and metallicity. Shaded areas are stellar evolution predictions from rotating single-star models of Georgy et al. (2009), for SN II (pink), Ib (light green), and Ic (blue-green). (Kuncarayakti et al. 2018).

5.11.3 Isophote Shapes of Early-type Galaxies

We studied isophote shapes of early-type galaxies with a dedicated analysis code developed by Kazuma Mitsuda, a former graduate student. It is well known that early-type galaxies are classified into two types morphologically, boxy and disk. Some of theoretical models predict that the ratio could be a good indicator to study merging history of galaxies. We carefully measured early-type galaxies of deep images taken with the Hubble Space telescope and of images by the Sloan Digital Sky Survey to study possible evolution between redshift of 1 and 0. There was no significant evolution found, and theoretical models are constrained.

References

- Mitsuda, K. et al. 2017, ApJ, 146, id.109

5.12 Kotaro Kohno (and IoA radio astronomy group)

The IoA radio astronomy group consists of 1 professor (K. Kohno), 2 assistant professors (B. Hatsukade and F. Egusa), 5 postdocs (including 1 visiting researcher from RIKEN), and 7 graduate students (including 1 visiting student from University of Science and Technology of China), as of December 2019. There are 4 women (1 assistant professor, 2 postdocs, 1 graduate student), and 3 are from abroad (2 from China, 1 from Taiwan).

We are primarily focusing on millimeter/submillimeter-wave (mm/submm) observations of galaxies at $z = 0 - 8$ and beyond, including the molecular gas in the Milky Way and gravitationally-lensed galaxies at the epoch of reionization (EoR). Currently, most of our science outcomes are based on ALMA and existing (multi-wavelengths) facilities, but we are also contributing developments of new observing instruments and techniques.

Here, we present some highlights of such achievements in 2013–2019. Research highlights by Drs Hatsukade and Egusa are described in separate subsections (5.21 & 5.22).

5.12.1 Deep galaxy surveys using ALMA

We have conducted deep galaxy surveys using ALMA at $\lambda \sim 1$ mm to obtain “confusion-free” contiguous maps of deep fields with rich ancillary data including SXDF-UDS-CANDELS (~ 2 arcmin²: Tadaki et al. 2015; Hatsukade et al. 2016; Kohno et al. 2016; Yamaguchi et al. 2016; Wang et al. 2016), and GOODS-S/HUDF (~ 26 arcmin², “ASAGAO”: Ueda et al. 2018; Hatsukade et al. 2018; Fujimoto et al. 2019; Yamaguchi et al. 2019). See the research highlight by B. Hatsukade (5.21) for more details of these ALMA deep surveys.

Another ALMA deep survey on SSA22, one of the most extreme overdensity regions at $z = 3.1$, has been led by H. Umehata (Umehata et al. 2017, 2018). By combining deep MUSE and ALMA observations, we have shown that the majority of the dusty starburst galaxies are hosting accreting (growing) super-massive black holes (SMBHs), and they are residing along the large-scale (~ 1 cMpc scale) Ly α filaments for the first time (Umehata et al. 2019, published in Science), giving the first direct evidence for the relation between the intergalactic medium and growths of galaxies and SMBHs in the early universe.

Based on these efforts, we have launched the ALMA Lensing Cluster Survey (ALCS), one of the on-going cycle-6 large programs, to observe high magnification regions of 33 lensing clusters, covering 88 arcmin² in total, to a depth of 80 μ Jy (1.2 mm, 1σ). The sample comes from the best-studied massive clusters blessed with HST treasury programs, i.e., CLASH, HFF, and RELICS. The ALMA observations are still on-going (carried over to cycle-7), but initial outcomes reveal a number of magnified ALMA sources without HST WFC3/F160W (H-band) counterparts, i.e., intrinsically-faint, HST-dark (H-band dropout) ALMA sources. These sources have faint IRAC counterparts, and the measured 1.2-mm to IRAC flux ratios suggest these are very distant ($z > 4 - 6$) galaxies and/or forming massive galaxies at $z \sim 4$, which are often completely invisible even in the deepest WFC3/HST images. In fact, we have revealed that such “H-band dropout ALMA galaxies” are also uncovered in GOODS-S (Yamaguchi et al. 2019) and our clustering analysis suggests that they are progenitors of present-day massive elliptical galaxies (Wang, T. et al. 2019, published in Nature).

References

- Fujimoto, S., Ouchi, M., Kohno, K., et al. 2018, ApJ, **861**, 7
 Hatsukade, B., Kohno, K., Umehata, H., et al. 2016, PASJ, **68**, 36
 Hatsukade, B., Kohno, K., Yamaguchi, Y., et al. 2018, PASJ, **70**, 105
 Kohno, K., Yamaguchi, Y., Tamura, Y., et al. 2016, IAU Symp., **319**, 92
 Tadaki, K.-i., Kohno, K., Hatsukade, B., et al. 2015, ApJ, **811**, L3
 Ueda, Y., Hatsukade, B., Kohno, K., et al. 2018, ApJ, **853**, 24
 Umehata, H., Tamura, Y., Kohno, K., et al. 2017, ApJ, **835**, 98
 Umehata, H., Hatsukade, B., Smail, I., et al. 2018, PASJ, **70**, 65
 Umehata, H., Hatsukade, B., Kohno, K., et al. 2019, Science, **366**, 97
 Wang, T., Yoshimura, Y., Kohno, K., et al. 2019, Nature, **572**, 211
 Wang, W.-H., Kohno, K., Hatsukade, B., et al. 2016, ApJ, **833**, 195
 Yamaguchi, Y., Tamura, Y., Kohno, K., et al. 2016, PASJ, **68**, 82
 Yamaguchi, Y., Kohno, K., Hatsukade, B., et al. 2019, ApJ, **878**, 83

5.12.2 Interstellar medium in galaxies and quasars in the EoR

We have used ALMA to detect redshifted fine structure lines such as [CII] 158 μ m and [OIII] 88 μ m lines to characterize the nature of ISM and star-formation history of galaxies in the EoR (e.g., Tamura et al. 2019 and references therein). Our [CII] 158 μ m observations of Subaru-HSC-selected quasars (SHELLQs; see also 5.4), which are significantly less luminous

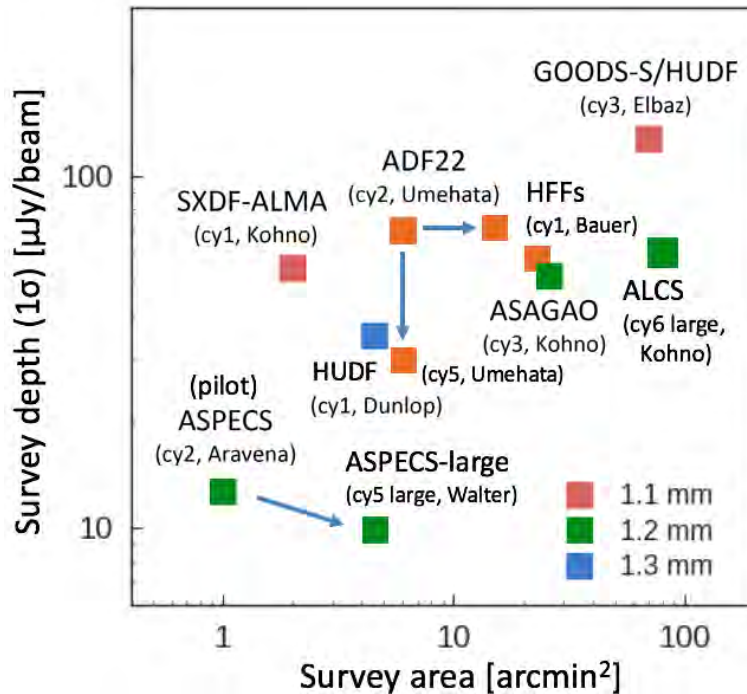


Figure 5.21: A summary of ALMA deep surveys at $\lambda \sim 1$ mm. KK is leading ALMA Lensing Cluster Survey (ALCS), one of the cycle-6 ALMA large programs.

compared with the previously known $z > 6$ quasars, have revealed that such less luminous (ergo “more typical”) quasars tend to follow the present-day M - σ relation, implying that such a galaxy-SMBH scaling relation has already been formed even in $z \sim 6$ (Izumi et al. 2019).

References

- Izumi, T., Kohno, K., et al. 2019, PASJ, **71**, 111
 Tamura, Y., Hatsukade, B., Kohno, K., et al. 2019, ApJ, **874**, 27

5.12.3 Physical and chemical properties of giant molecular clouds in the Milky Way and galaxies

We have unveiled the chemical richness at the heart of the starburst galaxy NGC 253, where a significant variation of complex organic molecules such as CH_3OH among the ~ 10 pc scale clumps (Ando et al. 2018; Figure 5.22). This leads to the ALMA large program ALCHEMI, which conducted Band 3/4/5/6/7 spectral scans of the central region of NGC 253.

We find that giant-molecular-cloud (GMC) scale (i.e., 100-pc-scale) chemical properties (such as $\text{CH}_3\text{OH}/^{13}\text{CO}$ ratios) vary depending on the large-scale (i.e., $>$ kpc-scale) structures of galaxies (such as spiral arms, bars, etc.) in the disk region of NGC 1068 (Tosaki et al. 2017). Extragalactic H_2CO measurements toward a GMC in M51 have been made to investigate the cloud-scale gas density structures using NRO 45-m and IRAM 30-m telescopes (Nishimura et al. 2019).

Physical and chemical properties of ISM at the vicinity of AGNs (such as NGC 1097 and Circinus) have been investigated in $<$ a few 10 pc resolution and we show that observed properties are consistent with the predictions by a “radiation-supported receding torus model” (Izumi et al. 2017, 2018).

Chemical properties of a distant molecular cloud have been investigated by observing molecular absorption lines (Ando et al. 2016). The H_2S ortho/para ratio of 2.9 ± 0.1 has been measured toward the molecular absorber toward B0218+357 at $z = 0.68$, indicating that the contribution of grain surface formation to the gas-phase H_2S abundance is not dominant in the system (Yoshimura et al., submitted).

See also the research highlight by Fumi Egusa (5.22) for further outcomes in the field of nearby galaxies.

References

- Ando, R., Kohno, K., et al. 2016, PASJ, **68**, 1
 Ando, R., Nakanishi, K., Kohno, K., et al. 2018, ApJ, **366**, 97
 Izumi, T., Kohno, K., et al. 2017, ApJ, **845**, L5

ALMA Band-4 compatible SIS receiver “B4R” for LMT We have developed the Band-4 SIS receiver (“B4R”) for the Large Millimeter Telescope (LMT) in Mexico, which aims at 2-mm band heterodyne spectroscopy by exploiting ALMA Band-4 receiver technologies. This project is led by NAOJ, under the collaboration with the IoA/U.Tokyo, University of Electro-Communications, Keio Univ., Nagoya Univ., INAOE, UMASS, so on. See the research highlight by B. Hatsukade (5.21) for details.

new off-point-less observing method for mm/submm heterodyne spectroscopy using “FMLO” We have proposed a new off-point-less observing method for mm/submm heterodyne spectroscopy with a frequency-modulating local oscillator (FMLO; Taniguchi et al., in press). Unlike conventional switching methods, which extract astronomical signals by subtracting the reference spectra of off-sources from those of on-sources, the FMLO method does not need to obtain any off-source spectra; rather, it estimates them from the on-source spectra themselves. The principle uses high-dump-rate (10 Hz) spectroscopy with radio frequency modulation achieved by the fast sweeping of a local oscillator of a heterodyne receiver. Because sky emission (i.e., off-source) fluctuates as $1/f$ and is spectrally correlated, it can be estimated and subtracted from time-series spectra (a time-stream) by principal component analysis. Meanwhile, astronomical signals remain in the time-stream since they are modulated to a higher time-frequency domain. The FMLO method therefore achieves (1) a remarkably high observation efficiency, (2) reduced spectral baseline wiggles, and (3) software-based sideband separation. We developed an FMLO system for the Nobeyama 45m telescope and a data reduction procedure for it. This is a joint development with Nagoya University and NAOJ.

References

- Endo, A., Tamura, Y., Taniguchi, A., Takekoshi, T., Kohno, K., et al., *Nature Astronomy*, **3**, 989
Nakajima, T., Kohno, K., et al. 2013, *PASP*, **125**, 252
Oshima, T., Takekoshi, T., Kohno, K., et al. 2018, *Journal of Low Temperature Physics*, **193**, 996
Takekoshi, T., Oshima, T., Kohno, K., et al. 2018, *Journal of Low Temperature Physics*, **193**, 1003
Takano, S., Nakajima, T., & Kohno, K., 2019, *PASJ*, **71**, S20
Taniguchi, A., Tamura, Y., Kohno, K., et al., *PASJ*, in press.

5.13 Takashi Miyata, Takafumi Kamizuka, Kentaro Asano

5.13.1 Development of Field Stacker for precise monitoring in MIR

Time variation of the atmosphere cause a serious uncertainty of the photometry in monitoring observations at mid-infrared wavelengths from the ground. To overcome this problem, IoA mid-infrared group led by T. Miyata has developed a new device called “Field Stacker.” It is an optomechanical device that combines two discrete fields inside a telescope’s field-of-view into a single field, before feeding it into a camera. It enables us to carry out simultaneous observations of a science target and a reference star, and improve the photometric accuracy by real-time calibration. This device was installed on the top of our mid-infrared camera MIMIZUKU developed for TAO. Details of this device and results of the first light observation were published reported in five SPIE papers such as Kamizuka et al. (2014, 2016, 2018) and Uchiyama et al. (2016, 2018).

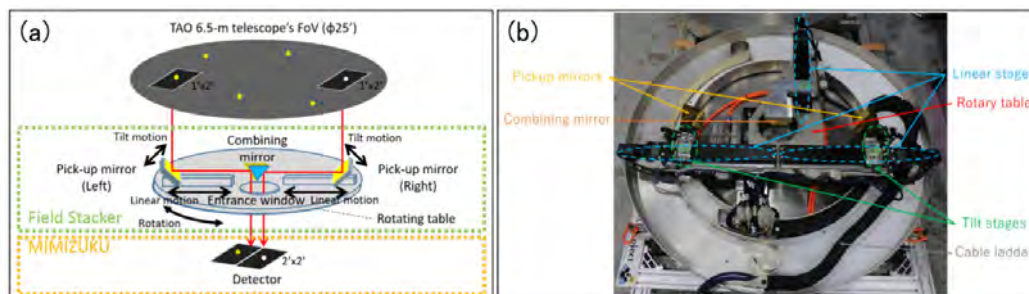


Figure 5.23: 1. (a) a conceptual diagram of the Field Stacker. (b) Top-view of the Field Stacker

5.13.2 Structure of protoplanetary disks

Protoplanetary disks are very important objects to understand formation process of planets. Especially spatially resolved images in thermal infrared wavelength provide us information on disk structures. T. Miyata and T. Kamizuka carried out mid-infrared observations of the disks by using Subaru/COMICS and Gemini-S/T-ReCS with their collaborators.

One of our targets is a transitional disk around a Herbig Ae star IRS48. We obtained spatially-resolved multi-color images in mid-infrared wavelength region with using Subaru/COMICS. The N-band (7 to 13 μ m) images show that the flux distribution is centrally peaked with a slight spatial extent, while the Q-band (17 to 25 μ m) images show asymmetric double peaks. This can be interpreted as a shadow of the inner disk casted on the outer disk. We also carried out mid-infrared observations of other 22 Herbig Ae/Be stars and revealed the relation between the spectral energy distribution and the disk structure. Those results were published as Honda et al. (2015, 2018).

5.13.3 Studies on solar system objects

Since solar system objects such as planets, satellites, asteroids, and comets show strong time variation in general, time domain observations is a key to understand their nature. Followings are two results of monitoring observations with using miniTAO and our developed mid-infrared camera MAX38.

Huge volcanic activities on Io In order to study volcanic activities of a Jupiter moon Io, we carried out monitoring observations at mid-infrared wavelength. During the monitoring, a very bright spot was discovered around a place called Daedalus Patera in 2011. It was enormous, and its total power reached to 10^{13} W which is almost comparable that of the most powerful volcanic spot Loki Patera. This result was published as Yoneda et al. (2014)

Observation of near earth asteroid 2005 YU₅₅ In 2011, an asteroid 2005 YU₅₅ approached very close to the Earth (0.85 lunar distance). This was a rare opportunity to study details of small near earth asteroids. We monitored this object in mid-infrared wavelengths during this approach and successfully obtained its infrared fluxes at the closest phase. This data gave a strong constraint on the albedo and the size of the asteroid (Müller et al. 2013).

5.13.4 Dust formation and alteration processes around young and evolved stars

Dust grains are ubiquitous in the universe. However, its formation and alteration processes are still under debate. Evolved stars such as red giant stars are important objects as the origin of dust grains. Young stars are also important to

understand the life of dust grains, since alteration processes are expected in planet formation processes. For understanding these processes, we performed ALMA observations to reveal the spatial distributions of dust-forming molecules such as AlO and SiO.

AlO and SiO molecules around W Hya AlO and SiO molecules are thought to be the ingredients of alumina and silicate grains, respectively. Takigawa et al. (2017) revealed the spatial distributions of these molecules around an oxygen-rich asymptotic giant branch star, W Hya. Their distributions suggest that alumina grains condense from AlO molecules in the vicinity of the star and that silicate grains are not formed sufficiently around the star. This result gives a new possibility that stellar wind from asymptotic giant branch stars may be driven by alumina grains.

AlO molecule around Source I in Orion-KL Alumina grains are sometimes found in meteorites as a form called calcium-aluminum-rich inclusions. It is thought to be formed in high-temperature environment in protoplanetary disks. ALMA observations performed by Tachibana et al. (2019) revealed the spatial distribution of AlO molecules around the famous young-stellar-object candidate, the Source I in Orion-KL. AlO molecules show a confined distribution at the base of the outflow, and it suggests that alumina grains can be formed from the AlO molecules in the stellar outflow.

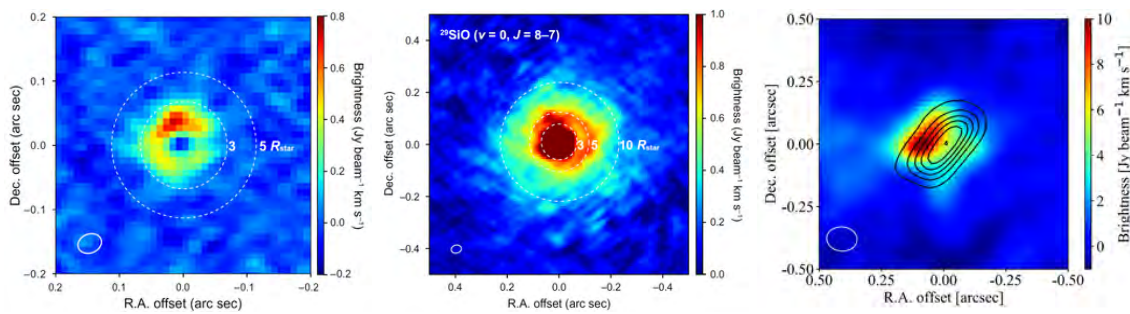


Figure 5.24: Dust-forming molecules around young and evolved stars. Left: AlO emission around W Hya. Center: SiO emission around W Hya. Right: AlO emission around Source I in Orion KL. Black contour shows continuum emission from the equatorial disk of Source I.

References

- Kamizuka et al. 2014, Proc SPIE, 9147, 3
- Kamizuka et al. 2016, Proc SPIE, 9908, 3
- Kamizuka et al. 2018, Proc SPIE, 10702, 2
- Honda, M. et al. 2018, PASJ, 70, 3, 44
- Honda, M. et al. 2015, ApJ, 804, 2, 143
- Müller, T. G. et al. 2013, A&A, 558, A97
- Takigawa, A. et al. 2017, Science Advances, 3, 11, id eaao2149
- Tachibana, S. et al. 2019, ApJ, 875, 29
- Uchiyama et al. 2016, Proc SPIE, 9912, 5
- Uchiyama et al. 2018, Proc SPIE, 10702, 2
- Yoneda, M. et al. 2014, Icarus, 236, 153

5.14 Masuo Tanaka

5.14.1 Near-infrared Narrow-band Imaging Observations in the 1.87 and 2.07 μm of Massive Star Clusters with miniTAO at Atacama: Classification of Stellar Components

Massive stars essentially affect the structure and evolution of galaxies through their huge radiative and mechanical energy output, and also their production of plentiful heavy elements during their very short lifetimes and release them into the interstellar space especially during their late evolutionary stages. These phenomena are critically important not only for chemical evolution of galaxies and next-generation star formation, but also for formation of earth-type planets and the origin of lives. In spite of the importance of the massive stars, we have not yet had enough knowledge of the birth and evolution of massive stars.

We have ever studied variety of evolved massive stars including Wolf-Rayet (WR) stars, Luminous Blue Variables (LBV), Yellow Hyper-giants (YHG), and red/blue supergiants (RSG/BSG), together with main-sequence O-type stars, mainly spectroscopically in near-infrared. On the basis of these observational results, we have developed a new survey method by using small number of near-infrared narrow-band filters, which is effective not only for the observations of highly reddened regions, but also for direct detection of the major spectral features to classify the various kinds of massive stars.

We have carried out narrow-band imaging observations in 1.87 μm and 2.07 μm with a 1.0 m infrared telescope (miniTAO) at the summit of Cerro Chajnantor (an altitude of 5640 m) in Atacama, northern Chile. Thanks to this extremely high altitude and dry climate, precipitable water vapor is as low as 0.5mm, the atmospheric window opens at the wavelength range around 1.87 μm . This wavelength range contain strong Paschen α (HI $n=4-3$) and He II ($n=8-6$, 6-5) emission lines which are valuable probes for searches of evolved massive stars. Pa α is the strongest hydrogen recombination line in the case of observations for deeply embedded sources highly-reddened by interstellar and circumstellar dust. However, it is difficult to observe it from ground based telescopes and is thought to be observed only by using *Hubble Space Telescope*. In practice, we have observed some massive-star clusters toward the galactic center, other galactic clusters, and LMC/SMC, and have detected many emission line sources including WRs and LBVs in this wavelength. The quality of the data is essentially comparable to that of *Hubble Space Telescope*.

We have obtained a set of three images for each target: the standard Ks (2150 nm)-band and two new narrow-bands of 1875 nm for Pa α and He II, and 2072 nm for C IV. These sets of images directly make us pick up emission-line sources of massive stars. Tanaka et al. (2018) detected some candidates of WR stars together with almost all known WR stars and LBVs in three clusters (Galactic Center cluster, Quintuplet cluster, Arches cluster) of the Galactic center. Color-color diagrams made from the set of the images show clear excess in 1.87 μm for WN-type Wolf-Rayet stars, Luminous Blue Variables, and Ofpe stars, and also clear excess in 2.07 μm for WC-type Wolf-Rayet stars. The 1.87 μm excess of WN stars show a clear correlation to the K_S magnitude. The correlation suggests that the 1.87 μm excess originates in recombination line emission of H and He, and the K_S magnitude includes free-free radiation. On the other hand, the color-color diagrams also enable us to find extinction for each star to draw extinction maps. Furthermore, almost all Mira variables are detected in our images. By using the extinction maps, several tens of extremely red sources except for Mira variables are detected. They are considered to be low-temperature ($T < 1000$ K) objects (possibly YSO).

References

Tanaka, M. et al. 2018, MNRAS, 480, 1507

5.15 Naoto Kobayashi

5.15.1 NIR High-resolution Spectroscopy of Optical Quality with WINERED

With a large collaboration (University of Tokyo: Kobayashi (PI), Noriyuki Matsunaga (Project Scientist), Sohei Kondo, Chikako Yasui (now at NAOJ), Satoshi Hamano (now at NAOJ), Yuki Sarugaku (now at Kyoto Sangyo Univ.), Hiroaki Sameshima; Koyama Astronomical Observatory, Kyoto Sangyo University: Yuji Ikeda, Hideyo Kawakita, and more than 15 engineers/students from both universities), we had developed a near-infrared (0.9-1.35 μ m) high-resolution spectrograph *WINERED* (Warm INfrared Echelle spectrograph to REalize Descent near-infrared high-resolution spectroscopy), to exploit a novel sciences with high-quality spectroscopy that is equivalent to that achieved in the optical wavelengths. The spectral resolutions are $R = 28,000$ (WIDE-mode, covering an entire WINERED 's wavelength region with a single exposure) and $R = 70,000$ (HIRES-modes, covering either Y- or J-band with a single exposure) (Ikeda et al. 2016, Otsubo et al. 2016).

The most important characteristics of this instrument is the high-sensitivity that doubles throughput compared to typical high-resolution spectrographs by making use of 1. Narrow wavelength range, which makes high-throughput coating available, 2. Shorter infrared wavelength range, which makes warm optics possible, 3. Highly-sensitive 1.7- μ m cut-off HAWAII-2RG 2048 \times 2048 array and originally developed thermal cut filter, that enable very low-background even for warm optics.

Owing to the high-throughput optics (> 0.5) and the very low noise of the system, WINERED has the potential to detect the faintest objects when attached to 10 m class telescopes. The instrument was developed as a PI-type instrument that can be attached to various telescopes with a Nasmyth focus. The WIDE mode and two HIRES modes were successfully commissioned in 2013 and 2016, respectively, with 1.3m Araki telescope at KAO in Kyoto. In the beginning of 2017, WINERED was relocated from Japan to the ESO 3.58 m New Technology Telescope (NTT) in La Silla Observatory, Chile, and began its scientific observations. By March of 2018, 30 nights in total were allocated for observation with the WINERED at the NTT. WINERED routinely provides spectra of the SNR > 500 for bright stars, and realized the detection of those of SNR = 30 for faint objects of $J = 16.4$ mag (for WIDE mode) and $J=15.0$ (for HIRES mode) with the exposure time of 8 hours using the narrowest slit at the NTT (even without AO) (Ikeda et al. 2018). A variety of scientific programs were conducted to successfully provide high-quality spectra of e.g., Cepheids/Miras in the Galaxy, LMC/SMC, DIB absorption lines, symbiotic stars, Nova, P Cyg stars (e.g., Mizumoto et al. 2018), YSOs (e.g., Yasui et al. 2019), AGNs, QSOs, etc. Collaborating with Carnegie Observatories, we are transferring WINERED from La Silla Observatory to Las Campanas Observatory to attach WINERED to Magellan 6.5m telescope. We hope to realize an unprecedented sensitivity of NIR high-resolution spectroscopy from next academic year.

References

- Ikeda, Y., Kobayashi, N., Kondo, S. et al. 2018, SPIE, 10702, 107025U
 Ikeda, Y., Kobayashi, N., Kondo, S. et al. 2016, SPIE, 9908, 99085Z
 Otsubo, S., Ikeda, Y., Kobayashi, N., et al. 2016, SPIE, 9908, 990879
 Yasui, C., ...Kobayashi, N. 2019, ApJ, 886, 115
 Mizumoto, M., Kobayashi, N. et al. 2018, MNRAS, 481, 793
See more scientific results at Matsunaga's section.

5.15.2 Near-infrared DIBs

Diffuse interstellar bands (DIBs) are absorption bands in the optical-near-infrared (NIR) spectra of the reddened stars, which originate from foreground interstellar clouds. The number of DIBs detected till now exceeds 500 and can be detected ubiquitously in the interstellar medium of our Galaxy, nearby galaxies, and even in the high- z quasar absorption-line systems. Despite more than 500 DIBs found in the near-UV and optical wavelength range, the nature of their carriers are still unclear. From their behaviors they are thought to be mainly contributed by organic compounds (Sarre 2008). Recently the carrier of several DIBs at 0.96 μ m was finally identified as ionized buckminsterfullerene (C_{60}^+) by laboratory experiments (Cambell et al. 2015, Nature, 523, 322). This became the first identification of DIBs carriers. DIBs can be a unique tool to trace the large organic molecules in the interstellar medium and to investigate the processes of "astrochemistry".

Compared to the optical, the NIR spectroscopy have some advantages in the DIBs study: 1) we can study the correlations of anonymous DIBs with the DIBs from C_{60}^+ at 0.96 μ m, which falls in the short NIR range, 2) the electronic transitions of ionized PAHs are expected to fall in the NIR region, and 3) the lines-of-sight with heavy extinction can be observed. Despite the advantages, DIBs in the NIR wavelength range have not been studied very well because of the low quality of the NIR high-resolution spectrographs compared to optical and the forest of the atmospheric absorption lines in the infrared. Due to the recent progress of NIR spectrographs, the search of DIBs in NIR spectra finally became possible

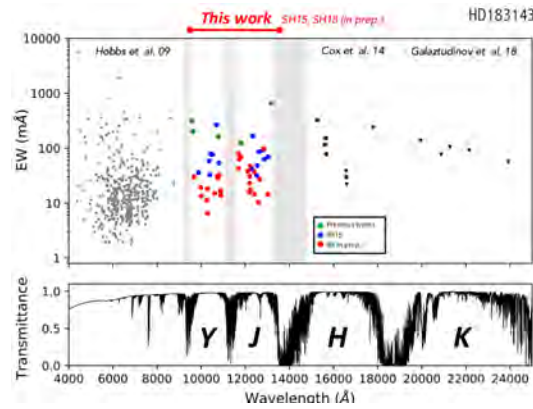


Figure 5.25: NIR DIBs detected by WINERED. Most of the NIR DIBs absorption lines ($>0.9 \mu\text{m}$) were found by the present work (Hamano et al. in prep.).

in this decade. As one of the main scientific programs of WINERED, we have extensively carried out a comprehensive survey of NIR DIBs using WINERED, which offers a high sensitivity in the wavelength coverage of $0.91\text{-}1.36 \mu\text{m}$.

Because S/N of more than 300 can be routinely achieved with WINERED, we managed to detect many new faint DIB lines in the NIR. More than 50 new NIR DIBs are firmly detected, and some of them are detected at the wavelengths close to the peaks of the absorption bands of PAH cations (Initial results are presented in Hamano et al. 2015). In addition, the high transmittance of the NIR wavelength range enables us to explore the environmental dependence of the DIBs carriers in the dusty environment for the first time and to constrain the properties of DIBs carriers (Hamano et al. 2015, 2016). We also detected $\text{C}_2 \text{ A}^1\Pi_u\text{-X}^1 \Sigma_g^+ (0,0)$ and $\text{CN A}^2\Pi_u\text{-X}^2 \Sigma^+ (0,0)$ absorption bands in the interstellar medium for the first time. The A-X (1,0) bands of C2 and CN were also detected simultaneously. These near-infrared bands have larger oscillator strengths, compared with the A-X (2,0) bands of C2 and CN in the optical. Thanks to the large oscillator strengths of these (0,0) NIR bands, we could improve the accuracy of the physical parameters estimated from the rotational distributions of both C2 and CN (Hamano et al. 2019).

Many of those works have been done at the 1.3 m Araki telescope in Kyoto, Japan, proving that a novel instrument could produce science even with the small telescopes. We are currently working on newly obtained data at NTT 3.6 m telescope in Chile to study the correlations between NIR DIBs and the C60+ lines.

References

- Hamano, S., Kawakita, H., Kobayashi, N. et al. 2019, ApJ, 881, 143
 Hamano, S., Kobayashi, N. et al. 2016, ApJ, 821, 12
 Hamano, S., Kobayashi, N. et al. 2015, ApJ, 800, 137

5.15.3 Development of Immersion Grating

An immersion grating composed of a transmissive material with a high refractive index ($n > 2$) is a powerful device for high-resolution spectroscopy in the infrared region. Although the original idea is attributed to Fraunhofer about 200 years ago, an immersion grating with high diffraction efficiency has never been realized due to the difficulty in processing infrared crystals that are mostly brittle. While anisotropic etching is one successful method for fabricating a fine groove pattern on Si crystal, machining is necessary for realizing the ideal groove shape on any kind of infrared crystal.

Collaborating with CANON Inc., we have finally realized the first machined immersion grating, which is made of single-crystal CdZnTe with a high diffraction efficiency that is almost identical to that theoretically predicted by rigorous coupled-wave analysis (Ikeda et al. 2015).

Immersion gratings will play important roles for infrared astronomy in the next generation. We have been developing immersion gratings with a variety of kinds of infrared crystals. After the success with CdZnTe, we have succeeded in fabricating a high-efficiency immersion grating with germanium (Ge), which has a high refractive index close to 4. We also managed to put a reflection coating on the grating surface and an AR coating on the entrance surface, realizing an immersion grating as ready for cryogenic application (Sarugaku et al. 2016). The grating will be installed in a K-, L-, and M-bands (2-5 μm) high-resolution ($R=80,000$) spectrograph, VINROUGE, which is a prototype for the TMT MIR instrument.

References

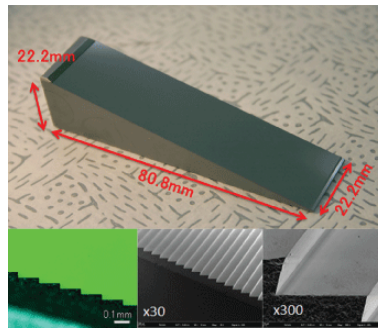


Figure 5.26: World first immersion grating made of machine-cutting. (Top) Fabricated CZT immersion grating. Magnified pictures of the (bottom-left) groove shape from the side view and the (bottom-center and bottom-right) SEM-machined surfaces (Ikeda, Kobayashi, Sarugaku et al. 2015).

Ikeda Y., Kobayashi, N., Sarugaku, Y. et al. 2015, Applied Optics, 54, 5193
Sarugaku, Y. et al. 2016, SPIE, 9906, 990637

5.16 Kentaro Motohara

5.16.1 Star Formation Activities in Nearby LIRGs Probed by Paschen α Imaging

Luminous infrared galaxies (LIRGs) are dusty galaxies with active star-formation, and an ideal environment to study galaxy formation. However, due to their large amount of dust, it is usually difficult to probe their star-formation activities.

We therefore carried out NIR Paschen α ($1.875\mu\text{m}$) narrow-band imaging survey of 38 nearby star-forming galaxies by miniTAO/ANIR (Konishi et al. 2015). Thanks to the high altitude (5640m) and dry climate of Co Chajnantor, we have successfully obtained an excellent dataset. The star-formation rates (SFRs) obtained from Paschen α shows a good agreement with those from infrared luminosities, suggesting that Paschen α is a good indicator of SFR (Tateuchi et al. 2015).

Utilizing this dataset, we also probe bulge formation in LIRGs. Recent research found there are two types of bulges at the center of galaxies, one is a “classical bulge” mainly supported by velocity dispersion, and the other is a “pseudobulge” mainly by rotation. They also have many differences such as metallicity, Sersic indices, and age of stellar population, and expected to have undergone different processes; classical bulges may have formed through drastic process such as major mergers, whereas pseudobulges through secular gas inflow. We have applied bulge-disk decomposition analysis to the 20 non-merger LIRGs in our dataset, and obtained Sersic indices of their bulges. Comparing it with the effective radius of star-forming regions obtained from Paschen α images, we have found that classical bulges ($n_b > 3$) has compact star-forming regions within the bulge, whereas pseudobulges ($n_b < 3$) has extended star-forming regions outside of bulges (Tateuchi et al. 2019). These results indicate that classical bulges may have grown through gas inflow to their centers, which may also feed supermassive blackholes (SMBHs) sitting there, and are consistent with Kormendy et al. (2011) that mass of SMBHs correlates well with mass of classical bulges, while not well with pseudobulges.

References

- Konishi, M. et al. 2015, PASJ, 67, 4
 Tateuchi, K. et al. 2015, ApJS, 217, 1
 Tateuchi, K. et al. 2019, PASJ, 71, 64
 Kormendy, J et al. 2011, Nature, 469, 374

5.16.2 Development of Integral Field Unit for SWIMS

Integral field spectroscopy (IFS) is one of the latest observing mode in the optical-NIR wavelength range to obtain spectral information of extended objects. To add this IFS function to SWIMS, we have been developing a compact-size image-slicer type integral field unit (IFU) for it. Its main features are:

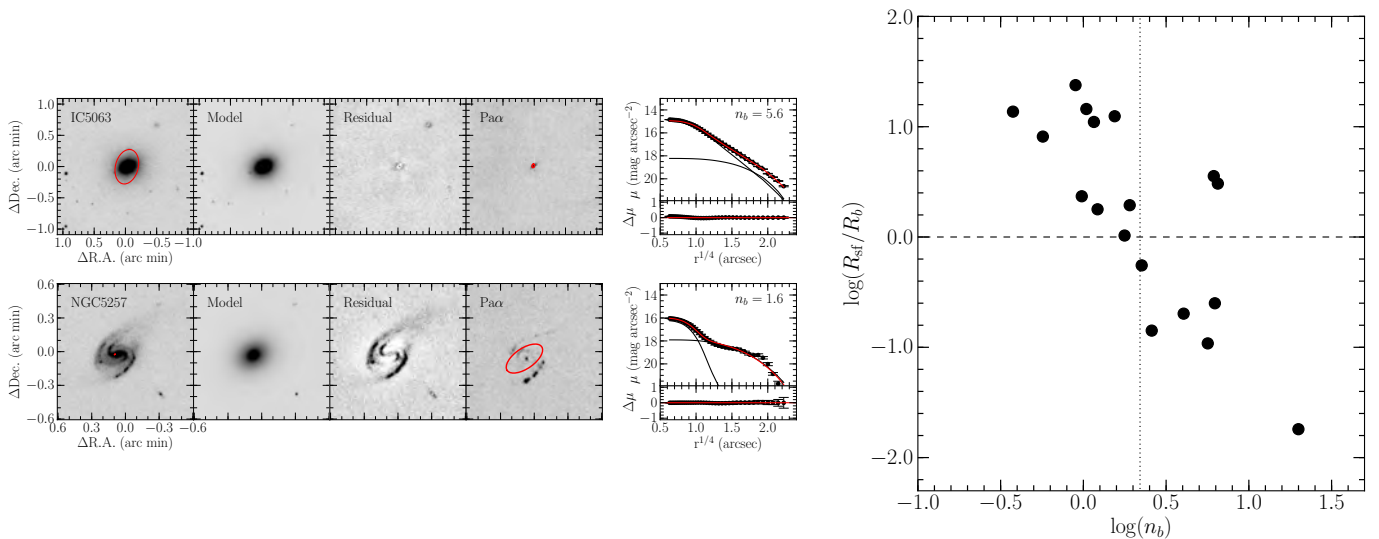


Figure 5.27: Left : A K_s -band image, model image of a bulge and a disk, a residual after the model subtraction, and Pa α emission line images of LIRGs observed. Right : Relation between Sersic indices of bulges (n_b) and ratios between half-light radii of Paschen α and bulge. While classical bulges ($n_b > 3$) show star-formation activities within bulge, pseudobulges show extended star-formation outside of bulges.

- Among the IFU of 6-10m class telescope, it has the largest field of view of $18.4'' \times 13.7''$ sliced into 26 $0.5''$ -width slitlets.
- To handle and store it in multi-object slit exchanger unit (MOSU) of SWIMS, its size is compact as $60\text{mm} \times 170\text{mm} \times 220\text{mm}$, and all the optics is packed in there utilizing some nonspherical surfaces.
- Its optics consists of 26 channels, each having 3 mirrorlet surfaces. To fabricate such complicate optics, we utilize high-precision machining technology in collaboration with RIKEN high-precision group.
- To be used under cryogenic environment, all the components, including mirror-arrays and structures are made of aluminum alloy. Mirror arrays are made of special aluminum RSA6061, which is pore-free aluminum on which optical-quality mirror surfaces can be made my high-precision machining.

We have finished its optical and mechanical design, as well as the development of the key technology, the high precision machining, and currently fabricating the final mirror arrays. We have completed one of the three mirror arrays, the slit-mirror array (S3), currently working on the pupil mirror array (S2). All the components are planned to be completed by 2020, and we expect to assemble and install the IFU in SWIMS in 2021.

References

- Kono, Y. et al. 2018, Proc. SPIE, 10706, 107063F
 Kitagawa, Y. et al. 2016, Proc. SPIE, 9912, 991225
 Kitagawa, Y. et al. 2014, Proc. SPIE, 9151, 91514P



Figure 5.28: Left : Optical layout of SWIMS-IFU. The size of the optics is strongly limited by the dimension of the storage of SWIMS. Middle : Mechanical layout of SWIMS-IFU. Right : Fabricated slit-mirror array (S3).

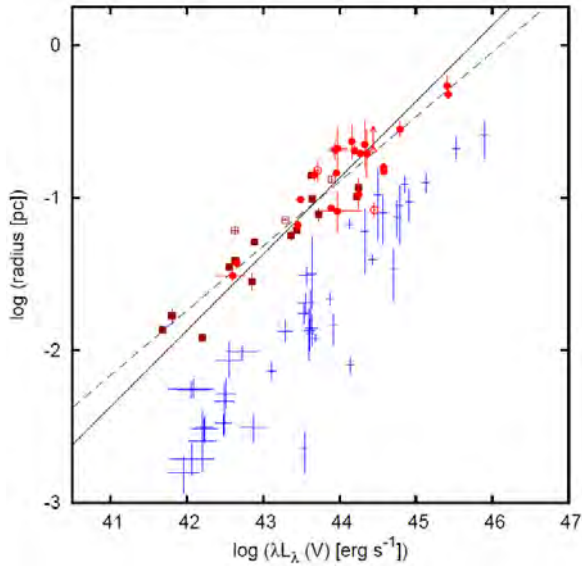


Figure 5.29: The size-luminosity relations for the innermost dust torus (brown and red circles) and a broad emission-line region (blue crosses).

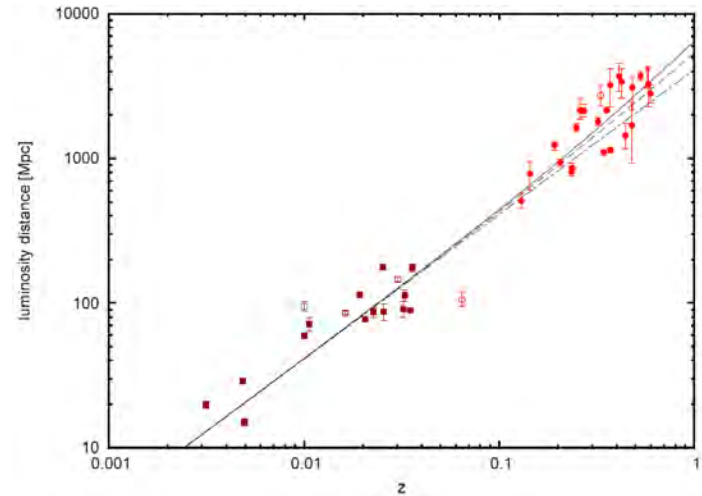


Figure 5.30: The Hubble diagram based on the dust-reverberation distance of AGNs. The solid line represents the standard cosmological model indicating the accelerated expansion of the Universe.

5.17 Takeo Minezaki

5.17.1 Reverberation Mapping of Active Galactic Nuclei

A dust torus is an important structure in an active galactic nucleus (AGN). It is a potential gas reservoir for fueling mass to the accretion disk where the enormous radiation energy of the AGN is produced, and is also a key structure in the unified scheme of AGNs in which the diversity of type 1 and type 2 AGNs is explained by the viewing angle and obscuration by the dust torus. Dust in the torus is illuminated by the strong UV–optical continuum emission from the accretion disk, and it absorbs the radiation energy and then re-radiates it as thermal emission at infrared wavelengths. As a result, the infrared flux variation of an AGN responds to its optical flux variation with a lag corresponding to a light-travel time from the accretion disk to the dust torus. Dust-reverberation mapping analyzes these source and response light curves to investigate the geometrical structure of the dust torus. This is a very unique and important technique because the innermost dust torus cannot be resolved by direct imaging.

A systematic dust-reverberation survey for a number of type 1 AGNs has been performed by the Multicolor Active Galactic Nuclei (MAGNUM) project (PI Yuzuru Yoshii). T. Minezaki played key roles in all aspects of the projects, such as instrumentation, observation, data analysis, interpretation, and student advising. We established a radius–luminosity relation for the innermost dust torus over a range of approximately four orders of magnitude in AGN luminosity, which was found to be consistent with the model prediction assuming radiation equilibrium of dust grains at the innermost dust torus (Figure 5.29). We also presented a direct observational evidence for the AGN unified scheme for the Seyfert type, that is, the reverberation lags of the broad emission lines were found to be smaller than that of the dust torus emission in all luminosity range (Figure 5.29). The initial compilation of the observational results was presented by Suganuma et al. (2006), and the second compilation was presented by Koshida et al. (2014). These results have been cited as baseline results for the inner structure of AGN by many publications and major reviews (282 and 92 citations, respectively). Now, T. Minezaki et al. (2019) presented the latest results for 36 type-1 AGNs, which will take the place of them.

The MAGNUM project also aims to measure the luminosity distance of AGNs to investigate the cosmic expansion. Based on the radius–luminosity relation, the AGN luminosity can be estimated when the dust-torus radius is obtained by reverberation mapping. This is an alternative method to that using Type Ia supernovae (SNe Ia) as a standard candle, which has led the studies of the cosmic expansion so far. Yoshii et al. (2014) built a model for the radiation equilibrium of dust grains in the innermost dust torus to obtain the luminosity distances of AGNs without requiring any distance ladder. They estimated the Hubble constant from these data and found it to be in good agreement with the current standard estimates. Koshida et al. (2017) compared the distance calibration of Yoshii et al. (2014) to the distances of SNe Ia that occurred in the AGN host galaxies and found that they are consistent. Minezaki et al. (2019) estimated the luminosity distances of AGNs at redshifts $z < 0.6$ based on their dust-reverberation lags, and found that the data in the redshift–distance diagram are consistent with the current standard estimates of the cosmological parameters (Figure 5.30). These results indicate that the reverberation distance is a promising new tool for investigating the cosmic expansion.

References

- Minezaki, T. et al. 2019, ApJ, 886, 150
 Koshida, S. et al. 2017, ApJ, 842, L13
 Koshida, S. et al. 2014, ApJ, 788, 159
 Yoshii, Y. et al. 2014, ApJ, 784, L11
 Suganuma, M. et al. 2006, ApJ, 639, 46

5.17.2 Development of Optical Adaptive Optics for Small Telescopes

T. Minezaki has lead development of an optical adaptive optics (AO) system for small telescopes. An AO instrument in optical wavelength mounted on a 1-2 m class telescope located at a good seeing site will make it possible to achieve high angular resolution of 0.1-0.2 arcsec. Such capability will enable us to perform unique astronomical programs such as surveys and monitors of bright objects with high angular resolution, as well as to provide good opportunity in education for both astronomy and engineering.

In order to examine the AO capability on small telescopes, we developed an experimental AO instrument, in which inexpensive commercial devices are extensively used to reduce cost for development. We designed the weight and the physical size so small that it is portable and easy to be mounted on a small telescope, which is a unique feature of our AO instrument. In collaboration with staff in Hiroshima University and University of Hyogo, we mounted it on 1.5-m Kanata telescope and 2.0-m Nayuta telescope to perform engineering observations in 2016.

Then, in collaboration with staff in Pontificia Universidad Católica de Chile and Universidad Católica del Norte, we mounted it on the 1-m telescope of the European Southern Observatory of La Silla in Chile in March 2018 to examine the performance at good seeing sites. We found that there were approximately 4 times and 5 times improvements in the full-width-half-maximum (FWHM) and Strehl ratio of the PSF from the natural seeing, respectively. The best AO-corrected PSF obtained during the observation achieved FWHM=0.18 arcsec and the Strehl ratio = 0.18. Based on the detailed analysis of the time-series wavefront and deformable-mirror-operation data, further improvement in AO performance is expected by adjusting the system parameters. We succeeded in demonstrating the feasibility of an inexpensive optical AO system for small telescopes.

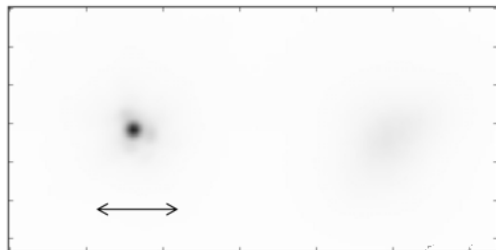


Figure 5.31: The obtained stellar images (colored darker when brighter). The left side shows the image corrected by the AO system, and the right side shows the uncorrected image. The arrow represents the angular size of 1 arcsec.

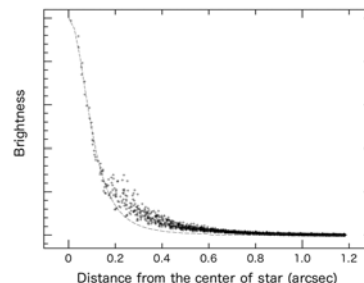


Figure 5.32: The radial brightness profile of the stellar image corrected by the AO system. The full width at half maximum of the stellar image is 0.18 arcsec, close to the angular resolution of the diffraction limit of 0.16 arcsec.

5.18 Toshihiko Tanabé

5.18.1 Search for the MOLsphere

Tsuji et al. (1997) found 2.5 and 2.7 μm H_2O absorption in β Peg (M2III) by the observations with *Infrared Space Observatory* (ISO). Because the temperature of the photosphere of M2 star is too high for H_2O to form there, they concluded that H_2O molecules must be located above the photosphere. Such a ‘quasi-static circumstellar envelope’ or the MOLsphere (coined by Tsuji 2000) is later confirmed geometrically by many high-spatial and/or high-spectral resolution observations (for example, Ohnaka et al. 2019) in K to M giant stars, Mira variable stars and red supergiant stars. The MOLsphere is thought to be related to the driving mechanism of the mass loss process in red giant stars, which is one of the long-standing unresolved issues. We started to search for the MOLsphere photometrically.

Thanks to the altitude of TAO site (5640m), a new atmospheric window around 1.9 μm appears. This provides us a unique opportunity to observe H_2O molecular band in stars at 1.9 μm (Ω band). Using the Near-Infrared Camera (ANIR) attached to the miniTAO 1-m telescope at TAO site, we made imaging observations of stars with known spectral type (M-type). ANIR is equipped with 1.875 μm and 1.910 μm narrow band filters as well as normal J , H and K_s bands and colors such as $m_{1.875} - K_s$ and $m_{1.910} - K_s$ can be used as water index.

We chose M-type stars in the fields of the SMC and LMC from the list of Blanco et al. (1980) and Frogel & Blanco (1990). Galactic M-type stars with known spectral type are too bright in the near-infrared even for 1-m telescope. We observed 5 SMC stars and 87 LMC stars. From their luminosities, they are all thought to be in the AGB. Fig. 5.33 left shows water index, $m_{1.910} - K_s$ against spectral type. Stars with large water index have strong H_2O absorption around 1.9 μm and are candidates of the star with MOLsphere. We also plot the same index vs. $J - K_s$ color in Fig. 5.33 right. We can see a general tendency that the water index increases with $J - K_s$ color between $0.0 < m_{1.910} - K_s < 0.2$. This is interpreted that photospheric water absorption increases toward red, cooler stars. We calculated synthetic colors using MARCS models ($Z = -0.5$ and $\log g = 0.5$) to check the photospheric water absorption. Red dotted line indicates photospheric colors from 4000 K to 3000 K. For photospheric component (color index 0.0–0.2), there is a good agreement between observed colors and theoretical photospheric ones. Therefore, stars with color index larger than ~ 0.3 are not explained by the photospheric water and are indicative of non-photospheric water, i.e. the MOLsphere. Our survey shows that the MOLsphere can be detected photometrically from TAO site and that stars with MOLsphere exist even in the low metallicity environment, such as the LMC and SMC.

References

- Blanco V.M., McCarthy M.F. Blanco B.M., 1980, ApJ, 242, 938
 Frogel J.A. Blanco V.M., 1990, ApJ, 365, 168
 Ohnaka K., Hadjara M., Maluenda Berna M. Y. L., 2019, A&A, 621, A6
 Tsuji T., Ohnaka K., Aoki W., Yamamura I., 1997, A&A, 320, L1
 Tsuji T., 2000, ApJ, 540, L99

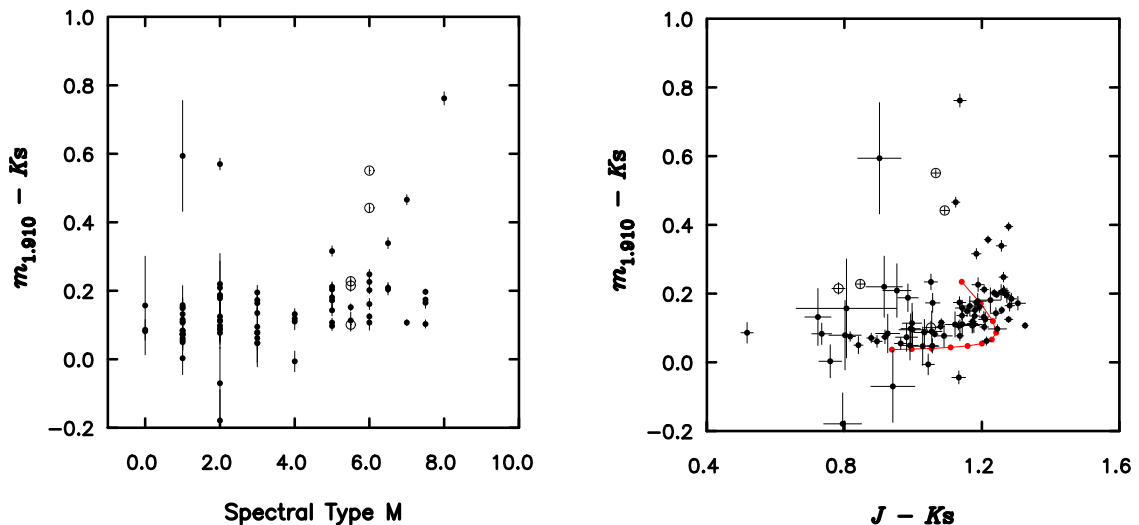


Figure 5.33: Left: $m_{1.910} - K_s$ vs. spectral type. Open circles are SMC stars while black dots are LMC stars. Right: $m_{1.910} - K_s$ vs. $J - K_s$. Red dotted line is synthetic colors calculated using MARCS models.

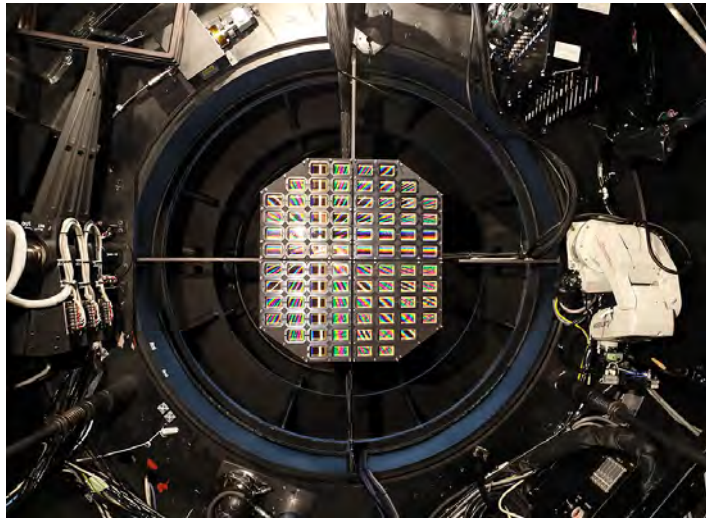


Figure 5.34: Tomo-e Gozen camera with 84 chips of CMOS sensors mounted on the prime focal plane of the Kiso Schmidt telescope.

5.19 Shigeyuki Sako

5.19.1 Development of Tomo-e Gozen: Kiso Wide-field Video Observation System

Tomo-e Gozen is an optical wide-field video observation system with a mosaic CMOS camera on the Kiso 105-cm Schmidt telescope and intelligent observation software. The camera is capable to take consecutive images in 2 fps maximum with a field-of-view of 20 deg^2 by 84 chips of $2\text{k} \times 1\text{k}$ CMOS image sensors (Figure 5.34). The low read noise and low dark current allow us to operate them in a non-vacuum system without mechanical coolers and realize a large and lightweight focal plane unit. The camera is directly connected to an onsite computing system with 200 CPU cores, 1 PB storage, and 10 Gbps networks. Since a size of obtained video data is too large, 30 TB night^{-1} , to keep them for a long time on site, they are deleted from the storage in seven days. Real-time data reduction software with several machine learning techniques implemented produces stacked images and photometry tables and saves them in a long-term storage before the raw data are deleted. The reduction software also mines attractive information including fast-moving and rapidly variable objects in the sky-big-data. Control software automatically arranges an efficient survey and reoptimizes it according to changing weather conditions and additional information on targets. Over 100 nights every year, Tomo-e Gozen carries out a monochromatic video survey over $7,000 \text{ deg}^2$ with more than three visits in a night. This survey enables us to detect transient phenomena brighter than 18th mag, including those with short timescales of 1 second to 1 hour. We started a development of a prototype model of the Tomo-e Gozen camera with 8 chips of CMOS sensor in 2013 and completed it in 2015 (Sako et al. 2016). After performance evaluations on the Kiso Schmidt telescope, a development of the Tomo-e Gozen camera with 84 CMOS sensors and the computing system were started in 2015 and completed in Oct. 2019.

References

- Sako, S. et al. 2018, SPIE, 10702, 107020J 17pp (invited)
 Sako, S. et al. 2016, SPIE, 9908, 99083P 15 pp.

5.19.2 Observations of the solar system small bodies with Tomo-e Gozen

A large part of small NEOs remain to be discovered. According to the estimate of Harris (2010), almost 99.9% of the NEO smaller than 140m have not been observed yet. This situation should be improved in order to characterize the small bodies around the Earth as well as in terms of the planetary defense. Small NEOs become sufficiently bright to be observed only in the vicinity of the Earth. A close asteroid, however, moves fast. Such fast apparent speed hampers a systematic and efficient survey of small NEOs. A video survey with Tomo-e Gozen have the advantage of detecting fast-moving objects ($\sim 1'' \text{ s}^{-1}$) over other large surveys. S. Sako and R. Ohsawa have launched a survey of fast-moving NEOs as small as 20 m with Tomo-e Gozen. Fast-moving NEOs have been extracted from enormous survey big data with a specially-developed algorithm supported by a machine learning technique. Kojima et al. (2019) successfully discovered a NEO 2019FA in April 2019. Two more small NEOs have been discovered in 2019 (*e.g.*, Beniyama et al. 2019). S. Sako demonstrated the advantage of Tomo-e Gozen in detecting small NEOs. About 100 NEOs smaller than 20 m are expected

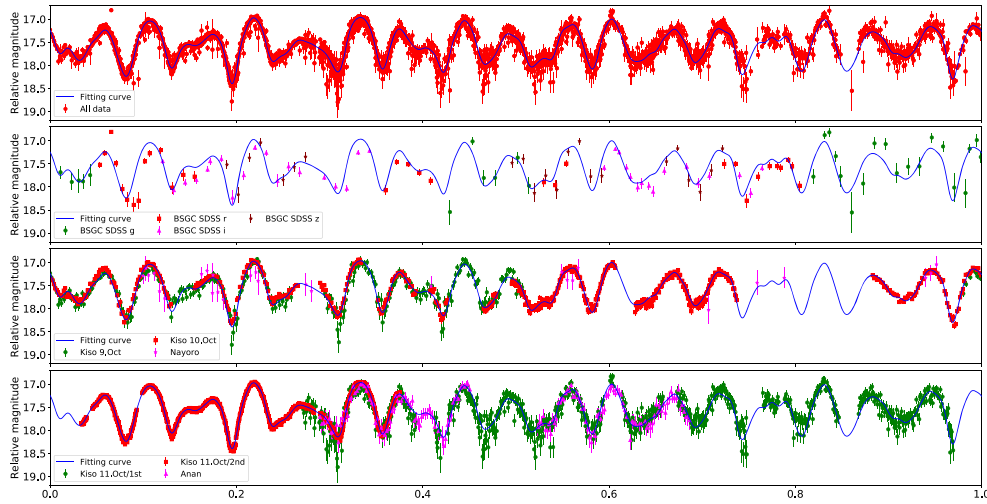


Figure 5.35: The light curves of 2012 TC₄, adopted from Urakawa et al. (2019). The data obtained with Tomo-e Gozen are illustrated in the red square symbols in the bottom two panels.

to be detected in the survey with Tomo-e Gozen.

Urakawa et al. (2019) performed observations of a near-Earth object (NEO), 2012 TC₄ in optical and near-infrared. The NEO 2012 TC₄ approached close to Earth at a distance of about 50,000 km in 2017 October. This close approach provided a practical exercise for planetary defense. This apparition was also an appropriate opportunity to investigate 2012 TC₄, which is a monolithic asteroid. S. Urakawa conducted the observation campaign of 2012 TC₄ using six telescopes. The high time resolution light curves of 2012 TC₄ were provided with Tomo-e Gozen. The light curves are illustrated in Figure 5.35. The shape and rotational motion models of 2012 TC₄ were derived from the analysis of the light curves. Assuming that 2012 TC₄ was a triaxial ellipsoid rotating in the long-axis mode, the rotational and precession periods were 8.47 ± 0.01 minutes and 12.25 ± 0.01 minutes, respectively. This indicates that 2012 TC₄ is a tumbling and monolithic asteroid. Plausible axial lengths were $6.2 \times 8.0 \times 14.9$ m or $3.3 \times 8.0 \times 14.3$ m. The flattened and elongated shape indicates that 2012 TC₄ is a fragment produced by an impact event. The impact event happened within $\sim 3 \times 10^5$ yr, suggesting that 2012 TC₄ has a fresh surface.

References

- Beniyama, J. et al. 2019, MPEC, 2019-V87
 Harris, 2010, Proc. the International Conference “Asteroid-Comet Hazard 2009”, 312
 Kojima, Y. et al. 2019, MPEC, 2019-F19
 Urakawa, S. et al. 2019, AJ, 157, 155

5.19.3 Observations of faint meteors with Tomo-e Gozen

The Earth is surrounded by small dust grains produced by comets and asteroids. Tons of such grains plunge into the Earth’s atmosphere hourly. Part of their kinetic energy excites and ionizes the surrounding atmosphere, which is observed as a meteor phenomenon. Optical observation of meteors is an effective tool to constrain the size distribution of interplanetary dust particles around the Earth. Ohsawa et al. (2019a) reported imaging observations of faint meteors on April 11 and 14, 2016 with a prototype camera of Tomo-e Gozen, Tomo-e PM, mounted on the 105-cm Schmidt telescope. Tomo-e PM can monitor a sky of 1.98 deg^2 at 2 Hz. The numbers of detected meteors are 1514 and 706 on April 11 and 14, respectively. The detected meteors are attributed to sporadic meteors. Their absolute magnitudes range from +4 to +10 mag in the V-band, corresponding to about 8.3×10^2 to 3.3×10^4 g in mass. The present magnitude distributions were well explained by a single power-law luminosity function with a slope parameter $r = 3.1 \pm 0.4$ and a meteor rate $\log_{10} N_0 = -5.5 \pm 0.5$. The results demonstrated a high performance of telescopic observations with a wide-field video camera to constrain the luminosity function of faint meteors.

Radar and optical simultaneous observations of meteors are important to understand the size distribution of the interplanetary dust. Faint meteors detected by high power large aperture radar observations have not, however, been detected until recently in optical observations, mainly due to insufficient sensitivity of the optical observations. R. Ohsawa et al. (2019b) conducted two radar and optical simultaneous observations. The first observation was carried out in 2009–2010 using Middle and Upper Atmosphere Radar (MU radar) and an image-intensified CCD camera. The second

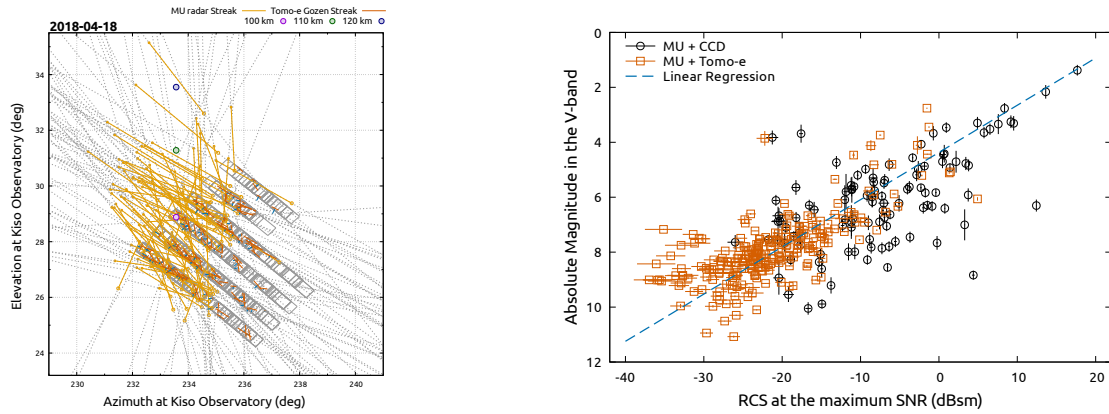


Figure 5.36: (*left*): Figure 1 of Ohsawa et al. (2019b), where simultaneous meteors detected on April 18 are shown in the altitude-azimuth coordinate; (*right*): Figure 5 of Ohsawa et al. (2019b), illustrating a relationship between the radar cross section and the optical magnitude.

observation was carried out in 2018 using the MU radar and a mosaic CMOS camera, Tomo-e Gozen, mounted on the 1.05-m Kiso Schmidt Telescope. The left panel of Figure 5.36 illustrates the meteors simultaneously detected in radar and optical. In total, 332 simultaneous meteors were detected. The relationship between radar cross sections and optical V -band magnitudes was well approximated by a linear function (the right panel of Figure 5.36). A transformation function from the radar cross section to the V -band magnitude was derived for sporadic meteors. The transformation function was applied to about 150,000 meteors detected by the MU radar in 2009–2015, large part of which are sporadic, and a luminosity function was derived in the magnitude range of -1.5 – 9.5 mag. The luminosity function was well approximated by a single power-law function with the population index of $r = 3.38 \pm 0.08$. The present observation strongly indicates that the MU radar has capability to detect interplanetary dust of 10^{-4} – 10^1 g in mass as meteors.

References

- Ohsawa, R. et al. 2019a, P&SS, 165, 281
 Ohsawa, R. et al. 2019b, P&SS, submitted

5.19.4 Development of data-driven approaches toward astronomical big data

Optical wide-field surveys with a high cadence are expected to create a new field of astronomy, so-called “movie astronomy,” in the near future. The amount of data from the observations will be huge, and hence efficient data compression will be indispensable. Morii et al. (2017) proposed a low-rank matrix approximation with sparse matrix decomposition as a promising solution to reduce the data size effectively while preserving sufficient scientific information. M. Morii et al. (2019) apply one of the methods to the movie data obtained with the prototype model of the Tomo-e Gozen mounted on the 1.0 m Schmidt telescope of Kiso Observatory. Once full-scale observation with the Tomo-e Gozen commences, it will generate ~ 30 TB of data per night. M. Morii demonstrated that the data are compressed by a factor of about 10 in size without losing transient events like optical short transient point sources and meteors. The intensity of point sources can be recovered from the compressed data. The processing runs sufficiently fast, compared with the expected data-acquisition rate in the actual observing runs.

Chopping observations with a tip-tilt secondary mirror have conventionally been used in ground-based mid-infrared observations. However, it is not practical for next generation large telescopes to have a large tip-tilt mirror that moves at a frequency larger than a few hertz. Ohsawa et al. (2019) has proposed an alternative observing method, a “slow-scanning” observation. Images are continuously captured as a video, while the field of view is slowly moved. The signal from an astronomical object is extracted from the movie data by a low-rank and sparse matrix decomposition. The performance of the “slow-scanning” observation was tested in an experimental observation with Subaru/COMICS. The quality of a resultant image in the “slow-scanning” observation was as good as in a conventional chopping observation with COMICS, at least for a bright point-source object. The observational efficiency in the “slow-scanning” observation was better than that in the chopping observation. The results suggest that the “slow-scanning” observation can be a competitive method for the Subaru telescope and be of potential interest to other ground-based facilities to avoid chopping.

References

- Morii, M. et al. 2017, ApJ, 835, 1

Ohsawa, R. et al. 2018, ApJ, 857, 37

5.20 Tomoki Morokuma

5.20.1 Electromagnetic Counterpart Identification of Gravitational Wave Sources

The Advanced Laser Interferometer Gravitational-wave Observatory (LIGO) detectors started the first observing run (O1) from September 2015 and conducted its second observing run (O2) in 2016-2017. We have organized an observing group to conduct systematic follow-up observations with Japanese telescopes (J-GEM; Japanese Collaboration for Gravitational-Wave Electro-Magnetic Follow-up; PI: Prof. M. Yoshida in NAOJ/Subaru Telescope). M. Doi, K. Motohara, S. Sako, T. Morokuma, R. Ohsawa, and Y. Niino joined the J-GEM collaboration mainly for conducting wide-field surveys with Kiso Schmidt telescope.

The first gravitational wave (GW) source GW150914 was detected as a binary black hole coalescence (Abbott et al. 2016a) and we made follow-up imaging observations in optical wavelengths with the Kiso Schmidt telescope in Japan and B&C telescope in New Zealand (Abbott et al. 2016b; Morokuma et al. 2016).

In the final one month of O2, the Virgo detector in Europe joined the GW observations and the three detectors were operated in August 2017. They detected a gravitational wave, GW170817, from a binary neutron star coalescence (Abbott et al. 2017). A Chilean telescope discovered a likely counterpart close to a nearby galaxy NGC 4993 (40 Mpc distance from the Sun). We conducted optical and near-infrared imaging observations with the Subaru, IRSF, MOA-II, and B&C telescopes and obtained multi-band light curves over ~ 2 weeks. The object showed 2.5 mag decline in z -band for the first 1 week after the coalescence, indicating that the object is very different from supernovae. The color also got redder. These properties are consistent with expectation for a kilonova that is powered by the radioactive decay of newly synthesized r -process nuclei. Compared with theoretical models for kilonovae, we found kilonova models with Lanthanide elements can reproduce the the observed properties well, suggesting that r -process nucleosynthesis beyond the second peak takes place. The object was brighter than originally expected, indicating more ejecta mass or additional energy source. These are expected to be understood by observations of more events in the 3rd observing run (O3; currently being conducted) and future observing runs.

In the 3rd observing run (O3) starting from April 2019, the UT group is conducting systematic follow-up observations with Tomo-e Gozen (20 deg² field-of-view; Sako et al. 2018) on the 1.05-m Kiso Schmidt telescope for detected gravitational sources if the weather permits. As of Nov. 30, we carried out imaging observations for 12 events among ~ 40 GW events (Murata et al. 2019; Tanaka et al. 2019; Niino et al. 2019; Kawabata et al. 2019).

References

- Abbott, B. P. et al. 2016a, ApJ, 826, 13
 Abbott, B. P. et al. 2016b, ApJS, 225, 8
 Morokuma, T. et al. 2016, PASJ, 68, 9
 Yoshida, M. et al. 2017, PASJ, 69, 9
 Utsumi, Y. et al. 2017, PASJ, 69, 101
 Tanaka, M. et al. 2017, PASJ, 69, 102
 Utsumi, Y. et al. 2018, PASJ, 70, 1
 Tominaga, N. et al. 2018, PASJ, 70, 28
 Sako, S. et al. 2018, SPIE, 10702, 107020J
 Kawabata, K. S. et al. 2019, GCN, 24350, 1
 Niino, Y. et al. 2019, GCN, 24299, 1
 Tanaka, M. et al. 2019, GCN, 24113, 1
 Murata, K. L. et al. 2019, GCN, 24064, 1

5.20.2 Electromagnetic Counterpart Identification of High-Energy Neutrino Sources

Observational studies on high-energy neutrinos have attracted much attention, especially in terms of identification of its origin. This is important to understand the diffuse emission of the high-energy cosmic neutrinos. The first identification except for the Sun and supernova 1987A was achieved for IceCube-170922A (IceCube Collaboration et al. 2018). Motivated by a discovery of rapid near-infrared variability of a BL Lac-type blazar by our group using 1.5-m Kanata telescope, intensive multi-wavelength observations including optical spectroscopic observations to determine the redshift to the blazar were carried out (Tanaka et al. 2017). These include our own imaging observations with the 1.05-m Kiso Schmidt telescope and 3 other domestic telescopes, polarimetric observations with the 1.5-m Kanata telescope (Yamanaka et al. 2018), and spectroscopic observations with the 8.2-m Subaru (Morokuma et al. 2017) and Gemini telescopes. After careful examination of the Fermi/LAT γ -ray data of other blazars, we found that TXS 0506+056 is likely to be the origin of the neutrino with 3.1σ significance.

References

- IceCube Collaboration et al. 2018, *Science*, 361, 1378
 Morokuma, T. et al. 2017, *The Astronomer's Telegram*, 10890
 Tanaka, Y. T. et al. 2017, *The Astronomer's Telegram*, 10791
 Yamanaka, M. et al. 2018, *The Astronomer's Telegram*, 11489

5.20.3 Effective Selection of Low-Mass Black Holes via Optical Rapid Variability

We proposed a new method for effectively selecting objects which may be low-mass active black holes (BHs) at galaxy centers using high-cadence optical imaging data. One candidate was successfully identified to be an active $2.7 \times 10^6 M_{\odot}$ BH at $z = 0.164$. This active BH was originally selected due to its rapid optical variability, from a few hours to a day, based on Subaru Hyper Suprime-Cam g-band imaging data taken with a 1 hour cadence. Broad and narrow H α lines and many other emission ones are detected in our optical spectra taken with Subaru FOCAS, and the BH mass is measured via the broad H α emission line width ($1,880 \text{ km s}^{-1}$) and luminosity ($4.2 \times 10^{40} \text{ erg s}^{-1}$) after careful correction to the atmospheric absorption around 7580-7720Å. The Eddington ratio and find it to be as low as 0.05, considerably smaller than those in a previous SDSS sample with similar BH mass and redshift, which indicates one of the special potentials of our Subaru survey. The $g - r$ color and morphology of the extended component indicate that the host galaxy is a star-forming galaxy. We also show the effectiveness of our variability selection for low-mass active BHs.

References

- Morokuma, T. et al. 2016, *PASJ*, 68, 40

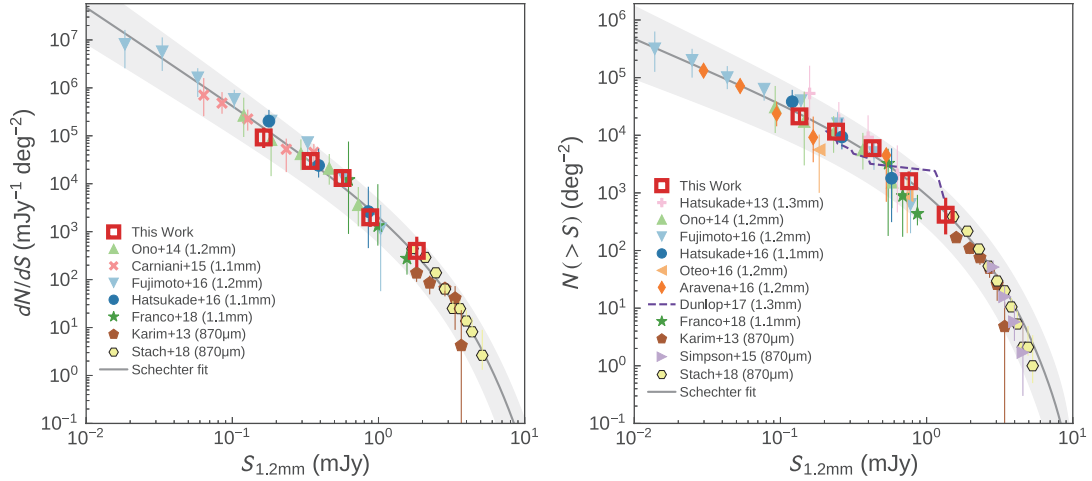


Figure 5.37: Differential and cumulative number counts at 1.2 mm (Hatsukade et al. 2018)

5.21 Bunyo Hatsukade

5.21.1 A Census of the Population of Faint Submillimeter Sources

In order to reveal the origin of the extragalactic background light (EBL) at millimeter/submillimeter (mm/submm) wavelengths, it is essential to study fainter submm populations ($S_{1\text{mm}} < 1$ mJy). ALMA enables us to explore fainter submm sources compared to previous single-dish surveys because of its high sensitivity and high angular resolution. Based on the ensemble of serendipitously detected sources in ALMA observations, we successfully constrained the faint end of 1.3 mm number counts (Hatsukade et al. 2013). The flux range probed in the study is more than an order of magnitude fainter than previous studies. We found that $>50\%$ of the EBL is resolved into discrete sources, making a breakthrough compared to the previous results of 10%–20%.

We conducted “unbiased” surveys of submm sources in the Subaru/XMM-Newton Deep Survey Field (SXDF-ALMA) to obtain a census of the population of faint submm sources. We derived number counts in the flux range of 0.2–2 mJy by using 23 sources detected in a continuous 2-arcmin² area of the SXDF (Hatsukade et al. 2016). This is the first blank-field survey in a continuous area by using ALMA.

To obtain a larger map and sample, we also conducted the ALMA twenty-six arcmin² survey of GOODS-S at one millimeter (ASAGAO). ASAGAO is a 1.2 mm deep and wide area (26 arcmin²) survey on a contiguous field, which provides the largest sample of sources (45 sources at 4.5σ) among ALMA blank-field surveys (Hatsukade et al. 2018). Multi-wavelength analysis of the ASAGAO sources found that the median redshift is 2.4 and they are located on the massive end of the main sequence. We created IR luminosity functions (LFs) at $z = 1\text{--}3$, and constrain the faintest luminosity of the LF at $2 < z < 3$. The LFs are consistent with previous results based on other ALMA and SCUBA-2 observations, which suggests a positive luminosity evolution and negative density evolution with increasing redshift. We found sources without counterparts in deep H and K -band images, whose spectral energy distributions suggest that they are at $z \geq 3\text{--}5$. Their contribution to the cosmic SFR density can be consistent with or larger than that of bright SMGs, demonstrating the importance of ALMA unbiased survey for detecting dust-obscured star formation activity in the early universe, which has been missed in previous optical/NIR surveys (Yamaguchi et al. 2019).

References

- Hatsukade, B. et al. 2013, ApJL, 769, 27
Hatsukade, B., Kohno, K. et al. 2016, PASJ, 68, 36
Hatsukade, B., Kohno, K. et al. 2018, PASJ, 70, 105
Yamaguchi, Y., Kohno, K., Hatsukade, B. et al. 2019, ApJ, 878, 73

5.21.2 Host Galaxies of Gamma-ray Bursts (GRBs) and Superluminous Supernovae (SLSNe)

Molecular Gas in the Host Galaxies of GRBs

Long-duration gamma-ray bursts (GRBs) are associated with the explosions of massive stars. Due to the short lifetime of massive stars, GRBs are thought to trace galaxies with ongoing star formation. Because GRBs are bright enough to be observable in the cosmological distances, they are expected to be a new tool to probe the star-forming activity in the distant universe. However, it is still a subject of debate whether GRBs can be used as an unbiased tracer of star formation. It is important to understand the environment of GRBs by studying their host galaxies. Observations of molecular gas, the fuel of star formation, is essential to understand the properties of host galaxies.

We have been working on CO search toward GRB hosts. We successfully detected for the first time in GRB hosts, and derived molecular gas mass, star-formation efficiency, and spatial distribution of molecular gas and dust (Hatsukade et al. 2014). We conducted a pioneering work and achieved a breakthrough in this research field, which has opened a new door for studying GRB environments in terms of molecular gas. Recently we detected two CO transitions in a $z = 2$ GRB host by using VLA and ALMA, which makes the host the first case in GRB hosts with more than two CO transitions together with the results in the literature, allowing us to examine excitation conditions in GRB hosts (Hatsukade et al. 2019). We are extending this research to increase the sample (>20) for statistical studies (Hatsukade et al. 2019, ApJ, submitted).

References

- Hatsukade, B. et al. 2014, Nature, 510, 247
 Hatsukade, B. et al. 2019, ApJ, 876, 91

Obscured Star Formation in the Host Galaxies of SLSNe

SLSNe are extremely luminous explosions with peak absolute magnitudes of ≤ -21 mag, which are ~ 10 – 100 times brighter than ordinary Type Ia and core-collapse SNe. They are detected at high redshifts ($z \sim 4$), and therefore can be powerful indicators of environments in the distant universe. The physical nature of the progenitor of SLSNe is still a matter of debate. In order to constrain the progenitor models, it is essential to understand the properties of their host galaxies. An important factor to consider is the effect of obscuration by dust. The observations of SLSN hosts have been made exclusively in the UV/optical wavelengths, which are subject to dust extinction in contrast to longer wavelengths, and it is possible that we are missing dust-obscured star formation in SLSN hosts.

We conducted 3-GHz radio continuum observations of the eight host galaxies of SLSNe at $0.1 < z < 0.3$ by using VLA and found that three host galaxies have an excess in radio SFRs by a factor of >2 , suggesting the existence of dust-obscured star formation, which cannot be traced by optical studies (Hatsukade et al. 2018). Our radio observations also place a constraint on a pulsar-driven SN model, which predicts quasi-steady synchrotron radio emission. Because the radio emission is predicted to reach its peak at around 10 years after the explosion, long-term follow-up observations are important. We demonstrated that radio observations are a powerful tool to constrain theoretical models of SLSNe.

References

- Hatsukade, B. et al. 2018, ApJ, 857, 72

5.21.3 Commissioning of a New 2-mm Receiver and Spectrometer System on LMT

The Large Millimeter Telescope (LMT) is a 50-m diameter telescope situated on the summit of Sierra Negra at an altitude of 4600 meters in Mexico. We have carried out a project of installing a new 2-mm heterodyne receiver and spectrometer system (“B4R”). I have been involved in this project as a Project Scientist since 2018, and conducted planning of commissioning, test observations, and initial science sessions. We successfully detected molecular lines from galactic and extragalactic objects (including lensed SMGs at $z = 2$ – 3) at the test observations in 2018 and 2019.



Figure 5.38: LMT (left) and the B4R receiver (right).

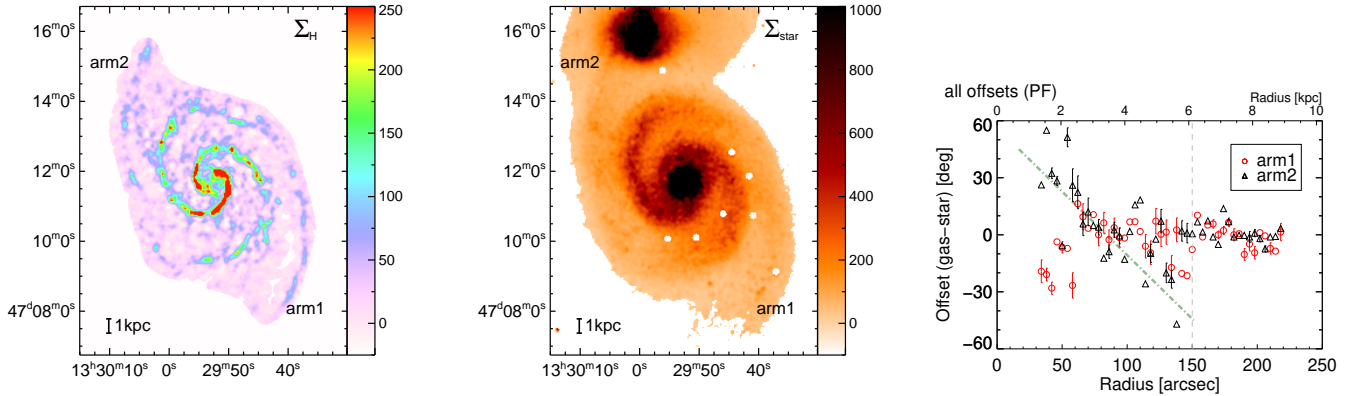


Figure 5.39: (Left and Middle) Gas and stellar mass distribution in M 51. (Right) Gas-star offset against radius for the two arms. Only the inner part of arm2 is consistent with the steady arm model (green dot-dashed line).

5.22 Fumi Egusa

5.22.1 Lifetime of Spiral Arms in Nearby Galaxies

In the local universe, more than half of galaxies are categorized as spiral galaxies (e.g. Delgado-Serrano et al. 2010). However, we do not have a conclusive answer to the very fundamental question: “*What is the nature of spiral arms?*” A number of theoretical models have been proposed, but here we focus on their lifetimes: steady (long-lived) or dynamic (short-lived).

Baba et al. (2015) performed numerical simulations of disk galaxies with steady and dynamic spiral arms, and found that the location of gas spiral arms (relative to stellar arms) is different between the two models. Based on this theoretical study, F. Egusa and collaborators investigated gas-star offsets in the nearby grand-design spiral galaxy M 51 (Egusa et al. 2017; Fig. 5.39), and found that its two spiral arms exhibit different offset dependences against radius. One arm is consistent with a steady arm, while the other is consistent with a dynamic arm. We deduce that this difference is likely due to a tidal interaction with the companion galaxy (Pettitt et al. 2018).

We now aim to extend this research to other nearby spiral galaxies with a variety of spiral arm properties, such as barred spirals, multi-armed spirals. Because the above analysis requires a spatially resolved stellar mass distribution, we have been working on applying the SED fitting code CIGALE (Boquien et al. 2019) to multi-wavelength high-resolution images. Once we establish the methodology, we will be able to (i) measure locations of stellar arms; (ii) measure gas-star offsets; and (iii) deduce the lifetime of the spiral arms, for tens of nearby spiral galaxies. It will be an important result to understand a relationship between the nature of spiral arms and other physical properties.

This project has been supported by KAKENHI 17K14259.

References

- Baba, J. et al. 2015, PASJ, 67L, 4
- Boquien, M. et al. 2019, A&A, 622, 103
- Delgado-Serrano, R. et al. 2010, A&A, 509, 78
- Egusa, F. et al. 2017, MNRAS, 465, 460
- Pettitt, A. R. et al. 2018, MNRAS, 480, 3356

5.22.2 Molecular Gas and Star Formation in the Nearby Barred Spiral Galaxy NGC 1365

NGC 1365 is the nearby ($D = 18.1$ Mpc) barred spiral galaxy with a star forming ring around a Seyfert 1.8 nucleus. F. Egusa and Yulong Gao (a visiting student from University of Science and Technology of China, from Sep. 2019 to Aug. 2020) use ALMA data to investigate molecular gas properties in this galaxy. With an angular resolution of $\sim 2''$ (corresponding to ~ 180 pc), galactic structures within the field of view (e.g. center, bar, bar-arm transition) are clearly resolved. We find that molecular gas is mostly confined to leading edges of the bar, forming a ring-like structure in the center, while the emission is rather faint in the bar-arm transition.

R_{21} : CO(2–1)/CO(1–0) ratio

CO is the most abundant molecular species after H_2 , and thus has been used as a tracer of molecular gas. While CO($J=1-0$) has been regarded as a tracer of bulk cold molecular gas, CO($J=2-1$) has come to be similarly popular because of the high sensitivity of ALMA. Recently, it is a common strategy to assume that the ratio between the two transitions is constant (e.g. $R_{21} = 0.7$; Sun et al. 2018) for deriving the H_2 mass. However, it is clear that R_{21} depends on physical conditions such as density and temperature.

Koda et al. (2012) presented its spatial variation at a kpc scale in M 51. In this spiral galaxy, R_{21} tends to be higher at the downstream side of spiral arms, suggesting the impact of star formation on R_{21} . They also found high R_{21} where star formation is not active, which might trace dense gas before star formation.

In NGC 1365, we find that overall structures traced by the both CO transitions are similar, but R_{21} varies significantly within the FoV. Our preliminary investigation suggests that the variation is much larger than that is found in M 51, which likely reflects the difference of spatial resolution. We compare the R_{21} map with the GALEX NUV map which traces young stars, and find that the scatter of R_{21} is large where NUV is faint while R_{21} slightly increases with NUV where NUV is bright. As for the M 51 case, we deduce that high R_{21} with low NUV corresponds to dense gas without (or before) star formation, and high R_{21} with high NUV corresponds to warm gas due to recent star formation. We are now working on the absolute flux calibration of ALMA data and deriving the extinction-corrected SFR to finalize our conclusion.

Star formation and young massive star clusters

Y. Gao is leading the investigation of star formation activity in the bar and central ring in NGC 1365. With ALMA CO data and optical IFU images from VLT/MUSE (Venturi et al. 2018), we can derive a number of physical properties such as stellar mass, SFR, gas mass, and SFE.

Based on the ALMA radio continuum images, we find several bright star forming regions along the bar leading edge and in the ring. The extinction map from VLT/MUSE data suggests that some of the regions are highly embedded. As the SFE is also high for these regions, we deduce that they are in the very young stage of massive star clusters (e.g. Sakamoto et al. 2007). We are now investigating the impact of large-scale gas dynamics for triggering the star formation. One possibility is the gas streaming motion along the bar that can accumulate gas in the central region (Elmegreen et al. 2009). Another is outflow from the nucleus that can increase gas density at the interface to ambient ISM, i.e. positive AGN feedback. Using the tilted-ring model (Di Teodoro et al. 2015), we try to distinguish these two possibilities based on molecular gas dynamics.

References

- Di Teodoro, E. M. and Fraternali, F. 2015, MNRAS, 451, 3021
 Elmegreen, B. et al. 2009, ApJ, 703, 1297
 Koda, J. et al. 2012, ApJ, 761, 41
 Sakamoto, K. et al. 2007, ApJ, 654, 782
 Sun, J. et al. 2018, ApJ, 860, 172
 Venturi, G. et al. 2018, A&A, 619, 74

5.22.3 Molecular Gas Properties in the Nearby Barred Spiral Galaxy M 83 from PDF Analysis

We have obtained CO(1–0) data toward the nearby ($D = 4.5$ Mpc) barred spiral galaxy M 83 (NGC 5236) using ALMA and NRO 45m Telescope (Hirota et al. 2018). With the combination of interferometer and single-dish telescope, the CO data achieved both high angular resolution ($2'' \sim 40$ pc) and high fidelity.

F. Egusa led an analysis with a “probability distribution function (PDF)” technique (Egusa et al. 2018). A PDF is simply a histogram of a physical property or observed quantity. This technique thus has an advantage over “clump

find” technique in which clump properties depend on how clumps are defined and gas components outside the clumps are excluded for further discussion. In the observed area of M 83, we defined the center, bar, and arm regions and compared PDF profiles of integrated intensity (I_{CO}), peak temperature, and velocity dispersion among these regions. We found that the I_{CO} PDF for the bar shows a bright-end tail while that for the arm does not. As the star formation efficiency is lower in the bar, this difference in PDF shape is contrary to the trend in Milky Way studies where the bright-end tail is found for star-forming molecular clouds. While the peak temperature PDFs are similar for the bar and arm regions, velocity dispersion in the bar is systematically larger than in the arm. This large velocity dispersion is likely a major cause of the bright-end tail and of suppressed star formation. We also investigated an effect of stellar feedback to PDF profiles and found that the different I_{CO} PDFs between bar and arm regions cannot be explained by the feedback effect, at least at the 40 pc scale.

In collaboration with Jin Koda (Stony Brook, USA) and Kazushi Sakamoto (ASIAA, Taiwan), CO(1–0) and CO(2–1) data for the entire disk of M 83 are now available. With the wider field of view as well as the addition of CO(2–1) transition, we plan to explore differences of PDF profiles (if any) between inner and outer disks, and between the two transitions.

References

- Egusa, F. et al. 2018, ApJ, 854, 90
Hirota, A. et al. 2018, PASJ, 70, 73

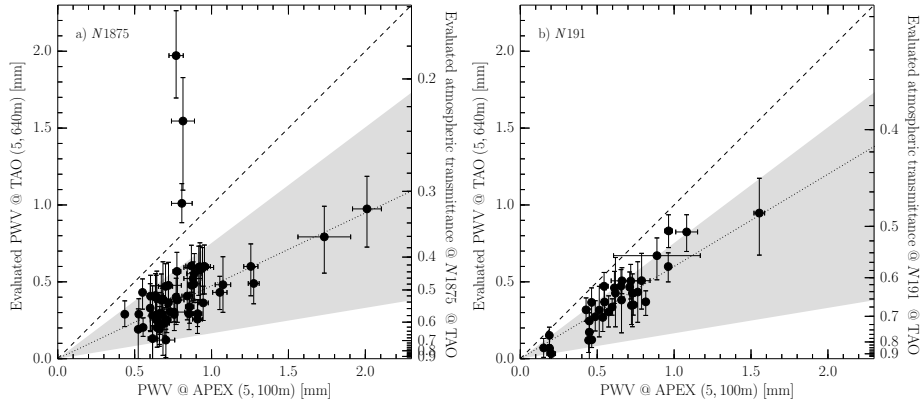


Figure 5.40: PWV values evaluated with the total throughputs of the $N1875$ (left) and $N191$ (right) narrow-band imaging data compared to those from radiosonde measurements at the base of the TAO site.

5.23 Masahiro Konishi

I have joined to Institute of Astronomy, Graduate school of Science as a TAO project assistant professor in 2009, and have been appointed as an assistant professor in 2019. Here is my recent (2013–2018), selected research results.

5.23.1 The evaluation of atmospheric transmittance in the NIR at the TAO site

The summit of Cerro Chajnantor (an altitude of 5,640m above the sea level) in the north of Chile has been selected as the site for the University of Tokyo Atacama Observatory (TAO) based on satellite data and radiosonde measurements carried out at the vicinity of the site that concluded that the area including the site (Chajnantor area) has very dry atmosphere. And thus at the site, a high atmospheric transmittance has been expected from the very low precipitable water vapor ($PWV < 1$ mm). We therefore have developed the near-infrared camera ANIR (Atacama Near-Infrared camera) for the miniTAO 1.0-meter telescope constructed at the site. The instrument has two narrow-band (NB) filters ($N1875$ and $N191$). Their central wavelengths are located between the H -band and K -band where it is very sensitive to PWV content.

Using those NB imaging data combined with the H and K -band data, we have developed a method to evaluate the atmospheric transmittance (τ_{atm}) and the corresponding PWV content above the site (Tateuchi et al. 2012). Assuming that the H -band and K -band data are temporally stable in τ_{atm} (i.e., less sensitive to τ_{atm}) and hence in the total throughput, we calculated τ_{atm} at the wavelength of the NB filters by comparing the total throughputs of the NB data (sensitive to τ_{atm}) with those of the H and K -band data. We also obtained PWV from τ_{atm} values using an atmospheric transmittance model ATRAN. As the result, we obtain the median PWV and its dispersion of 0.40 ± 0.30 mm ($N1875$) and 0.37 ± 0.21 mm ($N191$), which are remarkably ($\sim 50\%$) smaller than the radiometer measurements at the base of the site (5,100m altitude) (Figure 5.40). We find that the decrease in PWV can be explained by the different altitude of the sites. If the vertical distribution of the water vapor is approximated with an exponential profile, the PWV at a altitude is obtained by integrating the profile. In this situation, the decrease in PWV we obtained above is explained with a exponential profile having scale heights within 0.3–1.9 km that is consistent with the radiosonde measurement. We thus conclude that the TAO site has high atmospheric transmittance and is indeed suitable for ground-based Pa α observations. This work has been published as Konishi et al. (2015).

References

- Konishi, M., et al. 2015, PASJ, 67, 4
 Tateuchi, K., et al. 2012, Proc. SPIE, 8446, 84467D

5.23.2 TAO enclosure design and wind analysis

The baseline design of the TAO summit facilities (the enclosure and the operation building) was based on the well-established system of the Magellan telescope at Las Campanas Observatory. The system adopts a passive ventilation procedure, i.e., takes the natural wind flow into the enclosure and controls its velocity by adjusting ventilation windows and a wind shield, and thus it maintains temperatures inside the enclosure and brings good and stable observing performance.

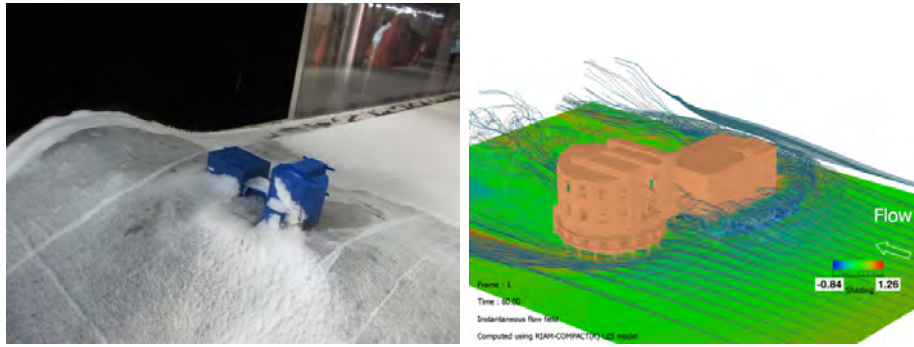


Figure 5.41: *Left*: Result of the wind tunnel experiment after 15-minute snow drift. *Right*: CFD simulation of the wind velocity field around the TAO summit facilities.

To adapt the system to work well at the TAO site, We have carried out the wind studies by using (i) the wind tunnel experiments with snow drift and (ii) the computational fluid dynamics (CFD) numerical simulation (Figure 5.41). Compared to the previous studies (for other observatories), this CFD study is unique and first-ever in that the software used deals with unsteady and non-linear wind flow to take into account temporally complex wind behavior. That approach has been already established in industrial studies such as construction of wind turbines, and We applied it for the first time in designing of astronomical facilities.

The wind tunnel experiments showed that the wind is accelerated due to the topographic effect before reaching the summit, and is disturbed by the facilities. As the result, the experiments confirmed that while snow accretion is observed on down-wind surfaces of the facilities, the open space between the facility and the ground works as intended and snow accretion around those area is significantly less, which is important for prompt recovery of the observatory function. The CFD simulation not only reproduced the acceleration and turbulence of the wind flow observed in the wind tunnel experiments, but also showed the wind behavior below and in the enclosure in detail. The open space below the enclosure is also found to be effective to drift away the air turbulence near the ground level which could significantly affect the dome seeing. From the wind velocity field derived, typical air change rate is calculated to be 20–30 per hour, which is comparable to those reported in the previous studies on other observatories, and is expected to be sufficient to expel warm and turbulent air and reduce the dome seeing. These results, published as Konishi et al. (2016), have been incorporated into the final design of the facilities.

References

Konishi, M., et al. 2016, Proc. SPIE, 9906, 99062M

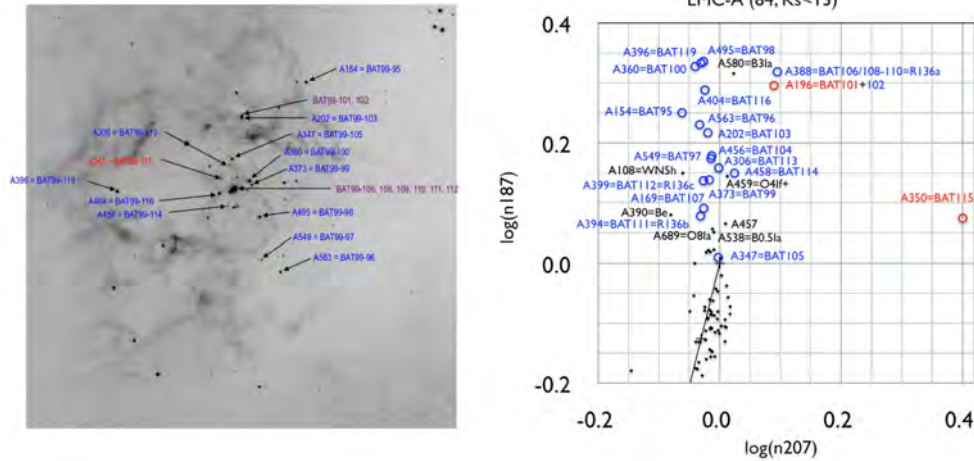


Figure 5.42: Left panel : Distribution of pick-uped Wolf-Rayet stars around R136. Image size is ~ 5 arcmin (\sim FOV of ANIR). Right panel : The color-color diagram of $\log(n207)$ vs $\log(n187)$. (n^{***} means normalized value of each band by standard star spectra (λ^{-4} .) The extinction line is also drawn. Dots which are distributed along the extinction line shows normal stars. The color excess of WR stars (open circle) are seen in this diagram.

5.24 Hidenori Takahashi

5.24.1 Investigation of Property of Massive Star Cluster by Near-Infrared Imaging Observation

In order to reveal origin, birth and evolution of massive stars (Wolf-Rayet (WR) stars, Luminous Blue Variable (LBV) stars, Yellow Hyper Giant (YHG) stars, Red Super Giant (RSG) stars, OB type stars), the discussions based on NIR narrow band imaging observation of massive star clusters by mini-TAO/ANIR (Atacama Near-InfraRed camera) are ongoing. As the filter set to pick up the massive stars, K_s wide-band filter, narrow-band filter which is optimized for CIV emission line ($2.07\mu\text{m}$) from WC/WR stars, and $1.87\mu\text{m}$ filter which can be detected HeII and $\text{Pa}\alpha$ line from WN/WR stars or LBV are used. The main observation targets are massive star clusters; e.g. galactic center clusters, Westerlund cluster, and LMC/SMC regions. As a result of the analysis, almost known WR stars in the WR catalog have been detected, and the effectiveness of our method has been confirmed. This shows that it is possible to discuss the spacial and numerical distribution of massive stars, and it leads to elucidate the evolution of massive starforming regions. Furthermore, from the color-color diagram, it is possible to estimate the extinction in the observed region and to detect “red objects” such as Mira-type stars and YSOs (Tanaka et al. 2018).

Recent main target is the region where the star formation activity and its ages is continuously changing from R136 around 30Doradus, where there are many massive stars among LMCs, to the N158–N160 region. In particular, the supermassive stars exceeding 150 solar mass seems to exist inside R136, the origin and evolution of these stars is considered to be different from clusters in the Milky Way. As a result of analysis of a plurality of regions, a difference in the distribution of stars on the color-color diagram for each region is confirmed. This indicates that it depends on the IMF and age of the cluster, as well as the surrounding environment and the metallicity.

References

Tanaka, M. et al. 2018, MNRAS, 480, 1507

5.24.2 Multi-wavelength Study of Starburst Galaxy NGC253

Data analysis of NGC253 by mini-TAO/ANIR is in progress. The data was acquired in a observation run in November 2013, and the spatial distribution of the ionizing region is explored using $\text{Pa}\alpha$ and $\text{Pa}\beta$ imaging data including continuum emission. In addition to the spatial distribution of star formation, its evolution can be discussed. The hydrogen recombination line $\text{Pa}\alpha$ in the near-infrared range is at a longer wavelength than visible $\text{H}\alpha$ and so on, so it is resistant to dust extinction and can be seen through to inside the galaxy, that is; it is a good indicator of star formation activity

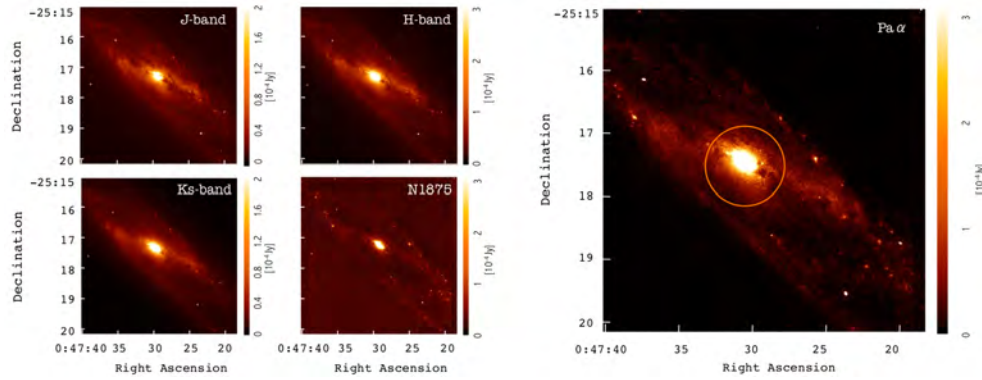


Figure 5.43: NIR images of NGC253. Pa α image which derived from N1875 and Ks–H band images approximately shows starformation activity.

especially in dust-rich star formation regions. NGC253 is a relatively near starburst galaxy that can be investigated star-resolving activity via spatially resolved images by ANIR. In addition to ANIR data, radio observations with VLA and NRO, and comparisons with AKARI and Herschel far-infrared data can give a strong limitation to spatially resolved physical conditions such as temperature and density. (Takahashi et al. 2012, 2017)

References

- Takahashi, H., Matsuo, H., and Nakanishi, K., 2012, PKAS, 27, 261
 Takahashi, H., Matsuo, H., and Nakanishi, K., 2017, JAXA-SP-17-009E, 329

5.24.3 Development of Tunable Filter for Spectroscopic Imaging Observation

Despite the tunable filter (wavelength scanning filter) has global demand strongly from various astronomy research fields, there are no examples of development yet. Its main purpose is to develop it and to install it as a front optical module for observation equipment of large-aperture telescopes, and to show its practicality. The scientific goal is to investigate the physical conditions of a large star forming region in a wide spatial dynamic range from the cluster level in the galaxy to nearby and distant galaxies continuously at high spatial resolution over near infrared wavelength range. As a result, the physical processes of star formation and to elucidate the evolution of massive stars and galaxies will be expected. Technically this research will be expected to become the touchstone of the development and demonstration of basic technology for tunable filters for the wide-field near-infrared imager (e.g. ULTIMATE project promoted by the Subaru Telescope at NAOJ).

Specifically, a spectroscopic module based on Fabry-Perot interferometer is being developed. As the optical element (etalon), a substrate in which a reflection film is coated on anhydrous quartz is used, in order to keep high reflectance along wide near infrared wavelength. A cryogenic driven piezo element is looked into its possibility as the parallelism control mechanism of the etalon that is directly influenced to the optical/spectral performance.

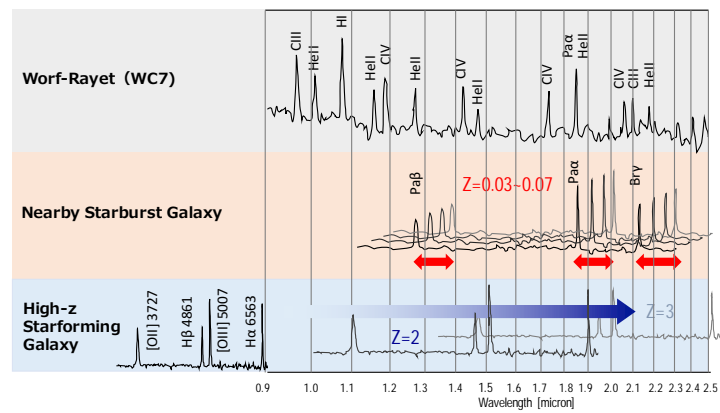


Figure 5.44: By covering the entire near-infrared wavelength for spectroscopy, it is possible to investigate star formation activity at any targets, distances, and the spatial scales.

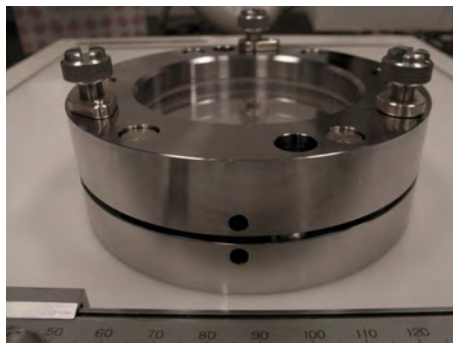


Figure 5.45: Prototype of Fabry-Perot Spectrometer (etalon holding mechanism).

Chapter 6

Kiso Observatory

The Kiso Observatory is the unique astronomical observatory of the University of Tokyo in Japan. By making use of the dedicated Schmidt telescope with wide-field capability, the observatory pursues the following three objectives: 1. Large survey with quick return for Japanese astronomical community, 2. Development of novel and experimental instruments for the strength of Institute of Astronomy as one of the main institutes of observational astronomy in Japan, 3. Outreach for social contributions(社会貢献) and regional return (地域還元) for the University of Tokyo.

6.1 Introduction

The Kiso Observatory was established on 11 April 1974 as the fifth observatory of the former Tokyo Astronomical Observatory of the University of Tokyo. When the Tokyo Astronomical Observatory was reorganized as the National Astronomical Observatory (NAO) in July 1988, the Kiso Observatory was transferred to the jurisdiction of the Institute of Astronomy, the University of Tokyo (IOA-UT), which made a debut at the same time, as its annex observatory. Under the priority measure for graduate schools implemented in 1998 by the government, the observatory became an observatory of the IOA-UT and this status still remains.

The Kiso Observatory was established with the following objectives at the beginning: *1) to pursue observational research of various astronomical objects in and outside of the Galaxy and to perform observation of night skylights using a 105cm Schmidt telescope, 2) to support observational research of astronomers and astrophysicists throughout Japan.* Equipped with a 105cm Schmidt telescope as its main equipment, the Kiso Observatory has been virtually open to astronomers throughout Japan since its beginning, and started the official open-use from 1988 when the Tokyo Astronomical Observatory was reorganized as NAO. The observatory has an advisory committee every year for the open-use and observatory operation.

Kiso observatory is well-maintained by experienced observatory staffs and served the University of Tokyo as well as Japanese astronomical community for science, education, and public outreach. All the activities of the Kiso Observatory, including the open-use researches, are summarized in an annual report published jointly by the DoA and IoA, the University of Tokyo. This section sometimes reports the status of all the activities from 1990's to show the long-term transition of this facility.

6.2 Observing Facilities

In the highest mountain area, Kiso is known to have one of the darkest sky in Japan. Despite the past rapid urbanization of local area in Japan, the area still keeps a dark environment that is close to that of the world best observing sites. The observatory has the 105cm Schmidt telescope with a wide field-of-view of 9-degrees in diameter to detect faint object by making use of the dark sky. In the following we will describe the telescope, past instruments, and the new instrument. During last period (2012-2019), we have completed an extremely wide-field CMOS camera, which has become the new work horse instrument of the observatory.

6.2.1 105cm Schmidt Telescope

The 105cm Schmidt telescope (Figure 6.1), which was built by Nikon, is the main telescope of the Kiso Observatory. The specifications are listed in Tables 6.1–6.3. A remote/automatic observation system of the 105cm Schmidt telescope was developed and has been used for last five years for efficient and comfortable observing.



Figure 6.1: Kiso Schmidt 105cm telescope (left) and the dome in the night (right). Pictures are by KOJI OKUMURA (Forward Stroke). Note sky images are synthesized.

	Aperture	Thickness	Material	Weight
Corrector plate	105cm	2cm	UBK7	48kg
Main mirror	150cm	24cm	CER-VIT	1350kg

Table 6.1: 105cm Schmidt telescope: main mirror and corrector.

Focal length	330cm
Image scale	62.2"/mm
Focal ratio	F/3.1
Field of view	9° in diameter

Table 6.2: 105cm Schmidt telescope: optics.

	Vertex angle	Aperture	Dispersion (at $H\gamma/A$ band)	Weight
Objective prism 1	2°	105cm	800/3800 Å/mm	121kg
Objective prism 2	4°	105cm	170/1000 Å/mm	245kg

Table 6.3: 105cm Schmidt telescope: objective prism.

6.2.2 Past Instruments

Since its inauguration, photographic plates had been used for a long time for the Schmidt telescope. However, strong demands for deeper imaging lead to the replacement of the photographic plates to state-of-the-art solid-state imaging devices for detections and precise measurements of faint objects. In 1987, a development of a 1K-CCD camera started and it had been open to the common-use since 1993. At the same time the development of a 2K-CCD camera with higher sensitivity and wider field-of-view was started. The camera became available for test use at the beginning of 1997 and for the open-use at the beginning of 1998. The 2K-CCD had been the main instrument for the Schmidt telescope for more than 10 years by making use of its large pixel size for detecting faint extended objects, such as dust trails of comets. In 1997, a near infrared camera (KONIC) became available to the open-use. Since 2003, a development of the Kiso Wide Field Camera (KWFC) with eight chips of $2k \times 4k$ CCDs covering a field-of-view seven times wider than that of the 2KCCD was started. The KWFC was used as the main instrument for the Schmidt telescope from 2012 to 2018.



Figure 6.2: The 2K-CCD camera with the dewar opened.

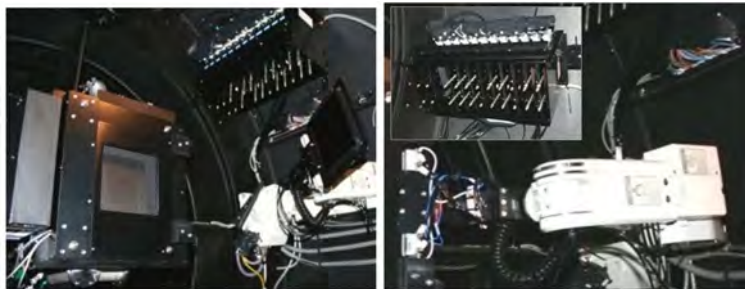


Figure 6.3: The 8-K pixel mosaic camera KWFC installed at the prime focus of the Schmidt telescope. A robotic arm (white structure) grabs one of filters in a magazine unit seen near the top of pictures to deliver to KWFC (a square instrument to the left in the left picture).

6.2.3 New Instrument – Tomo-e Gozen –

We have pursued development of a wide-field *video* observation system *Tomo-e Gozen* as a next generation facility instrument since 2013. Tomo-e Gozen is an optical wide-field video observation system with a mosaic CMOS camera on the Schmidt telescope and an intelligent observation software. The camera unit is capable of taking consecutive wide-field images of 20 deg^2 at 2-frames per second (fps) in full-frame read with an absolute time accuracy of 0.2 millisecond by 84 chips of $2k \times 1k$ CMOS image sensors. The sensors are operated without mechanical coolers owing to a low dark current at room temperature. A low read noise of 2-e- achieves higher sensitivity than that with a CCD sensor in short exposures. Big data of 30-TBytes per night produced in the 2-fps observations are processed in real-time to detect transient events

and issue alerts for follow-ups quickly. The camera unit is directly connected to an on-site computing system where real-time data reduction software with several machine learning techniques is implemented to search for fast-moving and rapidly variable objects in the sky-big-data. After evaluating component technologies of Tomo-e Gozen by a prototype model camera with 8 chips of CMOS sensor in 2013, we started a development of a final model of the Tomo-e Gozen camera with 84 CMOS sensors and the computing system. The Tomo-e Gozen system was successfully completed in Oct. 2019.

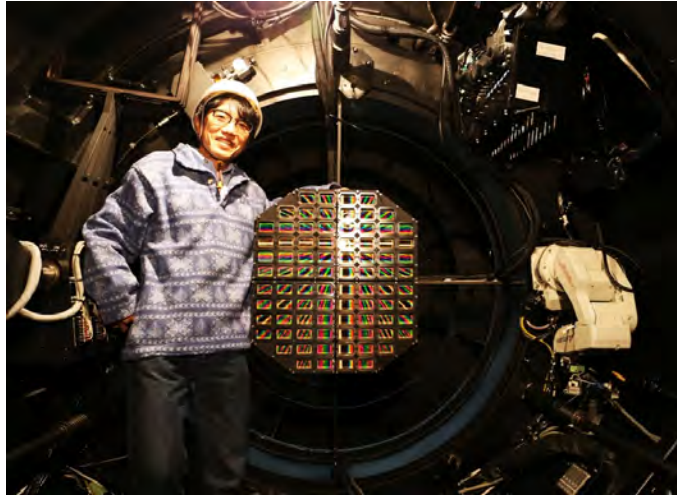


Figure 6.4: The Tomo-e Gozen camera installed on the focal plane of the Schmidt telescope.



Figure 6.5: Development scenes of Tomo-e Gozen.

Sensor	Canon 35-mm front-side-illuminated CMOS sensor (with micro-lens array and AR coated cover glass)
Sensor format	2,000×1,128 pix / chip
Sensor chips	84 chips
Field of view	2.2° × 2.2°
Pixel size and scale	19 μm/pix, 1".189/pix
Sensitive wavelength	370 to 730 nm
Filters	Transparent windows (default), optical filters, grisms
Max frame rate	2 fps in full-frame, 500 fps in partial-frame
Read noise (2 fps)	2.0, 4.1, 9.2 e- in High-, Mid-, and Low-gains
Well depth (linearity < 5%)	6,000, 25,000, 53,000 e- in High-, Mid-, and Low-gains
Dark current	0.5 e-/sec/pix at 290 K, 6 e-/sec/pix at 305 K
5σ limiting mag (High-gain)	16.7, 18.5, 19.9 mag at t_{exp} of 0.1, 1, 10 sec w/transparent windows
Absolute time accuracy of time stamps	± 0.2 millisecond
Data production rate (full-frame, 2 fps)	830 MBytes/sec, 30 TBytes/night
Size and weight of the camera body	515mm x 575 mm × t = 540 mm, 57 kg

Table 6.4: Specifications of the Tomo-e Gozen camera

6.3 Remote/Automatic Observing

Since AY2012 we have strongly promoted the development of remote and automatic observations for efficient operation to save resources. The hardware, such as weather station, and the software, which consists of observation management and queue-observation software, are fully implemented and have been steadily used for more than 5 years for KWFC observations. After we switched to Tomo-e, the same system is similarly used after some modifications.

The remote observing of the Schmidt telescope is currently possible virtually from anywhere in the world, and most of the observing have been conducted from Tokyo. This makes a significant reduction of the number of visiting observers to save the travel budget.

Also, most observations are currently done in automatic mode and the data acquisition through the night simply follows the queue input before the night, except for interruptions such as for observing NEO candidates or ToO objects. The observation (queue input) is mostly from Mitaka, Tokyo, and the observatory staffs focus on the maintenance and trouble-shooting. The software constantly monitors the weather condition/telescope status to judge if the present time is observable or not. If the state becomes observable from non-observable, the software automatically opens the dome, points the telescope to the target, then starts exposures.

6.3.1 Observing Efficiency

Figure 6.6 summarizes the observing efficiency in last 10 years. Blue points show the *classical* daily efficiency: any nights with > 20 exposures are counted as 1, while any nights with < 20 exposures is counted as 0, then averaged over month. Red points show the hourly efficiency: any hours with > 5 exposures are counted as 1, while any hours with < 5 exposures are counted as 0, then averaged over month. The hourly efficiency is about 50% on average except for rainy season (June to Aug): this should be regarded as the typical observing efficiency.

In the same plot the Green points show the weather-limited efficiency (hourly % of observable weather condition), from the software for evaluating observing conditions. This should trace the maximum possible efficiency and any decrease from the green point suggests telescope/instrument/operation trouble. During the steady observation phase with KWFC in 2014-2017, the red curve (real efficiency) nicely traces the green curve, meaning all the telescope, instrument, software etc. worked almost perfect. After the switch to Tomo-e (2018-), the real observing efficiency (red) sometimes dropped from the maximum possible efficiency (green). This is because Tomo-e was under R&D during this period, and in fact, the red curve has become almost identical to the green curve starting fall 2019 when Tomo-e got into the steady operation phase. We would expect this efficient observing continues for ~10 years as long as Tomo-e operation continues.

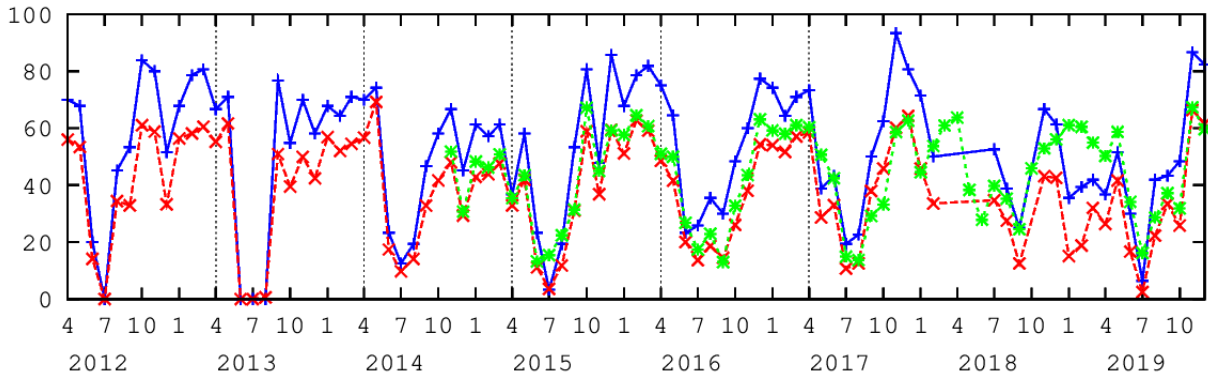


Figure 6.6: The observing efficiencies of the Schmidt telescope in last ten years. The vertical is in %. Red: real efficiency (based on hourly estimate). Green: predicted efficiency (= weather-limited efficiency estimated by automatic observation software). Blue shows real efficiency based on daily estimate and is just for reference. See the detail in the main text.

6.4 Science Operation

6.4.1 From Open-Use to Inter-university Collaboration

From the beginning most of the observing time of the Schmidt telescope had been subject to “classical” open-use for the community because it was the most important objective from the establishment of the observatory. However, we ended the open-use in AY2016 because 1) the new instrument, Tomo-e, is basically a survey instrument, which is not suitable for general open use, 2) the minimization of the operation cost was mandatory.

After ending the open-use, we had conducted several KWFC programs that require supplemental observing, then decommissioned KWFC at the end of AY2018. At the same time we started engineering runs for Tomo-e in AY2017 and AY2018. The Schmidt telescope is under a semi-automatic observing mode with Tomo-e since AY2019.

The observatory sponsors the *Kiso Symposium* every year to discuss the science, data, and instrument of the Kiso Observatory. It was originally for the open-use community, but we continue this good tradition with the Tomo-e collaborators from all over Japan even after the end of the open-use.

In the following we briefly summarize our open-use since our past experiences could be useful for future operations of this kind of astronomy facility by IoA or School of Science.

6.4.2 Open-Use

The number of programs for the open-use in AY2012 – 2016 term are listed in Table 6.6. As a reference, the same list for AY1995 – 2012 is also shown in Table 6.5.

The call for research proposals (normal program) had been released once every year to anyone in and outside the observatory as an open-use. From AY2007, we started “short program” with call for proposals with small number of nights once every three months to look for a fresh use of the telescope with new ideas. This attempt brought new users from non-optical astronomy fields and graduate students/posdocs, thus appeared to have been successful to stop the decrease of the number of proposals and to keep the community (Table 6.5). Obviously the number of programs significantly decreased from AY2000 as the 8-m class large telescopes (such as Subaru Telescope) became available to the community. Starting AY2012, we re-organized the categories of common-use observation by observing style rather than observing targets (Table 6.6) since classical observing was about to be obsolete for the needs of users.

All these gradual transformations appear to have been accepted favorably by the community and we managed to keep a good community for the telescope. Note those community members became the backbone of the Tomo-e development, and helped the observatory to shift to more like compact/efficient but a modern observatory that is suitable for small telescopes.

6.4.3 Publications

Figure 6.7 summarizes the number of refereed papers in last 10 years. On average 6.8 papers using Kiso data (cyan and blue blocks in the figure) are published per year, suggesting efficient production for such small observatory with low operational cost. The constant upgrade of instruments appears to keep the constant production of scientific papers. The main subjects are solar system small bodies, near-by open clusters, and transient objects, suggesting the wide-field of

Academic year	Galaxies	ISM	Stars	Solar system	Misc	Short	TOTAL
1995	21	9	11	7	9	–	57
1996	19	7	10	11	9	–	56
1997	18	2	14	12	11	–	57
1998	16	3	9	8	3	–	39
1999	11	2	8	3	3	–	27
2000	9	2	8	4	2	–	25
2001	10	2	5	3	2	–	22
2002	9	2	5	7	2	–	25
2003	7	0	5	8	2	–	22
2004	7	2	6	8	4	–	27
2005	7	2	4	8	5	–	26
2006	5	1	3	6	4	–	19
2007	5	2	2	6	6	6	27
2008	6	1	3	6	5	12	21
2009	6	2	4	5	5	5	22
2010	4	1	3	6	5	3	22
2011	4	0	3	6	8	7	28

Table 6.5: The number of open-use programs in the past (–AY2011)

Academic year	Normal	Monitoring	ToO	Education	Large	Misc	TOTAL
2012	8	2	1	5	2	–	18
2013	10	2	1	6	2	–	21
2014	6	4	1	6	2	2	21
2015	7	6	2	5	2	1	23
2016	7	3	1	4	2	1	18

Table 6.6: The number of open-use programs (AY2012–2016)

the Kiso Schmidt telescope is well-utilized. We hope a moderate or wide increase of the number of papers with the new instrument Tomo-e.

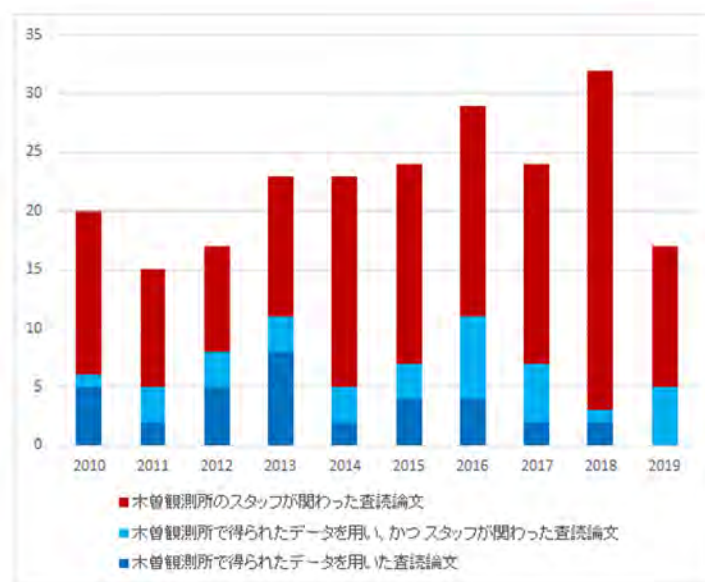


Figure 6.7: The number of refereed papers using Kiso data. Blue and red blocks show the number of papers using Kiso data and of papers by Kiso research staffs, respectively (Cyan shows papers using Kiso data with Kiso staffs as co-authors)

6.5 Observatory Long-term Science Programs

The Schmidt telescope has been fully used for open-use programs for long time. However, in this large telescope era, any small telescope should increase science productively with long-term programs by the dedicated use of the small telescope time. We first started such long-term programs with 8K mosaic camera KWFC besides the continuing common-use programs with 3-5 nights/program. Then, with the latest instrument Tomo-e, we have completely shifted to the dedicated use of the telescope only for several long-term programs.

6.5.1 Overview

With the completion of KWFC, a variety of science programs were proposed, including the survey of transient objects, asteroids, comets, unknown planets, transits by extrasolar planets, Galactic plane (especially the outer Galaxy), and near-by galaxies. While many of those have been carried out by common-use observers, we initiated two observatory long-term science programs that make use of the wide field of view of KWFC by focusing a large amount of telescope time on these programs: one is for extra-galactic supernovae (SNe) search and the other is for Galactic variable/transient object search. Those programs had been conducted in about 5 years (2012–2017), and they are briefly described in the following sub-sections.

Starting AY2019, we use the new instrument, Tomo-e, to start three long-term programs: 1) Follow-up observations of gravitational wave alerts, 2) SNe survey, and 3) NEO (Near Earth Objects) survey. Although those programs have been already producing promising results, we omit the description here since the programs have just started. See Ohsawa's section for initial results for NEOs. We have already completed the system for the program 1), and the follow-up observations of any alerts have been conducted as long as the target is on the sky during possible observing time.

6.5.2 KISO Supernova Survey (KISS)

We had conducted a SN survey with KWFC (PI: Tomoki Morokuma) for 3.5 years from April 2013 to September 2015 (in total 422-nights: including non-full night observations) with a primary purpose to detect *shock breakout*. The survey area of 50-100 square degree was observed with high cadence of 1hr (ideal for detecting shock breakout) with the limiting magnitude of $g=20$ -21mag. With this spec, ~ 1 shock breakout is expected.

We developed an efficient pipeline software system for the detection of SNe events to detect many candidates of which 27 are found to be genuine SNe by spectroscopic identification. We worked with excellent Japanese amateur astronomers to detect supernovae on the images. Although we have detected quite many candidates, most of them could not be spectroscopically followed up because of the lack of collaboration network with mid-class (3-4 m) telescopes with spectrograph, and no clear shock breakout was detected. However, we managed to construct the pipeline system, which is now utilized for the currently on-going Tomo-e survey. Also, we have constructed the follow-up scheme by collaborating with Japanese telescopes ($D=1$ -3 m).

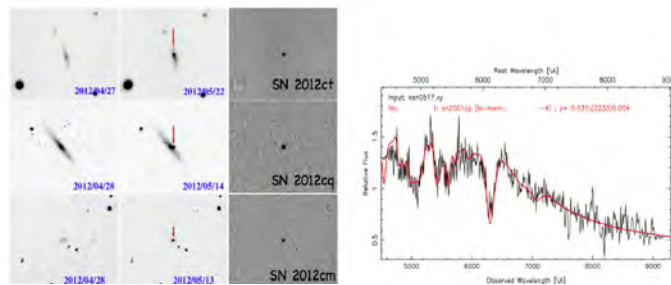


Figure 6.8: (Left) Three supernovae discovered with KISS at $z=0.028$, 0.026 and 0.039 from top to bottom. (Right) Spectrum of SN2012cm obtained with Kanata Telescope of Hiroshima University, showing it is a typical SN Ia.

The transient sky has been intensively explored in the last decade. However, transient phenomena with timescales shorter than 1 day are still largely unexplored. The past attempts with larger telescopes have shown the presence of rapid transients, but their nature is still unclear due to difficulty of real-time spectroscopy. We therefore initiated a high-cadence transient survey with a new wide-field CMOS camera, Tomo-e Gozen, on the basis of our experiences with KWFC. In this survey, $7,000 \text{ deg}^2$ sky is continuously monitored with cadences of 2 hours with 18 mag depth. Besides unexpected

objects, we expect to discover about 10 core-collapse SNe during their very early phase. We are currently obtaining a lot of data every night, and working on the software development for efficient detection of transients, for which the experiences with KWFC are quite useful.

6.5.3 KWFC Intensive Survey of the Galactic Plane (KISOGP)

KISOGP is one of the observatory survey projects that started in April 2012 using KWFC (PI: N. Matsunaga). This project is a photometric survey of variable and transient objects in the Galactic plane. Eighty fields of the KWFC view (320 deg^2 , see Figure 6.9). Until the end of the survey in the middle of 2017 March, 40–100 epoch images (one 5-sec and three 60-sec exposures per epoch) were collected with the frequency of once or twice every month. The limiting magnitude is around 16.5 mag (with $S/N=50$). The number of epochs depends on the Galactic longitude, but the regions with least visits, 40 (90–100 and 180–210 degrees in the longitude), still give sufficiently useful light curves for identification and classification of pulsating stars like Cepheids. The main targets are (1) pulsating variables like Cepheids and Miras, (2) young stellar objects, and (3) transient objects like (dwarf) novae. Cepheids and Miras can be good tracers of the Galaxy structure and evolution. Their period-luminosity relations can be used as distance indicators which enable us to determine the distribution of these objects accurately. Their ages can also be estimated based on the theory of stellar evolution. With follow-up spectroscopy, kinematics in the Galaxy and chemical abundance can be also obtained, and we have actually performed spectroscopic observations of candidates of Cepheids and Miras we had identified in preliminary analysis using the 1.9-m telescope at Okayama Astrophysical Observatory (NAOJ) and 2-m Nayuta telescope at Nishi-Harima Observatory (University of Hyogo). In spite of these advantages as tracers, the survey of variable stars in the Galaxy is far from complete. This is because most of the previous surveys of variable stars were carried out in visible wavelengths (e.g. typical extinction of 5–10 mag in the V-band corresponds to 2–5 mag in the I-band towards the Galactic plane). In the data analysis so far, we detected a couple of thousands of variable stars including approximately 100 Cepheids and more than 700 Miras. More than half of them were not previously reported as variable stars, indicating that there are still many relatively bright variables to be found in the Galactic plane. The data-sets are also useful for young stellar objects and transient objects like (dwarf) novae. Whereas it is known that young stellar objects show various kinds of light variation, 5 yr-long monitoring data for a large number of star-forming regions included in our survey field will give unique and comprehensive insights into their time variations. For transient objects, Japanese amateur observers are active in discovering and observing them, but our survey as deep as 16.5 mag in the I band would reveal a population that is located in the Galactic disk further than the previously known objects. We can investigate their distribution as well as population. In addition, there may be rare and/or new types of such objects from the large sample of KISOGP.

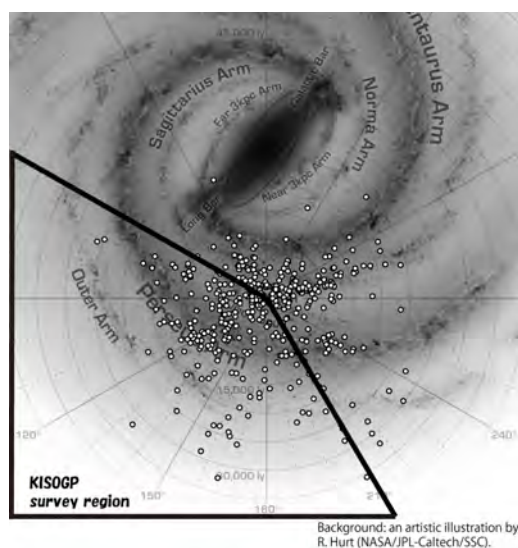


Figure 6.9: Survey range of KISOGP. The background image is an artistic illustration of the Galaxy (from Spitzer GLIMPSE), on which previously known Cepheids are plotted with circles. KISOGP can reveal variable stars embedded in Perseus arm as well as those located in the Outer Arm. More than 100 Cepheids are expected from this survey.

6.6 Education

Since the beginning the Kiso Observatory has been used for graduate educations for the University of Tokyo and other universities through the open-use observations. The number of thesis papers in last 10 years are summarized in Figure 6.10. About two master's thesis papers are published per year (green), and one doctor's thesis is published every two years (red) on average, suggesting this small observatory is effectively used for graduate educations.

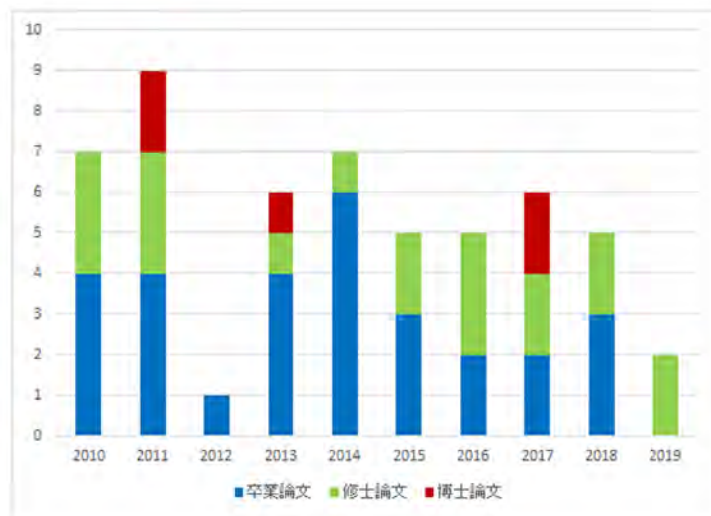


Figure 6.10: The number of thesis papers using Kiso data. Blue, Green, and Red blocks show the number of thesis papers of undergraduate, master, and doctor, respectively.

The Kiso Observatory has been used also for undergraduate education of the University of Tokyo for long time as a part of the observational astronomy course. Every summer, junior students come to the observatory for 3 to 5 days to learn basic skills such as observation planning, night-time observation, data reduction, and data analysis. The Observatory is also open to other universities for undergraduate education: currently eight universities (public: Tokyo Gakugei Univ., Mie Univ., Wakayama Univ., Shinshu Univ.; private: Bunkyo Univ., Japan Women’s Univ., Konan Univ., Otsuma women’s Univ.) utilize the observatory for observational astronomy course during summer/winter time. Kiso is now one of the most active places for university education/astronomy training in Japan. Some undergraduate students use the data from Kiso Observatory for their graduation thesis works (see blue bars in Figure6.10).

6.7 Public Outreach

The Kiso Observatory is now known as the center of astronomical outreach in Japan. Not only the normal outreach activities for the local community, such as open days and star gazing parties, a variety of top-class outreach programs are conducted through an academic year with funding from the government and support from the NPO (Science Station), which promotes outreach programs with graduate/undergraduate students. Through these activities, Kiso is quite contributing to Japanese astronomy community as well as to the local community (Nagano Prefecture or mid-Japan area).

6.7.1 Galaxy School (“Ginga Gakko”)

At the end of the fiscal year (March), we have an annual “Galaxy school” to invite 20-30 high school students from all over Japan. Students perform and experience real research programs by themselves from observations, data analysis, to final presentation. The 105cm Schmidt telescopes and the common-use instruments are used for the observations. This Galaxy School has continued for over 20 years since 1998 and about 600 students have experienced observational astronomy (Table 6.7).

Kiso Galaxy School is the first one of this kind in Japan. Some students who participated in past Galaxy Schools have enrolled in universities and graduate schools, and some of them became astronomer.

	Date	Subject	No. of participants
1st	1998 March 24-26	Visual and near-IR observation of nebulae	30
2nd	1999 March 22-24	Determination of the age of M3	12
3rd	2000 March 27-29	Construction of HR-diagrams of open clusters	15
4th	2001 April 3-5	Spectroscopy by using objective prisms	13
5th	2002 March 25-27	Multi-color imaging	18
6th	2003 March 28-30	Search for asteroids, size of the Galaxy, distance to clusters of galaxies	34
7th	2004 March 26-29	Temperature of Gemini stars, Spectral type of stars, Redshift of extra-galaxies	30
8th	2005 March 22-25	Variable stars in globular clusters, Nearby galaxies, Sun-like stars	31
9th	2006 March 21-24	Planetary nebulae, Star forming regions, Star formation in extra-galaxies	27
10th	2007 March 23-26	What is comets, Nearby field stars and stars in clusters, Various galaxies	29
11th	2008 March 28-31	Minor planets, The end of stars, Galactic clusters	25
12th	2009 March 28-31	The cometary nature and future, Nebulae, stars in the Galaxy	14
13th	2010 March 28-31	The evolution of comets as snowmans in the space , The Polaris flare, the Galactic feature	34
14th	2011 August 9-12	The Coma cluster, The Galactic rotation, the Galactic structure	27
15th	2012 March 27-30	The Galactic star formation history, The galactic star forming regions, The expanding universe	27
16th	2013 March 26-29	Search for Jupiter Satellites, Observation of Eclipsing binary, Find the shape of our Galaxy	33
17th	2014 March 25-28	Size distribution of asteroids, Distance,color,structure of nebulae, Polarization on light	36
18th	2015 March 24-27	Characterizing stars using star clusters, Origin of shape of galaxies, Progenitors of supernovae	35
19th	2016 March 22-25	Explore the Per-Cas region in the Milky, Supernovae and SNE, Interstellar dust from extinction	36
20th	2017 March 28-31	Dark future for bright comet?, Shape of our Galaxy, Gas without stars?	37
21th	2018 March 27-30	Origin of light from nebulae colors, Red flowers in galaxies: star formation	24
22th	2019 March 26-29	Who made explosion?, Hottest star in the Universe?	26
	Total		588

Table 6.7: Galaxy School.

6.7.2 Science Partnership Program (SPP)/Super Science High-school (SSH): “Hoshi no Kyoshitsu”

Under the support of the Ministry of Education, Research, Sports and Science (“Monkasho”), we conduct various outreach programs about five to ten times a year at the observatory for high-school students as Science Partnership Program (SPP) and/or Super Science High-school (SSH) program. For the nominal SPP (formerly SPP-A) and SSH classes, students are divided into a number of groups of about 5 students and try to estimate “the age of the universe” through various lectures, lessons, and data analysis (Figure 6.11). The program is conducted in two days by staying one night at the observatory (many students tend to continue discussing until midnight and some through overnight!), ending with the presentation session by students. This Kiso SPP program was selected as one of the best SPP programs by the Ministry, and the class scene was recorded to CD-ROM for open distribution. Over 3,600 students have already graduated this short class since 2002 (Table 6.8). The well-maintained facilities of the Kiso Observatory, such as the telescope, computers, dormitory, and the organization, are quite effectively used for this program.



Figure 6.11: “How did the universe inflate?” High-school students discussed with a support from the teaching assistant to the left (A scene from the SPP program).

Year	SPP-A	SPP-B	SPP-M	SSH	Total
2002	137(6)	—	48 (2)	—	185 (8)
2003	257(11)	—	45 (2)	—	302 (13)
2004	235(10)	—	55 (4)	42(4)	332 (18)
2005	248(9)	—	104 (6)	26(1)	378 (16)
2006	140(7)	107(3)	—	72(2)	319 (12)
2007	158(4)	102(5)	—	66(2)	326 (11)
Total	1175(47)	209(8)	252(14)	206(9)	1842(78)

Year	SPP-A	SSH	Total
2008	173(6)	66(2)	239 (8)
2009	191(6)	57(2)	248 (8)
2010	97(3)	90(3)	187 (5)
2011	69(2)	108(3)	177 (5)
2012	64(2)	102(3)	166 (5)
2013	31(1)	104(3)	135 (4)
2014	37(1)	105(3)	142 (4)
2015	91(4)	76(3)	167 (7)
2016	42(2)	80(2)	122(4)
2017	29(2)	88(2)	117 (4)
2018	36(1)	77(2)	113(3)
Total	860(26)	953(25)	1813(57)

Table 6.8: SPP program: number of students (number of high-school). The themes for SPP-A, SPP-B are Big-bang universe and the age of the universe, Building at telescope, respectively. SPP-M is for middle school students and they experienced and learned how to observe with the telescope.

6.7.3 Extracurricular Lessons and Star Watching Parties

As part of its outreach activities, the Kiso Observatory is sponsoring extracurricular lessons and star watching parties at primary, middle and high schools near the observatory (Table 6.9). Extracurricular lessons explain basics of astronomy, research topics, and latest results obtained by the Kiso and other observatories. At star viewing parties, celestial bodies are watched through the telescopes so that children and students can gain interest in the universe and stars. These extracurricular lessons and star watching parties are sponsored at about 20 schools every year.

Year	Extracurricular lessons	Star gazing parties	Observatory tour for study	Public talks
1994	3	2	—	3
1995	6	4	—	
1996	9	3	—	1
1997	8	2	—	
1998	11	2	—	
1999	14	1	—	1
2000	11	4	—	3
2001	12	1	—	3
2002	16	2	—	3
2003	7	5	—	0
2004	5	2	—	0
2005	16	8	—	2
2006	13	2	—	3
2007	11	5	—	3
2008	8	7	—	3
2009	8	5	—	6
2010	6	6	4	4
2011	5	6	7	3
2012	5	2	4	1
2013	5	5	5	2
2014	9	5	10	1
2015	6	3	9	1
2016	3	1	8	1
2017	2	0	7	4
2018	2	2	8	3

Table 6.9: Number of Extracurricular lessons and star gazing parties.

6.7.4 Open House

The Kiso Observatory sets open-house days each summer to show its facilities and research results to the public (Table 6.10). Started in 1976, this year's (2018) open house is 43th open house. From 1994, a star gazing party is also held in the evenings of the open-house days. As the observatory becomes visible to the public through a variety of media in last five years, the visitors are steadily increasing, as is seen in Table 6.10.

Note the observatory is accepting many visitors and group tours every year, which are not counted in this report.

Date	No. of participants	Star gazing parties
1991 Aug. 3-4	440	
1992 Aug. 1-2	380	
1993 Aug. 7-8	240	
1994 Aug. 14-15	440	first held
1995 Aug. 5-6	170	bad weather
1996 Aug. 3-4	270	held
1997 Aug. 9-10	180	bad weather
1998 Aug. 8-9	240	held
1999 Aug. 7	200	held
2000 Aug. 5	100	bad weather
2001 Aug. 11	100	bad weather
2002 Aug. 10	150	held
2003 Aug. 19	30	bad weather
2004 Aug. 7-8	350	bad weather
2005 Aug. 6	100	bad weather
2006 Aug. 12	100	held
2007 Aug. 4	150	held
2008 Aug. 9	100	—
2009 Aug. 1	100	bad weather
2010 Aug. 7-8	350	held
2011 Aug. 6-7	200	bad weather
2012 Aug. 4-5	240	held
2013 Aug. 3-4	200	bad weather
2014 Aug. 9-10	100	bad weather
2015 Aug. 8-9	400	held
2016 Aug. 6-7	400	held
2017 Aug. 5-6	400	held
2018 Aug. 4-5	600	held

Table 6.10: Open House.

6.8 Accommodation Facility

Among the astronomical observatory in Japan, the Kiso Observatory stands as a full accommodation facility for various parties from a single person to a large group of people up to 40.

The observatory is an ideal place for a group of researchers for workshop/discussions/writing papers in quiet environment. Note the observatory offers a spectacular view of high mountains of Japanese Alps during day time, and the dark night-sky in the evening.

The number of visitors stayed at Kiso Observatory is summarized in Table 6.11. Even after the open-use with classical observing is finished in AY2016, the observatory has been efficiently used as one of the center of interactions among Japanese astronomers/students. Also, the accommodation facility is ideal for outreach for high-school students to experience astronomy.

Institutes	1995		1996		1997		1998		1999		2000	
IoA-UT	19	39	18	26	36	198	32	178	7	10	20	47
Univ. of Tokyo	71	549	55	229	75	542	20	57	34	313	45	209
NAOJ	37	112	50	136	38	98	47	154	34	107	26	65
Other univ. in Japan	92	373	123	435	99	400	125	396	99	374	87	333
Foreign countries	9	25	11	41	14	36	3	9	5	14	1	2
Others	21	100	12	12	4	4	12	24	4	4	4	4
Total	248	1198	269	879	263	1278	239	818	183	822	183	660

Institutes	2001		2002		2003		2004		2005		2006	
IoA-UT	22	107	100	186	25	63	19	35	19	35	10	38
Univ. of Tokyo	27	92	20	70	24	119	47	146	47	146	19	89
NAOJ	16	55	20	86	27	123	23	51	23	51	8	32
Other univ. in Japan	114	445	81	326	143	653	133	512	133	512	95	354
Foreign countries	2	13	0	0	1	1	2	9	2	9	1	13
Others	4	4	7	7	3	3	12	24	0	0	0	0
Total	185	716	146	589	223	962	224	753	224	753	133	526

Institutes	2007		2008		2009		2010		2011		2012	
IoA-UT	13	36	7	30	12	63	11	53	12	110	23	179
Univ. of Tokyo	23	79	12	49	31	96	12	38	28	110	30	96
NAOJ	10	27	18	40	10	29	6	10	15	72	11	76
Other univ. in Japan	190	580	89	475	102	507	90	504	126	551	88	497
Foreign countries	1	27	3	23	3	22	1	4	2	14	1	9
Others	359	417	228	261	247	320	190	206	252	372	216	290
Total	596	1166	357	878	405	1037	310	815	435	1229	369	1147

Institutes	2013		2014		2015		2016		2017		2018	
IoA-UT	18	145	20	105	24	259	15	234	20	444	22	428
Univ. of Tokyo	42	162	29	87	29	115	12	57	24	65	24	82
NAOJ	10	75	10	34	10	41	12	57	8	28	5	18
Other univ. in Japan	101	459	86	400	88	280	107	334	75	239	71	237
Foreign countries	4	25	2	9	3	12	0	0	4	13	2	2
Others	185	268	276	361	248	325	221	309	171	221	180	255
Total	360	1134	423	996	402	1032	381	1010	302	1010	304	1022

Table 6.11: Number of visitors at Kiso Observatory (Left: Total number of visitors; Right: Total number of stay). Note the “Others” after AY2007 are mostly high-school students who visited with outreach educational programs (“Others” before AY2006 do not include high-school students since the number was not counted).

6.9 Future Plan

In this large telescope era, small/mid-class telescopes must seriously seek for best future plans with a limited amount of resources to meet with scientific and educational requirements. For last 10 years, we have been upgrading the facility and the organization of the observatory to accommodate to the situation. As a result, the Kiso Observatory is establishing a distinct position in Japanese astronomical community by pursuing: 1) capability of large survey by making use of the wide FOV of the Schmidt telescope, 2) base facility for young astronomers who are ambitious to try new astronomy/instrument projects (*high-risk/high-return* is fine), 3) basement for education/outreach programs at the professional observing site.

In AY2019, we have finally reached to the stage to start large continuous surveys with the extremely wide field-of-view camera, Tomo-e. We have already started routine surveys and plan to continue this for another 10 years. Still the data analysis system and data handling is a big issue for Tomo-e survey, and we are trying to clear the problems step-by-step, such as constructing fast network systems and the AI data reduction system for extracting useful objects from the survey data (see e.g., Ohsawa’s section).

Chapter 7

TAO project

7.1 Project Overview

The University of Tokyo Atacama Observatory (TAO) project is to construct a 6.5 m infrared telescope at an altitude of 5600 m in northern Chile, promoted by Institute of Astronomy, the University of Tokyo. Its major purpose is to carry out various science from cosmology, galaxy formation and evolution, to star formation and planet formation, as well as to educate next generation astronomers as a university-owned telescope. The telescope will be installed at the summit of Co. Chajnantor located in the Atacama plateau in northern Chile, the driest place on the Earth with annual precipitation of less than 10 mm. In combination with the extremely high altitude of the site, the precipitable water vapor (PWV) is less than 1 mm and thus atmospheric windows from near-infrared (NIR) to sub-mm wavelengths become accessible, especially at the mid-infrared (MIR) where new windows at 30–40 μm open and at the NIR where the windows at 1–2.5 μm become a single band (Figure 7.1). Thus, TAO will open a new window on sciences that were thought to be impossible for ground-based observations.

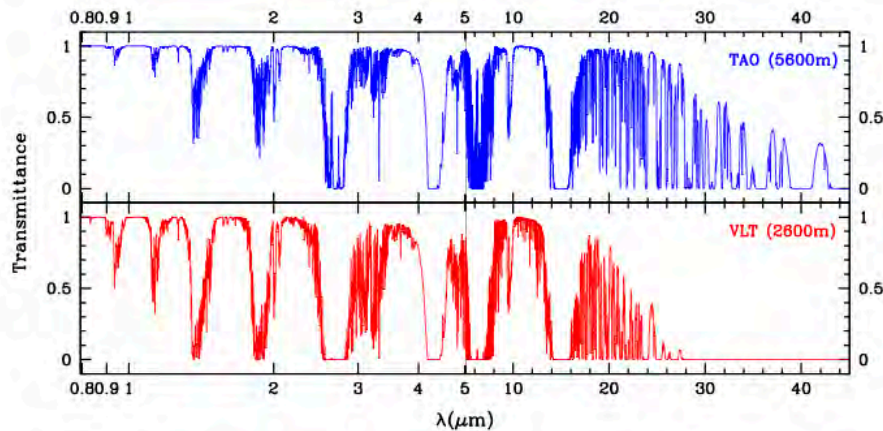


Figure 7.1: Simulated atmospheric transmission at the TAO site (upper panel) and VLT (lower panel).

The telescope design is based on that of the Magellan telescopes, having two Nasmyth foci for facility instruments and two folded-Cassegrain foci for carry-in instruments. The foci are switched by rotating the tertiary mirror. The telescope structure was fabricated by Nishimura Co. in Japan and its preassembly and test were completed in Jan, 2018. However, due to a hit of an extremely strong typhoon, most of the structure were damaged in August 2018 and they are now in process of re-fabrication. The 6.5 m primary mirror as well as secondary and tertiary were fabricated by Ricard F. Caris Mirror Lab. at the University of Arizona. The primary mirror is a monolithic honeycomb mirror and controlled by 104 actuators. The polishing process of these mirrors are all completed and preparation of transportation to Chile is now underway. These mirrors will be aluminized by a chamber installed at the summit building, which is now fabricated in China by Sanko Co.

Two facility instruments are being developed. One is a NIR instrument SWIMS for a wide-field ($9.6'\phi$) imaging and multi-object spectroscopy at 1–2.5 μm , and the other is an MIR instrument MIMIZUKU for imaging/spectroscopy at 2–38 μm . Their development started in 2010, and we successfully saw engineering first lights at Subaru in 2018. Site development is ongoing, and road expansion to the summit is now underway and the next step is excavation works at the



Figure 7.2: (Left) Completed primary mirror. (Right) The primary mirror is being installed into the primary mirror cell with the lifting fixture.



Figure 7.3: The aluminized secondary (left panel) and tertiary (right panel) mirrors. The blue film is for protection during the transportation.

summit and construction of the foundation. Installation of the dome enclosure and the telescope will follow, and the first light is expected in 2020.

References

- Yoshii, Y. et al. 2014, Proc. of SPIE, 9145, id. 914507
- Yoshii, Y. et al. 2016, Proc. of SPIE, 9906, id. 99060R
- Doi, M. et al. 2018, Proc. of SPIE, 10700, id. 107000W

7.2 Telescope Optics

The optics of TAO 6.5 m telescope adopts Ritchey–Chrétien design with a pupil located at the secondary mirror and a field-of-view of 25' diameter. To make the best use of good seeing at the site, requirements for image quality are 80% encircled energy diameter of 0.33 arcsec and FWHM of 0.22 arcsec for a point source. To utilize the good transparency of the atmosphere not only at the infrared wavelength but also at the ultraviolet, all the mirror surfaces are aluminized, not silver-coated. Also, the final F ratio is set to 12.2, which is same as that of the Subaru telescope to share instruments between the two telescopes.

Design and fabrication of the primary (6.5 m; Figure 7.2), secondary (0.9 m; Figure 7.3 left) and tertiary (1.1 m×0.75 m; Figure 7.3 right) mirrors and their support systems have been carried out by Richard F. Caris Mirror Lab of the Steward Observatory (previously SOML) at the University of Arizona. Fabrication of the three mirrors, as well as a dummy primary mirror, primary mirror cell, actuators, and etc. has been completed as shown in Figure 7.2. Final functional



Figure 7.4: The telescope mount preassembled in Japan.

tests for the mirrors including software tests have been ongoing as well as preparation for transporting the fabricated components from Tucson to Chile.

References

Morokuma, T. et al. 2014, Proceedings of the SPIE, 9145, id. 91453C

7.3 Telescope Mount

The telescope has a tripod-disk type altitude-azimuth mount (Morokuma et al. 2014). It has four foci, two of which are Nasmyth foci for facility instruments and the other two are folded Cassegrain foci for future carry-in instruments. An active focus is selected by rotating the tertiary mirror, and no instrument exchange during daily operation is necessary. To drive the giant telescope smoothly, hydrodynamic bearings and friction drives are adopted. Gravitational flexure of the structure and the primary mirror surface due to change in position are going to be compensated by actively controlling the primary mirror actuators and the position of the secondary mirror. They will be adjusted based on the wave-front error of the telescope optics that is measured using a reference star outside the field-of-view of an instrument during the observation.

The telescope mount is fabricated by Nishimura Co. It was preassembled and tested at a yard in Harima-Shinto island, Hyogo Prefecture (Figure 7.4). On January 28, 2018, a completion ceremony was held inviting astronomers and related companies, then the mount was disassembled, packed for the transportation and stored at an outdoor yard and a warehouse in Rokko island, Hyogo Prefecture.

Unfortunately, however, a strong typhoon critically damaged the disassembled telescope mount. A strong typhoon Jebi (No. 21) emerged at southern Pacific in the end of August 2018 and hit Rokko Island around 2PM on September 4. It caused a highest tide recorded, higher than that observed for typhoon Nancy in 1961, which resulted in disastrous damage around the island. The outdoor yard and the warehouse where the telescope mount was stored were also flooded by the tide. Although no item was lost by the incident, many of the parts stored outside were hit by cars and containers rushed in by the tide, and swept against the warehouse. All the packing was damaged and sea water intruded into the

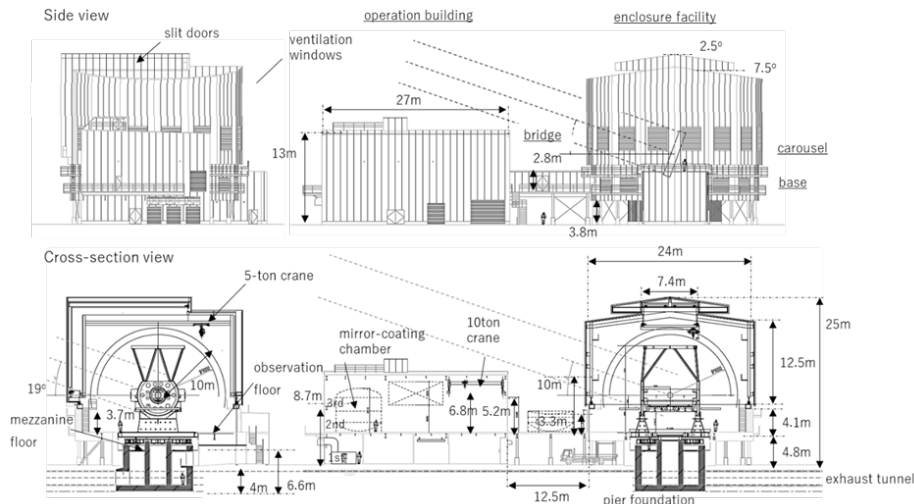


Figure 7.5: Layout of the summit facilities.

parts, even those stored inside the warehouse. Steel parts got rusted very fast, and surface accuracy for hydrostatic bearings and mechanical connections seemed to be severely damaged.

Considering difficulties to clean the giant and complicated parts completely and a risk of long-term rusting, we decided to refabricate all parts of the telescope mount. The refabrication of the telescope mount is started in 2019 based on the supplementary budget of the Japanese government for disaster recovery. Because of the restriction of the TAO project schedule, full assembly and functional test that had been done during the past preassemblage will be omitted, and only part-to-part connection checks will be performed. The refabricated telescope mount will be shipped from Japan in 2020.

References

Morokuma, T. et al. 2014, Proceedings of the SPIE, 9145, id. 91453C

7.4 Summit Facilities

The telescope will be installed in a carousel-type enclosure with a diameter of 25 m and height of 24 m. A moving part of the enclosure is 16 m high, and a base structure 9 m (Figure 7.5). The moving part has slit doors of 7.4 m wide, 14 ventilation windows, a 5-ton overhead crane, a windscreen, and a top screen, and is supported by 42 bogies. The telescope can observe fields higher than 19 degrees altitude. A telescope pier is 10.4 m in diameter and 2.6 m high, and the total weight is 200 ton. It consists of precast concrete parts, and is independent from foundation of the enclosure. The base structure has a control room, a compressor room, an electric room, a chiller room, and a 50 m tunnel which ventilates air in the enclosure, including that inside the pier.

Next to the enclosure is an operation building (two-floor, 27 m × 18.5 m × 13 m) having an observation room, an aluminizing chamber, laboratories, a lounge, a garage, an electric room, a generator room, and an evacuation room. Its 2nd floor is connected to an observation floor of the enclosure by a bridge of 12.5 m long. The primary mirror in the cell is moved to the aluminizing chamber in the building through this bridge.

The enclosure and the building are aligned to north-south direction which is vertical against the prevailing wind.

The moving part of the enclosure was preassembled at Nose, Osaka Prefecture in 2018 (Figure 7.6). After the assembly of steel frames, the 42 bogies and maintenance structures such as catwalks and stairs, all the other parts such as slit doors, ventilator windows (roll-up shutters), overhead crane, various motors and their controllers, and lights were installed. The operational tests were then carried out, and all the moving parts were confirmed to work properly. After disassembly of all the structure, repainting of the steel frames, and maintenance of the mechanical parts, all the moving parts of the enclosure were shipped from Kobe port to Chile in 2019. Steel frames, insulation walls, doors, floors and ventilation windows for the base structure of the enclosure were also fabricated in 2018. They were also shipped from Kobe port in 2019.

References

Sako, S. et al. 2014, Proceedings of the SPIE, 9145, id. 91454P



Figure 7.6: The preassembled enclosure.

Figure 7.7: (*left*): The moving part of the enclosure under preassembly; (*right*): Top view of the preassembly enclosure.

7.5 Aluminizing Chamber

The aluminizing chamber is necessary to re-deposit aluminum layer on the mirror surfaces to keep the optical throughput of the telescope. Process of the re-aluminization will be carried out as follows:

- The primary mirror and the cell are uninstalled from the telescope and handled by a moving/elevation cart. They are then transported to the operation building by the cart running on rails laid through the bridge.
- The primary mirror and the cell on the cart are first sent to a washing area of the building. Here, the mirror is washed and old aluminum layer is removed, which are done robotically by sequencer program. The mirror surface after the washing / removal is checked by human eyes.
- After the inspection, the mirror cell with the primary mirror in it is moved to an aluminizing area and sandwiched by the upper chamber and the lower lid. After the evacuation of the whole chamber, the surface of the mirror is cleaned to molecule level by ion-discharging.
- Finally the mirror is aluminized by evaporating aluminum, which is selected to achieve wide wavelength range from the optical to infrared. Thickness of the aluminum layer is set to 100–120 nm, in consideration of MIR observations. After the deposition, the mirror and the cell are sent back to the enclosure and attached to the telescope again.

Frequency of re-aluminization is expected to be every two years, although it depends on a speed of degradation of the mirror surfaces. Following conceptual design works in previous years, we made a production contract with Sanko Seikohjyo Co. Ltd., in 2018 which includes; fabrication of the main chamber, test for deposition, and transportation of the chamber to Chile. Conceptual design and experimental results of aluminization can be referred in Takahashi et al. 2014 and 2016.

The largest progress in a few years is completion of a detailed design of the main chamber and start of its production in Dalian, China. Procurement of materials such as stainless steel was completed in the end of 2018, and real production has started already; rough processing of parts for main chamber (upper part and lower lid) is completed, and the next

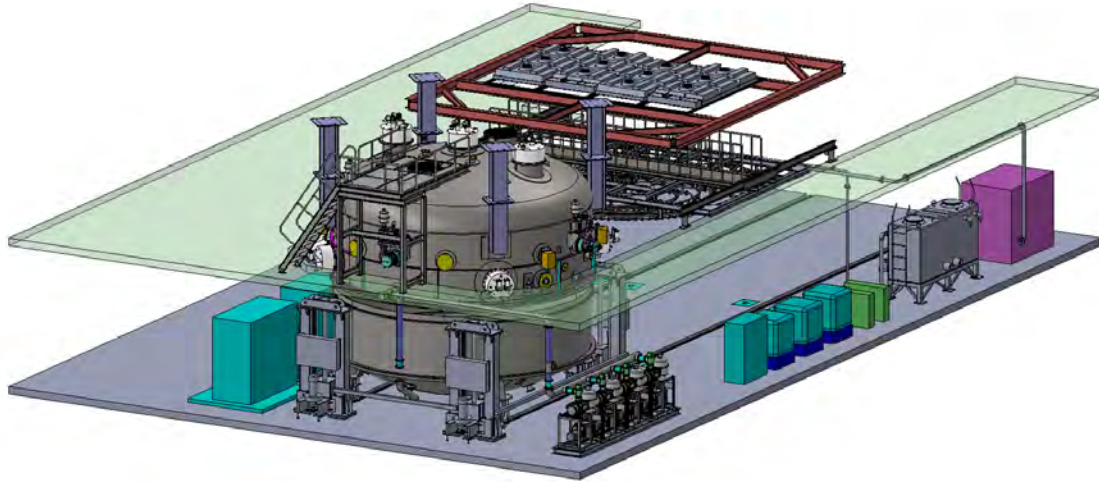


Figure 7.8: Installation of the coating facility in the support building. The cleaning system is arranged at the upper right of the chamber. The accessories on the 3rd floor are omitted for easy viewing.



Figure 7.9: (Left) The aluminumizing chamber joining upper part and lower lid. (Right) Inside floor of the chamber. The filaments are set on the floor and covered by dedicated box.

step was welding of these parts and drilling works. In the end of 2019, we will be able to see the final shape of the chamber. It has been confirmed that the upper and lower chambers were fitted with each other mechanically, and has been also confirmed to mate the primary mirror cell on the drawing. The requirements of the manufacturing accuracy are satisfied. Final design work for arrangement of aluminumizing filaments in the chamber and current/voltage setup is also underway, following the tests carried out in previous years. Arrangement of ancillary facilities in the operation building, such as pumps for washing, drain facilities, controller, and a power distributor, were also done. We also discussed the detailed installation scenario of the chamber with the design company of the building, as the chamber is very large and should be installed in the building during its construction. These all components will be sent and installed in a testing location in Japan, and the electrical operation check and the experiments of optimum conditions for aluminumization will be performed in early 2020 before transportation to the site.

References

- Takahashi, H. et al. 2014, Proc. of SPIE, 91457N
 Takahashi, H. et al. 2016, Proc. of SPIE, 99064Q

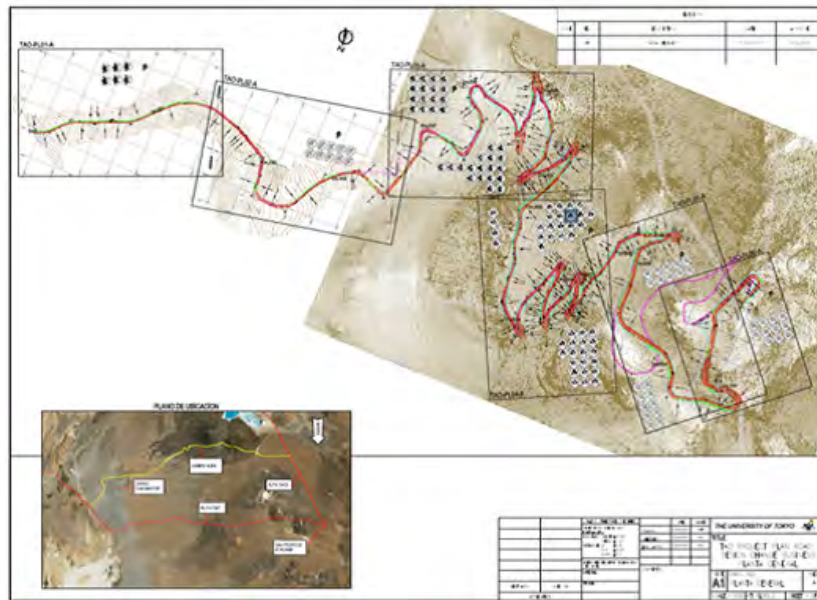


Figure 7.10: Summit access road to the TAO site

7.6 Site Construction Works

Development of the TAO site has been carried out by the University of Tokyo, which includes construction and maintenance of the summit area and its access road.

The existing access road was constructed in 2006 with a width of 3 m, which is not wide enough to transport the large parts of the 6.5 m telescope. Therefore, we have first started road expansion work prior to summit construction. After careful consideration, we found that minimum width of 6 m and inclination less than 12% at a straight part and 9 m and 2% at a curve meet the requirements. Figure 7.10 shows the design of the new road.

On-site work started on March 19, 2018. It was extremely difficult work because of harsh environment such as low air pressure, low temperature, dry atmosphere, and strong UV radiation. We have developed safety management program specialized for TAO in order to prevent medical illness for humans at the site. In this program all workers have to take medical examinations before their work starts. The results are reviewed by a licensed medical doctor. At the site all staff always need to use oxygen supply, and resting time is determined according to physical load of works. Another big problem was complicated geological structure. In the Chajantor mountain above 5,100 m.a.s.l. there are frozen layers everywhere, and if we remove surface soil on it, there is a possibility that a thermal input dissolves the layer and a slope may collapse. To evaluate this effect, we have carried out a joint research with Professor Yoshikawa at University of Alaska who is an expert of permafrost, and found that it is possible to make effective measures although risks of some slopes to collapse remain.

As of November 2019, the expansion work has almost finished. It has already reached the summit and a few curves remain to be finalized.

In parallel to the road expansion, we have started summit construction. The first step is to level out the ground, and then foundation work of the telescope and enclosure follows. As the temperature at the summit is below freezing, it is difficult to cast concrete on site. Thus we decided to incorporate precast concrete parts for the telescope pier and foundation of the the enclosure. As the pier is huge, we separate it into parts with 6 tons each. The production of the precast concrete parts completed, and preassemble test was successfully carried out (Figure 7.11). They are transported to the summit, and will be installed by the end of March. Assembly of the enclosure will also start in March 2020.

7.7 Schedule

After the completion of the civil works, we will finally move into the construction phase of the telescope. During this phase, all the parts except for the summit operation building are transported from Japan and assembled at the summit. Thus, transportation of each parts to the summit just in time is very important; it will be done by Nippon Express Co, who has many experiences in transportation for Subaru, ASTE and ALMA.

Due to troubles including the serious damage caused by the typhoon in 2018, we had to postpone the first light schedule that was initially expected to be in 2019. Fortunately, we had intense support from the government and the



Figure 7.11: The telescope foundation preassembled in a factory in Santiago

university, and started the reconstruction of the telescope as mentioned in the previous section. The first task after the civil works is assembly of the enclosure. Most of the parts have already arrived in Chile, and stored in a yard near Antofagasta port. The assembling work of the enclosure will start in March 2020.

Reproduction of the telescope mount will be done in parallel, and all the parts will be finished and tested by the end of FY2019. It will be shipped in May 2020 and assembled in the summit enclosure by October 2020. The mirrors and their control system will be shipped from Arizona in April 2020. Currently, engineering observations are expected to start in November 2020.

7.8 First-generation Instruments

7.8.1 SWIMS

SWIMS (Simultaneous-color Wide-field Infrared Multi-object Spectrograph) is an imager and multi-object spectrograph in the NIR wavelength of $0.9\text{--}2.5\ \mu\text{m}$ (Table 7.1). Having high versatility, it is capable of broad science from Galactic star formation, formation and evolution of nearby and distant galaxies, and cosmology.

The major feature of SWIMS is its wide FoV and wavelength coverage; the optical path is divided into two arms (*blue*: $0.9\text{--}1.4\ \mu\text{m}$ and *red*: $1.4\text{--}2.5\ \mu\text{m}$) by a dichroic mirror inserted in the collimated beam, which realizes a $\phi 9.6$ arcmin FoV with a pixel scale of $0.126\ \text{arcsec/pix}$ and two-color simultaneous sampling. Thus it is capable of taking images in two filter-band simultaneously in imaging mode, or $0.9\text{--}2.5\ \mu\text{m}$ multi-object spectra in spectroscopy mode, both with a single exposure. In combination with the high atmospheric transmittance at the site, where the NIR wavelength range becomes almost a single window, SWIMS enables us to obtain data of homogeneous quality with high observational efficiency. SWIMS was get funded and the development was started in 2009 in advance to the 6.5 m telescope. It was necessary to evaluate its performance by installing it on a telescope and observe celestial objects before going to the TAO site of 5,640 m altitude. Therefore, we have been contacting the Subaru telescope at Hawaii to carry out engineering observations there.

We had submitted an application for a carry-in instrument in 2014, and after several reviews over a few years, the application was approved and SWIMS was transported to Hilo in July 2017. In total, six nights have been allocated for on-sky commissioning observations, and it successfully saw the imaging first light in May 2018 and the multi-object spectroscopy first light in Jan 2019 (Figures 7.12 and 7.13). For the imaging mode, design performance of pixel scale of $0.095\ \text{arcsec/pix}$ with distortion less than 1 pix over the full FoV is confirmed, and the sensitivities are evaluated as high as expected ($\sim 40\%$ at a maximum in the *H*-band). For the spectroscopy mode, spectral resolutions are confirmed to be $2.40\ \text{\AA/pixel}$ (*blue*) and $4.57\ \text{\AA/pixel}$ (*red*) as designed, and the full-NIR-covered spectra show the similar or slightly lower sensitivities compared to the imaging data, which might be caused by stray light. We confirm the advantage of simultaneous two-color observations with high sensitivities.

SWIMS will be served to open-use operation at the Subaru telescope as a PI instrument from S21A semester for two years. After that, SWIMS will be transported to Chile in late 2022, and see the first light on the TAO 6.5-meter telescope in early 2023.

References

- Konishi, M., et al. 2018, Proc. SPIE, 10702, 1070226
- Kitagawa, Y., et al. 2016, Proc. SPIE, 9912, 991225
- Motohara, K., et al. 2016, Proc. SPIE, 9908, 99083U
- Terao, Y, et al. 2016, Proc. SPIE, 9915, 99151W
- Motohara, K., et al. 2014, Proc. SPIE, 9147, 91476K
- Takahashi, H., et al. 2014, Proc. SPIE, 9147, 91476N

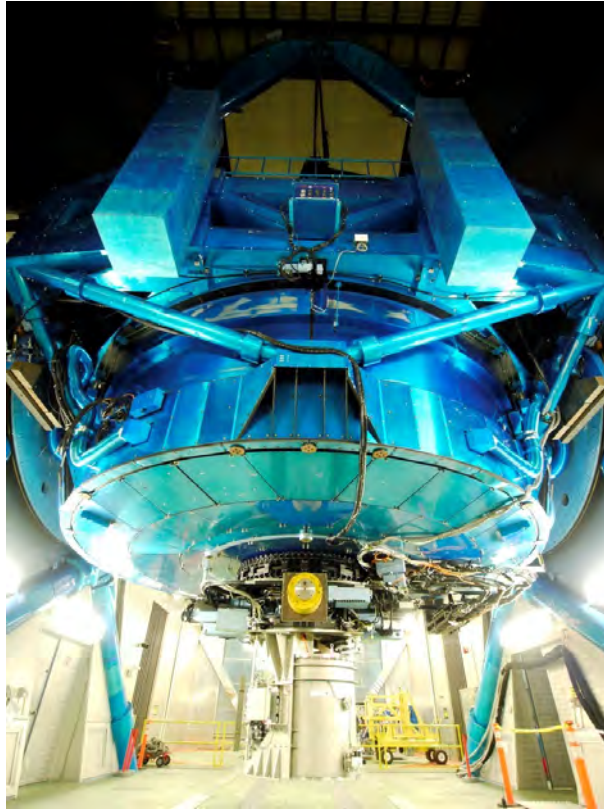


Figure 7.12: SWIMS installed on the Subaru telescope

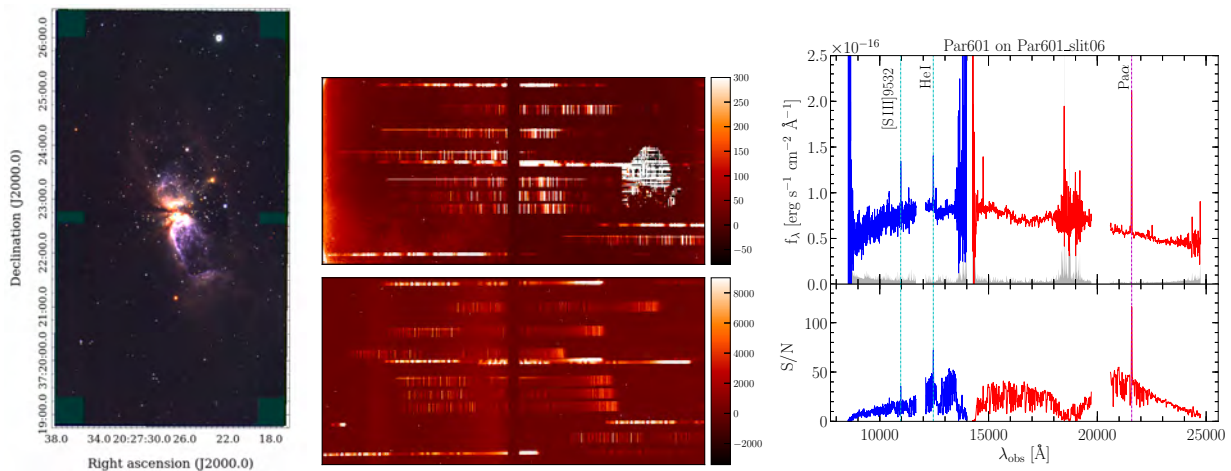


Figure 7.13: *Left*: The first-light image of SWIMS, a JHK_s three-color composite image of a star-forming regions Sharpless 2-106. *Middle*: The first-light MOS spectra (*upper*: blue spectra, *lower*: red spectra) taken at a field including a nearby luminous infrared galaxy at $z \sim 0.15$. *Right*: the reduced one-dimensional spectrum of the galaxy.

Todo, S., et al. 2014, Proc. SPIE, 9154, 91541L

Kitagawa, Y., et al. 2014, Proc. SPIE, 9151, 91514P

7.8.2 MIMIZUKU

Mid-Infrared Multi-field Imager for gaZing at the UnKnown Universe (MIMIZUKU) is a mid-infrared imager / spectrograph covering a wide wavelength range of 2–38 μm , to make the best use of the transparent atmosphere of the TAO site (Fig. 7.14; Table 7.2). In particular, 30- μm observation is a key feature of MIMIZUKU, where a ground-based observation is almost impossible at the other sites. Another feature is a high spatial resolution; it is capable of 0.4'' and 1.2'' diffraction

Table 7.1: Specifications of SWIMS

Observation Mode	Imaging Multi-object spectroscopy(MOS) Integral-field spectroscopy (IFS)
Field of View	
Current	$8'.2 \times 4'.1$ (Imag.), $3'.5 \times 4'.1$ (MOS), $14'' \times 5'.1$ (IFS : optional)
Goal	9.6ϕ (Imag.), $3'.5 \times 8'.2$ (MOS), $14'' \times 10'.2$ (IFS)
Spatial Resolution	$0.126''/\text{pixel}$
Wavelength Range	$0.9\text{--}1.4 \mu\text{m}$ (<i>blue</i> arm), $1.4\text{--}2.5 \mu\text{m}$ (<i>red</i> arm)
Detector	HAWAII-2RG 1.7 (<i>blue</i>) / 2.5 (<i>red</i>) μm -cutoff arrays
Filters (<i>blue</i> <i>red</i>)	
Broad-band	$Y, J H, K_s$
Medium-band	$J1, J2 H1, H2, H3, K1, K2, K3$
Narrow-band	$N1244, N1261, N1292, N1326 N1630, N1653, N1875, N1945, N2137, N2167$
Grism	YJ ($2.40 \text{ \AA}/\text{pix}$, $\lambda/\Delta\lambda \sim 720\text{--}1150$ w/ $0'.5$ slit) HK ($4.57 \text{ \AA}/\text{pix}$, $\lambda/\Delta\lambda \sim 610\text{--}1040$ w/ $0'.5$ slit)
MOS multiplicity	~ 20 (40 at goal) objects/mask (w/ $12''$ length per slit)
IFS parameters	Image-slicer IFU, 13 (26 at goal) slices, $0'.5$ sampling/slice
System Throughput	Imaging $\sim 40\%$, Spectroscopy $\sim 30\%$
Limiting AB mag. (1hr, 5σ)	
Imag.	$Y=24.6, J=24.5, H=24.3, K_s=24.2$
Spec.	$Y=\text{TBD}, J=20.6, H=20.2, K_s=20.3$



Figure 7.14: (Left) External view of MIMIZUKU. (Middle) The field stacker unit installed on the top of MIMIZUKU dewar. (Right) Principle of the field stacker.

limited image at 10 and $30 \mu\text{m}$, respectively. MIMIZUKU is also capable of high-precision correction of the atmospheric absorption; in MIR ground-based observation, correction of the absorption by the Earth atmosphere is necessary, by observing standard stars. However, as variation of the absorption has a rather short timescale, it is necessary to observe a target and a standard star simultaneously to achieve high precision correction. MIMIZUKU has a “field-stacker” unit to image separated two objects on the sky on to its small field-of-view, which enables us to compensate the temporal variation of the atmospheric absorption, and carry out high precision photometry or spectroscopy (Fig. 7.14).

After a decade of development (Kamizuka et al. 2014, 2016, 2018; Okada et al. 2014; Uchiyama et al. 2016; Mori et al. 2018), MIMIZUKU saw the first light on July 2018 at the Subaru telescope. The purpose of the observation run is to brush-up the instrument through real observations and realize smooth operation at the TAO 6.5-m telescope, as well as to demonstrate the efficiency of the field stacker unit which was totally a new concept and had never been tested before. Fig. 7.15 shows the first light image of Mars in $10 \mu\text{m}$, taken on July 3, 2018. During the first run in July, $10\text{-}\mu\text{m}$ imaging observations with the field stacker was completed. Another run was carried out in December 2018, and $20\text{-}\mu\text{m}$ imaging and spectroscopy in 10- and $20\text{-}\mu\text{m}$ bands with the field stacker were successfully completed.

Through these observations, it was confirmed that diffraction limited images were achieved both in 10 and $20 \mu\text{m}$, that wavelength resolution of the spectroscopy mode was as designed, and that high photometric accuracy in both 10 and $20 \mu\text{m}$ and stable $20\text{-}\mu\text{m}$ spectroscopy became possible by the field stacker. These results mean that all the hardware/software development of the MIR-S channel is complete, and is an important milestone for MIMIZUKU.

References

Figure 7.15: (Left) MIMIZUKU installed on the Subaru telescope. (Right) 10- μm image of Mars.

Table 7.2: Specifications of MIMIZUKU.

	NIR ch	MIR-S ch	MIR-L ch
Observation mode	Single-field Imaging/Spectroscopy Dual-field Imaging/Spectroscopy		
Field of view	1.2' \times 1.2'	2.0' \times 2.0'	31" \times 31"
Pixel scale	0.069"/pixel	0.11"/pixel	0.24"/pixel
Wavelength range	2.0–5.3 μm	6.8–26 μm	24–38 μm
Detector	HAWAII-1RG 5.3 μm -cutoff	Aquarius Si:As IBC	MF-128 Si:Sb BIB
Filters	(<i>J</i> , <i>H</i>) <i>K</i> _S , <i>L'</i> , <i>M'</i> , <i>H</i> ₃ ⁺	7.6 μm , 9.8 μm , 11.6 μm , 13.1 μm , 20.8 μm , 24.5 μm	32 μm , 37 μm
Grism	<i>KL</i> -band (2.1–4.0 μm /210), 2.7- μm band (2.4–3.0 μm /620), <i>LM</i> -band (2.8–5.3 μm /110)	<i>N</i> -band (6.8–14 μm /170), <i>Q</i> -band (17–26 μm /100)	
Sensitivity (1 σ 1sec)	0.01–100 mJy	20–200 mJy	300–1000 mJy

- Kamizuka, T. et al. 2014, Proc. of SPIE, 9147, id. 91473C
 Kamizuka, T. et al. 2016, Proc. of SPIE, 9908, id. 99083W
 Kamizuka, T. et al. 2018, Proc. of SPIE, 10702, id. 107022H
 Okada, K. et al. 2016, Proc. of SPIE, 9915, id. 991527
 Uchiyama, M. S. et al. 2016, Proc. of SPIE, 9912, id. 99125N
 Mori, T. et al. 2018, Proc. of SPIE, 10702, id. 107022N

7.8.3 NICE

NICE (Near-Infrared Cross-dispersed Echelle spectrograph; Yamamuro et al. 2007) is an echelle spectrograph developed by Institute of Astronomy, the University of Tokyo in 2000 (PI: M. Tanaka). It covers the wavelength range from 0.9 μm to 2.4 μm with four exposures, and has a wavelength resolution of $\lambda/\delta\lambda \sim 2600$. These capabilities enable us to simultaneously evaluate the continuum level and intensity of various lines of a spectrum with high accuracy over a wide wavelength range. NICE was first installed at the Cassegrain focus of the 1.5 m infrared telescope of National Astronomical Observatory of Japan (Figure 7.16), and achieved results such as obtaining wide-range NIR spectra of Wolf-Rayet (WR) stars. Figure 7.17 shows an example of spectra of WR stars obtained by NICE; the spectra consist of blackbody radiation, free-free radiation from an intense stellar wind, and strong broad emission lines such as H, He I, He II, C III, and C IV (Nishimaki et al. 2008). Later, NICE was moved and installed on the 1.6 m Pirka telescope of Hokkaido University at Nayoro in Hokkaido, Japan and operated for about seven years. In addition to observations of WR stars and LBV stars, we started a joint observation of Venus with Osaka Prefecture University and Hokkaido University since 2018. The goal of science is to elucidate the origin of the rotation of Venus atmosphere over several days



Figure 7.16: NICE at the Cassegrain focus of the 1.5m infrared telescope of National Astronomical Observatory of Japan.

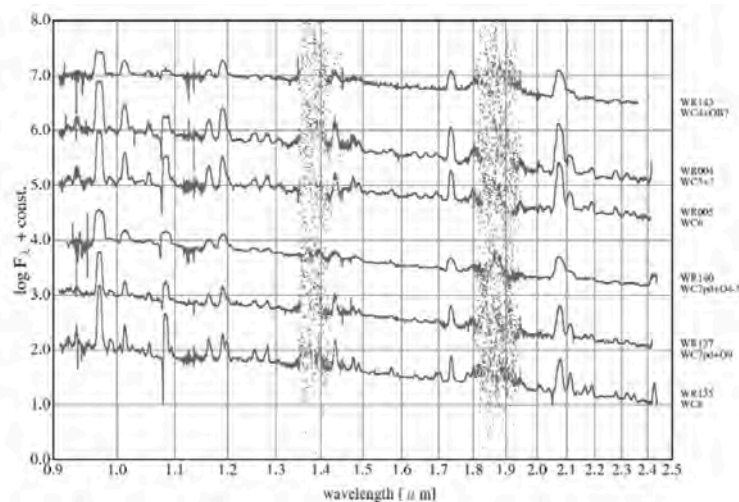


Figure 7.17: Near-infrared spectra of WC type Wolf-Rayet stars (Nishimaki et al. 2008).

and the difference in intensity distribution in the latitudinal direction using molecular emission lines in the near infrared.

To install on the TAO 6.5 m telescope in the future, NICE is currently in the process of upgrading cryogenics and computer systems in Japan. It will be transported to Chile in the second half of 2020 and will be used as a first-generation instrument for the early science observation phase. Thanks to the high altitude of the site and the extremely dry climate, almost continuous spectrum in the near infrared wavelength from 0.9 to 2.5 μm can be derived.

References

- Yamamuro et al. 2007, PASJ, 59, 387
 Nishimaki et al. 2008, PASJ, 60, 191

7.9 Key Science Objectives

TAO has two facility instruments, SWIMS and MIMIZUKU.

SWIMS is optimized for deep imaging/spectroscopy in the NIR wavelength, and capable of observation at the wavelengths from 0.2 to 2.5 μm utilizing the continuous atmospheric window at the site and covering wide redshift range for

emission-line observations. It also has wide field of view and capable of two-color simultaneous imaging / spectroscopy, which realizes high survey power. Thus, SWIMS is expected to carry out wide range of science cases from cosmology to galaxy formation and evolution.

MIMIZUKU covers the longer wavelengths from 2 to 38 μm , and especially 26–30 μm is only the wavelength range accessible from the ground by MIMIZUKU/TAO. As MIMIZUKU reaches far finer spatial resolution than that of existing satellite datasets, we can carry out observations to probe the origin of exoplanets and various materials in ISM. As high-precision relative photometry is realized by the “Field Stacker”, MIMIZUKU can also carry out time-domain observation in the MIR, which is impossible for existing ground-based instruments.

Utilizing the above features, we are planning to carry out the following key sciences by TAO.

7.9.1 Probe History of Baryon Accumulation by Observations of Quasars

It is now widely recognized that almost all the galaxies harbor supermassive black holes (SMBHs) at their centers, having masses of millions to billions of solar mass ($M_{\text{BH}} \sim 10^{6-9} M_{\odot}$). SMBHs are important to understand the history of baryon accumulation in the universe, not only as sources of the quasar phenomena emitting huge energy overwhelming their host galaxies, but also affecting the processes of formation and evolution of galaxies. Recent quasar surveys discover tens of quasars beyond redshift of 6, and many of their black hole masses are confirmed to exceed $10^9 M_{\odot}$ (e.g. Kurk et al. 2007; Mortlock et al. 2011; Wu et al 2015). As cosmic age at $z = 6$ is less than 1 Gyr, these discoveries put strong constraints on formation model of SMBHs heavier than $10^9 M_{\odot}$ (e.g. Tanaka & Haiman 2009).

Survey and Spectroscopic Follow-up for the Most Distant Quasars

Although many surveys have been carried out, only 3 quasars are discovered beyond $z = 7$ so far (and two of them are at $z \sim 7.0$) and thus further observations are necessary. Also, it is important to construct a large sample of high- z quasars covering large parameter space of space density, luminosity, and black hole mass that can be compared with various theoretical models. The reason for the difficulty of the detection of $z > 7$ quasars is that the Lyman break at 1216 \AA moves into the NIR wavelength at that redshift. Thus, we are planning a large quasar survey by TAO telescope with its wide-field imager SWIMS in collaboration with the HSC/Subaru wide-field imaging survey. The survey will spend 120 nights for the HSC-SSP-Wide field (1000°), which will reach $J = 23$ and $H = 22.5$, and is expected to discover up to 20 quasars at $z > 7.2$. The detected candidates will be followed-up by SWIMS with the spectroscopic mode, which will provide their black hole masses as well as precise redshifts.

Probe the Epoch and the Physical Process of the First Star Formation Using a Cosmological Clock

Investigation of chemical evolution in the early universe is expected to provide important clues for the formation of first (Pop III) stars. In the early universe, formation of iron will be delayed by ~ 1 Gyr than that of α elements, as it is expected to be formed by the long-lived progenitor of SNe Ia. Thus, iron ratio against α elements ($[\alpha/\text{Fe}]$) can be used as a probe for as a “clock” of galaxies, where its break against the cosmic age indicates the formation epoch of the first stars. The best target for this study is high- z quasars that have strong MgII and FeII emission lines, and many observations have been carried out. However, no break in the FeII/MgII flux ratio has been confirmed even at the cosmic age of 0.7 Gyr (De Rosa et al. 2014). We have revisited this problem and found that FeII/MgII flux ratio vs $[\text{Mg}/\text{Fe}]$ has strong dependence on gas density, and introducing a correction factor, succeeded in obtaining $[\text{Mg}/\text{Fe}]$ at $z = 0.7-1.6$ (Sameshima, Yoshii & Kawara 2017). We are planning to carry out NIR spectroscopic survey of high- z quasars with SWIMS/TAO and extend this measurement to $z = 7$, which will give us a new insight into metal formation in the early universe, and a clue to answer the question “When the first stars were formed?”.

References

- Kurk et al. 2007, ApJ, 669, 32
- Mortlock et al. 2011, Nature, 474, 616
- Wu et al. 2015, Nature, 518, 512
- Tanaka & Haiman 2009, ApJ, 696, 1798
- De Rosa et al. 2014, ApJ, 790, 145
- Sameshima, Yoshii & Kawara 2017, ApJ, 834, 203

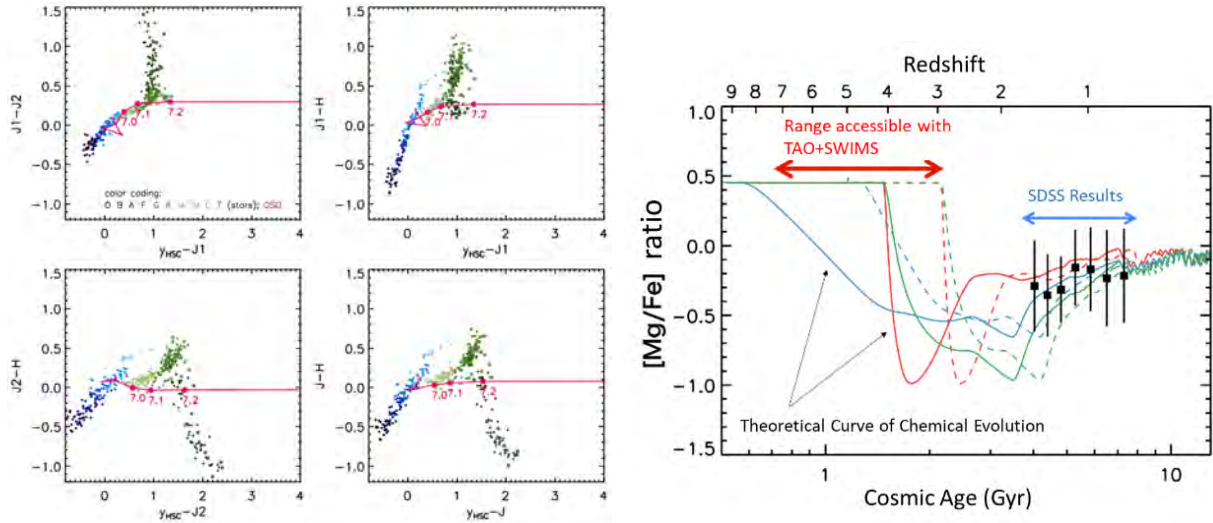


Figure 7.18: Left : Position of $z > 6$ quasars are shown as magenta lines on the color-color diagrams of $J1, J2, J, H$ -bands of SWIMS and y -band of HSC/Subaru. Filled points are distribution of Galactic stars. It can be seen that adding SWIMS data, we can select quasars at $z > 7.2$ efficiently. Right : $[Mg/Fe]$ obtained for SDSS quasars (black points), compared with the prediction of the chemical evolution model (Sameshima, Yoshii & Kawara 2017). TAO/SWIMS can put strong restriction to the model at high redshift.

7.9.2 Origin of Earth-Type Exoplanets

Giant Impact Events

In the current standard model of formation of the Solar System, dust particles collide and coalesce to form planetesimals and eventually grow into protoplanets. Final coalescence of protoplanets forms the planets, and it is called a “giant impact”, but little observational clue exists. MIR observation by TAO is a powerful tool to probe a giant impact event; once the giant impact occurs in a debris disk, cm-km size rocky fragments are formed and their cascade collisions result in formation of sub-micron size dust particles, emitting strong MIR-FIR emission.

There are two observational approaches to investigate the giant impact events with TAO.

One is a $30\text{-}\mu\text{m}$ imaging survey of stars with debris disks. According to simulations (e.g. Kenyon et al. 2004; Jascon et al 2012, 2014), the cascade collisions intensively occur at the impact position for about 1000 orbits which is an order of 1000 to 1 Myr according to the radius of the orbit. Therefore the disk that experienced the giant impact will show a localized bright spot in the mid-infrared wavelength. As $30\text{ }\mu\text{m}$ traces 80 K regions corresponding to 50–100 AU in radius, TAO/MIMIZUKU can resolve a giant impact event to 70 pc distance. About 30 stars out of 368 A-stars within 70 pc are expected to have traces of giant impacts and resolve it, assuming 30 events/lifetime for each star.

Another approach is a mid-infrared monitoring observation. The dust emission is brightest just after the impact event, and gradually weakens. Recent infrared monitoring have revealed that some disks show remarkable time variation (e.g. Melis et al. 2012; Meng et al. 2015; Thompson et al. 2019). This may be caused by a giant impact, but other possibilities such as instability of the disk and stellar variability cannot be ruled out completely. Further long-time monitoring observation is strongly desired. Spectral information of the dust is another key to understand the cause of the time variation. In particular, amorphous silica is a good indicator of a high speed collision. TAO/MIMIZUKU is the only instrument that can carry out accurate monitoring observations including spectroscopic monitoring in the mid-infrared.

Probing Atmosphere of Super-Earths around M-type Stars by Transit Observations

Transit observations discovers numbers of exoplanets, and studying physical properties of their atmosphere is the next step. In particular, atmosphere of super-earths ($\leq 10M_{\text{Earth}}$) are our interest. Super-earths are expected to be rocky planets, and different from gaseous planets, but their border is not clear yet. Therefore, spectroscopic transit observation to probe atmospheric composition is important to restrict their properties. SWIMS is suitable for such observations.

References

- Kenyon et al, 2005, ApJS 179, 451
- Jackson et al. 2012, MNRAS 425, 657
- Jackson et al. 2014, MNRAS 440, 3757

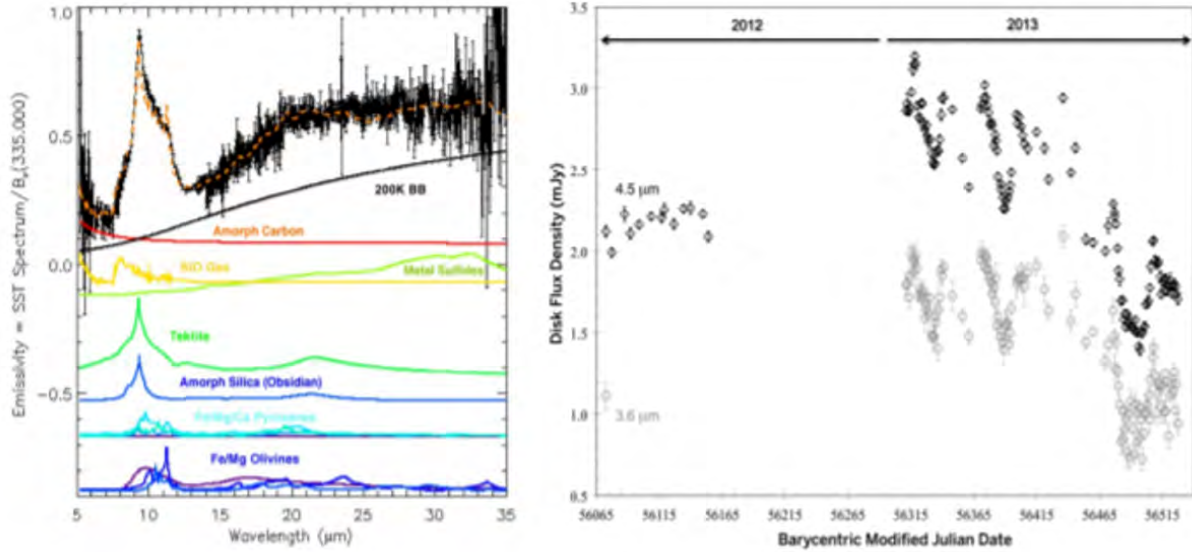


Figure 7.19: Spectral information (left, Lisse et al. 2009) and temporal evolution (right, Meng et al. 2014) of the infrared emission from some young stars provides the strongest evidence for giant impacts in the terrestrial planet region. Figures are from Wyatt+2018

Melis et al. 2012, Nature 487, 74

Meng et al. 2014, Science 345, 1032

Meng et al. 2015, ApJ 805, 77

Thompson et al. 2019, ApJ 875, 45

Lisse et al. 2009, ApJ 701, 2019

7.9.3 Time-Domain Observations

One of the advantages of SWIMS and MIMIZUKU on TAO is that they are installed on Nasmyth foci and can be switched easily by rotating the tertiary mirror. Thus, we can easily carry out flexible monitor observations in wide wavelength range from NIR to MIR.

Super-MAGNUM Project

The accelerated expansion of the universe, which was discovered in the end of the 20th century, is now the most intriguing problem in cosmology. It requires the introduction of mysterious “dark energy”, which consists three-quarters of energy density of the present-day universe. It goes without saying that the distance measurement for high redshift has critical importance on tracing the time variation of the dark energy and constraining cosmological models, however, it is difficult to reach beyond redshift of 2 by SNe Ia, which has led the studies of the cosmic expansion so far.

MAGNUM (Multicolor Active Galactic Nuclei Monitoring) group (PI : Yoshii) proposed and established an original method to measure the distance of AGNs (Yoshii et al. 2014, Minezaki et al. 2019). It uses the size-luminosity relation for the innermost dust torus, whose size is measured by reverberation mapping applied to the data of the multiwavelength monitoring observations of AGNs (Figure 7.20). They presented that the Hubble diagram of AGNs based on the dust-reverberation distance for $z < 0.6$ preferred accelerated expansion of the universe (Figure 7.21), which demonstrates that the reverberation distance is a promising new tool for investigating the cosmic expansion.

The reverberation-distance method can use the size-luminosity relation for the broad emission-line region as well (Watson et al. 2011; Czerny et al. 2013; Koshida et al. 2017), and we can observe strong UV emission lines even for very distant quasars. Utilizing TAO, we start the Super-MAGNUM project, which will execute multiwavelength photometric and spectroscopic monitoring observations of AGNs distributed over a wide redshift range to measure the distances of objects of $z \leq 7$ directly for the first time based on the reverberation method. Long-term monitoring observations required for this project are suitable for TAO, because flexible and strategic time allocation is available. This project will put constraints on the expansion of the universe in totally independent manner, which enables us to verify the gravity theory and temporal variation of dark energy.

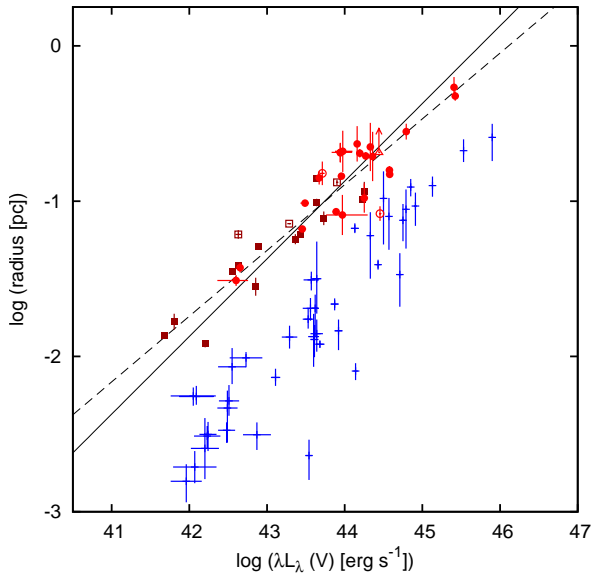


Figure 7.20: The size-luminosity relations for the innermost dust torus (brown and red circles) and a broad emission-line region (blue crosses).

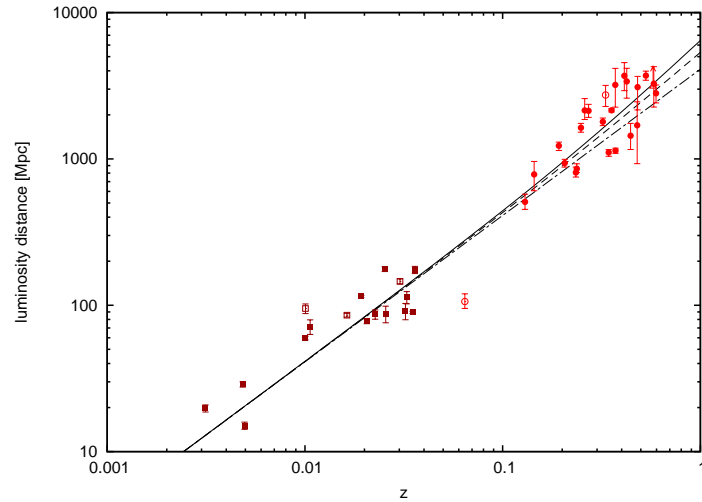


Figure 7.21: The Hubble diagram based on the dust-reverberation distance of AGNs. The solid line represents the standard cosmological model indicating the accelerated expansion of the Universe.

References

- Minezaki, T. et al. 2019, *ApJ*, 886, 150
 Koshida, S. et al. 2017, *ApJ*, 842, L13
 Yoshii, Y. et al. 2014, *ApJ*, 784, L11
 Czerny, B. et al. 2013, *A&A*, 556, A97
 Watson, D. et al. 2011, *ApJ*, 740, L49

Follow-up Observations of GW Events

Commissioning of Advanced LIGO and VIRGO, followed by their observational runs has resulted in discovery of first gravitational wave detection from a binary black hole GW150914 (Abbott et al. 2016), and later on, from coalescence of binary neutron star (NS-NS) GW170817 (Abbott et al. 2017). Various electromagnetic wave emission from gamma-ray to radio wavelength is detected by follow-up observations of GW170817 indicating that a NS-NS merger is a source of r-process elements, as well as progenitor of short-GRB event. At the time of the operation of TAO telescope, KAGRA in addition to Advanced LIGO and VIRGO will be operating. Follow-up observations of NS-NS GW events, especially NIR spectroscopy, is important to understand their properties (Pian et al. 2017), and TAO with SWIMS will be the best facility for this purpose. Galactic supernovae will also be a source of GW event, although the event rate is far lower than NS-NS mergers. As they will be located in the galactic plane, strong extinction is expected and infrared observation is essential. We will carry out wide field imaging follow-up observation by SWIMS, and once identified, both MIMIZUKU and SWIMS will be used for MIR observations and NIR spectroscopy to probe detailed properties.

References

- Abbott, B. P. et al. 2016, *ApJ*, 826, 13
 Abbott, B. P. et al. 2017, *ApJ*, 848, 12L
 Pian, E. et al. 2017, *Nature*, 551, 67

7.10 Operation Plan

Observing times of the 6.5 m telescope are divided into four categories; TAO project time, domestic time, partner time, and Chilean time. The partner time may be provided to a partner group with some contributions to the TAO project although possible contribution styles are being discussed in the TAO project. Observing time fraction for Chilean time is 10% of the total observing time and those for the partners are determined according to their contributions. After

subtracting the Chilean time and partner times from the total time, the rest observing times are divided into the TAO project time and domestic time with a ratio of 5 : 4.

The domestic time is open for astronomers in domestic universities and institutes. To seriously consider and determine the scheme of the domestic time, we will launch a new committee (“domestic SAC”) early 2020, consisting of about 4 UT faculty staffs and 4 scientists from other domestic universities and institutes based on an election in the Japanese optical-infrared astronomy consortium, “gopira”. We expect that the domestic SAC discuss various things related to the domestic time, for example, how to evaluate domestic time proposals considering those for the other large Japanese telescopes such as Subaru (8.2m, Hawaii) and Seimei (3.8m, Okayama), determine the scheme of the domestic time allocation committee (TAC), observing semesters, details of the rules about Chilean time, queue observation and target-of-opportunity systems, engineering observing times, outreach activities especially for initial results, education for young scientists and students, new instrumentation and strategic operation.